AN INVESTIGATION OF ROTATING MAGNETOSPHERES

Richard Daniel Ryan

A Thesis Submitted for the Degree of PhD
at the
University of St Andrews

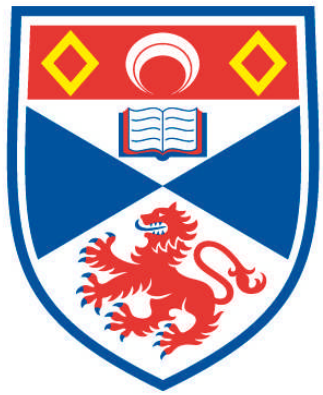

2002

An Investigation of Rotating Magnetospheres

Richard Daniel Ryan

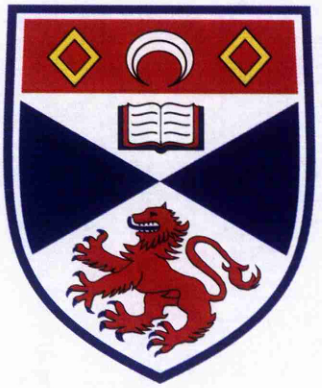

Thesis submitted for the degree of Doctor of Philosophy
of the University of St Andrews

ProQuest LLC.
789 East Eisenhower Parkway
P.O. Box 1346
Ann Arbor, MI 48106 – 1346

Declaration

1. I, Richard Daniel Ryan, hereby certify that this thesis, which is approximately 32,400 words in length, has been written by me, that it is a record of work carried out by me and that it has not been submitted in any previous application for a higher degree.

   date 23.11.02 ..... signature of candidate .....

2. I was admitted as a research student in September 1998 and as a candidate for the degree of PhD in September 1999; the higher study for which this is a record was carried out in the University of St Andrews between 1998 and 2002.

   date 23.11.02 ..... signature of candidate .....

3. I hereby certify that the candidate has fulfilled the conditions of the Resolution and Regulations appropriate to the degree of PhD in the University of St Andrews and that the candidate is qualified to submit the thesis in application for that degree.

   date 23 September 2002 signature of supervisor .....

4. In submitting this thesis to the University of St Andrews I understand that I am giving permission for it to be made available for use in accordance with the regulations of the University Library for the time being in force, subject to any copyright vested in the work not being affected thereby. I also understand that the title and abstract will be published and that a copy of the work may be made and supplied to any bona fide library or research worker.

   date 23.11.02 ..... signature of candidate .....

Acknowledgements

"Years ago my mother used to say to me, she'd say, "In this world, Elwood, you must be" – she always called me Elwood - "In this world, you must be oh so smart or oh so pleasant." Well, for years I was smart. I recommend pleasant. And you may quote me."

Elwood P. Dowd in *Harvey* (1950)

It is with pleasure that I would like to thank my supervisor, Dr. Thomas Neukirch for his tolerance, biblical patience and kind encouragement. I would also like to thank Dr. Moira Jardine for many useful discussions and insightful comments.

Special thanks to all my friends from St. Andrews, especially to long-suffering Zaharenia for her maternal care. This thesis would not have been possible without the unfailing support of my parents, Patrick and Kathleen Ryan, and of my brothers Luke, Dunk, Chris and Ferg.

Finally, I would like to gratefully acknowledge the financial support of PPARC

This thesis is dedicated to the memory of Beryl Hughes (1929-2000)

Contents

List of Figures

Chapter 1

Introduction

1.1 Rotating magnetic atmospheres: a background

1.1.1 The solar-stellar connection

The wealth of detailed optical, UV, EUV, radio and X-ray spectrum observations of both solar and of stellar atmospheric activity and the theory that has been developed alongside the observations, has contributed significantly to the reinforcement of the 'solar-stellar connection' paradigm from the 1970's to the present day. This refers to the complementary nature of solar and stellar studies, primarily (but not exclusively) with reference to the dynamic behaviour of the magnetic fields in the outer atmospheres. Given the proximity of the sun as the nearest star to the earth, it is inevitable that much greater observational detail has been amassed than has been possible for other stars. Clearly these

solar studies can inform our understanding of the physics of other solar-type stars but the converse is also true in that the diversity of stellar populations allows investigation of the relationship between the physical processes determining solar structure/dynamics and such general stellar properties as chemical composition, stellar mass, rotation rate and whether the system is binary or not. Magnetic activity in stars other than the sun has been measured since 1980 (e.g., Robinson et al. , 1980, Saar & Linsky , 1985) prior to which it had been inferred indirectly from periodic CaII H and K spectral line activity in slowly rotating late-type dwarfs (Wilson , 1966). Stars which are much more magnetically active than the sun have been estimated to have magnetic field strengths of the order of kiloGauss compared to the Sun with its photospheric mean surface magnetic-flux densities that are roughly two orders of magnitude weaker. Also, the coronal plasma temperatures have been inferred to be of the order of $10^7 - 10^8$K which is roughly two orders of magnitude higher than has been found in the solar corona.

Stellar rotation and magnetic activity

For the more rapidly rotating single stars of young clusters a correlation between increased chromospheric activity and stellar rotation rate, (see Noyes et al. , 1984) has been demonstrated and stellar rotation has therefore been shown to be a crucial parameter for the strength of activity in a star of a given spectral type (see Kraft , 1967, Durney , 1972). Indeed, a more explicit relation between magnetic activity and stellar rotation has also been well established (e.g., Parker , 1955, 1979) in terms of generation of large-scale flux from a dynamo, the efficiency of which will itself depend on the rotation of the

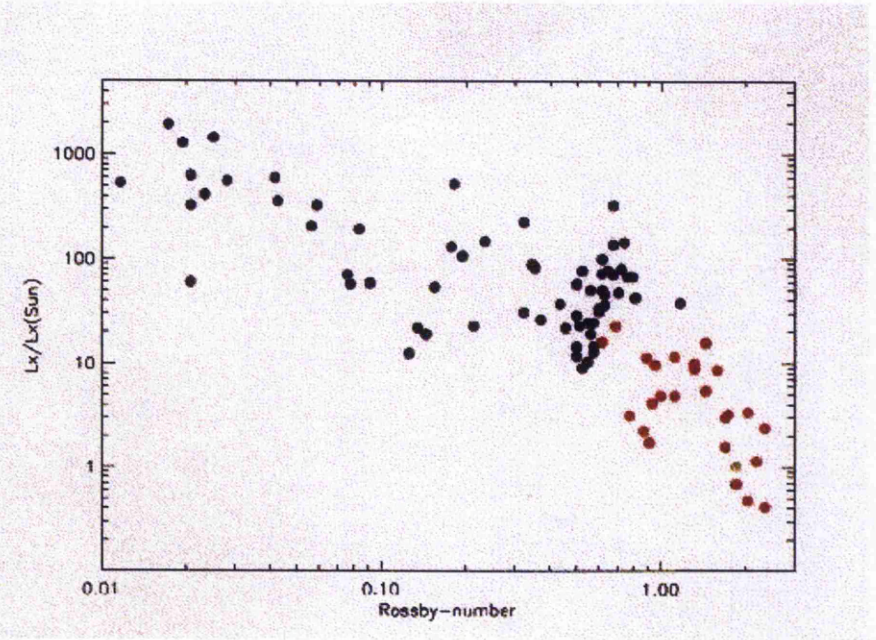

Figure 1.1: X-Ray luminosity is normalised to that of the Sun. The Rossby number gives rotation period in units of the eddy's lifetime. The position of the Sun is shown on the lower right.

fluid. Late-type stars (spectral types F to M) are observed to display all the usual measures of magnetic activity that are found in the solar atmosphere but are generally found to be 'scaled up' because their more efficient rotation dependent dynamos will generate a larger-scale magnetic field with a total flux that is systematically higher at a higher rotation rate. The magnetic field couples the sub-photospheric convection zone with the stellar chromosphere and corona allowing convective turbulent kinetic energy to be converted into excess magnetic energy which may then be dissipated, thereby allowing the maintenance of a hot stellar wind which acts as a 'brake' on the stellar rotation (for further details of angular momentum loss studies, see Collier Cameron et al. (1991) and Mestel

& Spruit (1987)). This leads to a subsequent decrease in the dynamo maintained flux and the coronal magnetic activity that is observed in the optical through to the X-ray spectrum bands (see figure (1.1)). The indicators of magnetic activity that have been found to be 'scaled-up' with respect to their properties in the solar atmosphere, include that of stellar emission measure, flares, prominences, starspot coverage and the dimensionless Rossby number, σ.

(i) Rossby number. The Rossby number, σ, is given by $\sigma = P/\tau$, where P is the rotational period and τ gives the convective turnover time at the base of the stars convective envelope (τ is may be computed by a number of different methods, e.g., Ventura et al. (1998)). A number of papers produced in the 1980's (e.g., Noyes et al. , 1984, Pallavicini et al. , 1981) demonstrated that with increasing Rossby number, the X-ray luminosity is observed to decrease in accordance with the simple dynamo/wind-braking picture outlined above. It is clear therefore that rotation of a star is a very important parameter influencing the magnetic activity of a stellar atmosphere. Furthermore, it follows that the considerably more intense magnetic activity observed in younger, less-evolved stars (with respect to that which is observed on the older, more evolved Sun) is related to the more rapid rotation of these stars. Whereas the Sun rotates once every 26 days (at the equator), some clusters of late-type stars have been observed to rotate at speeds up to around 180 times faster than the Sun. These rapid rotators will generally lose their angular momentum to their stellar winds as the stars evolve through the so-called "braking mechanism" (reviews of the relations between stellar magnetic dynamo characteristics,

rotation and coronal properties and observations are given in Saar (2001), Rosner et al. (1985), Moss & Smith (1981) and Schrijver & Zwaan (2000)).

The importance of the key role played by rotation in influencing the magnetic activity of stars is also supported by observations from RS CVn stars which are evolved stars in close binary systems that remain active with increasing age despite being subject to the same braking process outlined above because there is an additional angular momentum source in the orbital motion of the components of the system (details of this process are discussed in Mestel (1999) and Campbell (1997)).

(ii) Flares. In the case of flares, a number of very large events have been observed in recent years on a wide variety of stellar types and which have demonstrated peak luminosities comparable with the stellar bolometric luminosity (see Favata et al. , 2001) and may have have energies up to orders of magnitude larger than solar flares. Similarly, blue spectral shifts of up to 80 $\mathrm{km}s^{-1}$ have been observed, as opposed to about $10\mathrm{km}s^{-1}$ in solar flares so that in some cases (e.g. Houdebine et al. , 1993), it is the kinetic energy of the mass motions which dominates the flare energy budget. These flares are however, broadly similar to solar flares, in that some have been hydrodynamically modelled in a similar manner to solar compact flares whereas in other cases they have been modelled using reconnection, as solar-type two ribbon white-light flares (a review of these flare models is given in Reale (2001)).

(iii) Prominences. Both active and quiescent prominences or "coronal condensations"

of HI have also been widely observed over the last few years, transitting the stellar disc and scattering chromospheric Hα photons. These condensations are similar to solar prominences in that they consist of dense, relatively cool material embedded in the hot ambient medium of the stellar corona and in that they appear to be confined by strong coronal fields and insulated by a relatively poor cross-field thermal conductivity. However, the comparison is a rather loose one even though there are broad similarities. The masses deposited in these condensations are again 2-3 orders of magnitude larger (i.e., around the order of 10^{17}g) than is found in the solar quiescent prominences. One of the significant differences between these condensations and their solar analogues is their distribution at different distances from the star, e.g., the well observed young, rapidly rotating (its period is around 12.3 hours) K0 dwarf, AB Doradus (shown in figure (1.2) in X-rays) has a number of condensations at any given time, at cylindrical radii ranging from 2 to 8 $R_\star$ but the most favoured site for their formation is just inside the Keplerian corotation surface where the clouds are in enforced corotation with the star. The equatorial corotation radius, r_c, is defined as the radius at which the orbital period of a test particle in a circular orbit is equal to the star's axial rotation period, i.e., where the centrifugal and gravitational forces acting on a plasma are found to be in balance,

$$r_c = \left(\frac{GM_\star}{\Omega^2}\right)^{\frac{1}{3}} \tag{1.1}$$

where G is the gravitational constant, $M_\star$ is the stellar mass and Ω is the star's rotational angular velocity.

(iv) Starspots. Another indicator of stellar magnetic activity is that of starspot cov-

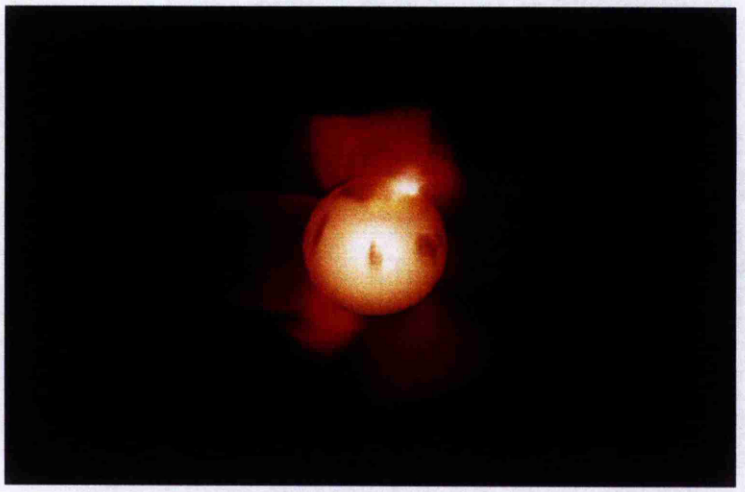

Figure 1.2: The X-ray emission from the high temperature plasma trapped in the closed field line regions of the corona of AB Doradus. Courtesy of M. Jardine

erage. Mapping of these starspots and their distributions are used as tracers of stellar differential rotation, dynamo activity and magnetic polarity patterns in a similar manner to the way in which coronal condensations are often used as tracers of complex coronal field topology and of the radial and longitudinal extent of the closed field corona (see Collier Cameron et al. , 2001). Approximately 0.1% of the quiescent solar surface is covered by spots which is in sharp contrast to the fact that many younger, active stars that may show filling factors of up to 70%. Furthermore, starspots have been well-observed from Doppler images (see Strassmeier & Rice , 1998) at both low and high latitudes especially (and of particular interest) at the stellar poles. The activity of these spots is also more vigorous than of those observed on the Sun, e.g., in RS CVn binaries, starspots can modulate the received flux from the star by a tenth of a magnitude as the star rotates.

1.1.2 Saturation and supersaturation of emission

The last indicator of magnetic activity to discuss is that of emission from stellar chromspheres, transition regions and coronae, principally in the EUV and X-ray bands. All the indicators of magnetic activity that we have discussed, have shown some form of 'saturation' or 'super-saturation' as the rotation rate increases for a given spectral type (e.g. Noyes et al. (1984), Vilhu & Walter (1987) and Hempelmann et al. (1995)). The most well known form of saturation is that seen in the coronal emission where the X-ray emission is observed not to simply increase with rotation as might be expected from a star that generates magnetic flux from a simple dynamo of the form $B \propto \Omega^q$ (with some scaling q) so that the stronger closed magnetic field lines would confine a more dense, emitting plasma. Instead the emission is observed (Stauffer et al. , 1997) to show an increase with rotation rate which then flattens off at higher rotation rates. More recently it has been shown that there is even a supersaturation effect whereby the emission initially increases with rotation but then starts to flatten slightly before showing a decrease, as shown in figure (1.3) for a sample of G-K and M dwarfs studied by James et al. (2000) and also demonstrated by Prosser et al. (1996) and Randich (1998). The saturation in emission is also seen in other parts of the spectrum. Onset of saturation is observed at roughly $vsini = 15kms^{-1}$ or rotation periods of around 3 days for coronal X-ray emission whereas for chromospheric and transition region emission the saturation is at periods of around $log\left(\frac{P}{\tau}\right) < -1$ (Doyle , 1996) or around 2 days for solar-type stars with the EUV emission saturating at slightly longer periods of around $log\left(\frac{P}{\tau}\right) < -0.6$ (Mathioudakis et al. , 1985). For starspots the saturation in coverage is observed only at

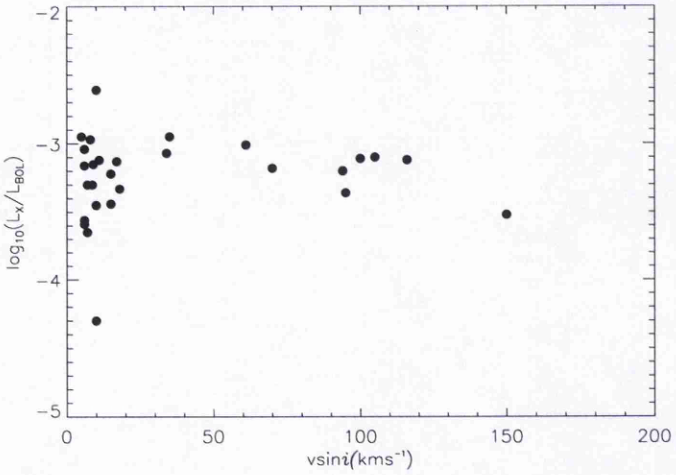

Figure 1.3: X-Ray luminosity, as a fraction of bolometric luminosity plotted against projected equatorial velocity for G-K dwarfs (Alpha Persei and IC 2391/2602 clusters and M-dwarfs (black circles from James et al. (2000))

periods of $P < 0.5$ days (O'Dell et al. , 1995).

The causes of these different forms of saturation have been extensively discussed in the literature since the observations were first reported and a number of possible explanations are often advanced.

(i) Dynamo saturation. Some form of saturation of the dynamo mechanism which arises from nonlinear interactions that take into account the back-reaction of the magnetic field on the fluid motions was initially invoked (in terms of classical mean field dynamo theory) as an explanation (see Krishnamurthi et al. , 1997, Charbonneau & MacGregor , 1992) that explained the presence of rapid rotators in the main-sequence of young clusters. A more extended discussion and background to alternative dynamo approaches to

the magnetic activity saturation problem is given by Rosner (2000).

(ii) Coriolis force deflection of flux tubes. In the work of Solanki et al. (1997), it is suggested that the concentration of magnetic flux near the poles of rapid rotators could provide an alternative explanation whereby the effect of Coriolis forces on the latitude of emergence of magnetic flux through the stellar surface achieves the same effect. This is because magnetic flux tubes rising buoyantly from the convective region through to the stellar surface will be deflected by Coriolis forces to higher latitudes and so if these flux tubes become open, they will exert a reduced braking torque compared to more low latitude flux tubes. Together with the results of O'Dell et al. (1995) this offers an argument against dynamo saturation at low rotation rates.

(iii) Emission region displacement. As stars rotate more rapidly, the proportion of the stellar surface that emits in X-rays begins to approach unity. Given that solar observations seem to show that X-ray and similar activity-related emission in the active regions comes primarily from those regions that surround the sunspots (Vaiana & Rosner , 1978), it may be the case that as an increasing fraction of the stellar surface is taken up with spots (as rotation is increased), the fraction of the surface from which the emission originates may decrease.

(iv) Saturation of the heating mechanism. This may occur either because the driving motions are being suppressed by the stronger fields or because the maximum available

power for the heating has already been fully exploited. There may also be a saturation in the total absolute magnetic flux because of increased flux cancellation rates between opposite polarities with increasing activity. Very active magnetic field production could conceivably lead to complex interactions between *in situ* field structures, which in turn lead to changing topologies of the magnetic field that may lead to declining X-ray emission. However, these suggestions are highly speculative and it has not been possible for further investigation of these ideas to date.

(v) Centrifugal stripping. Finally, Jardine & Unruh (1999) suggested that the X-ray emitting coronal volume of rapid rotators can be reduced by a process of centrifugal stripping which causes a rise in the pressure and density in the outer parts of the largest magnetic loops as the rotation rate (and therefore the centrifugal forces) increase. Such stresses may cause previously closed field lines to break open (as originally suggested by Mestel & Spruit (1987)) and destroy the X-ray emitting regions, if the centrifugal forces are sufficient to overcome the magnetic forces that confine the plasma and thereby reduce the extent of the closed corona. In these models it is the corotation radius that marks the heights at which the centrifugal stressing of the field begins and which are more susceptible to the onset of radiative instabilities due to the increased plasma density in those parts of the corona where many prominences are found to be situated. This allowed the authors to reproduce the observed saturation and show that centrifugal stripping may mimic dynamo saturation or disguise the rotation rate at which saturation sets in.

1.1.3 Planetary magnetospheres

Another major class of astrophysical bodies which possess an extended, active rotating magnetosphere is that of planets. Clearly solar planetary systems (particularly that of the Earth) have been more extensively subjected to observation than the magnetospheres of neutron stars or active galactic nuclei. There are a number of very broad similarities between stellar and planetary magnetospheric systems which might allow us to consider some aspects of these systems in a similar manner (see Kennel & Coronti (1977), Bagenal (1992) and Stern & Ness (1982) for comprehensive reviews of observations and models of these planetary systems). In Neukirch (1993a) a simple model of the deformation of an axisymmetric magnetic dipole field by trapped particles is considered. This model is based on the widely used parallel rotator model where the planetary rotation and magnetic field axes are aligned and the quasi-neutral magnetospheric plasma is held in corotation with the planet. It was found that there was always a maximum amount of plasma that could be confined in the magnetosphere by the field if the plasma density was used as a control parameter. These models may therefore act as a motivation for our work in modelling the behaviour of the emission from stellar magentospheres in prompting us to consider whether or not the observed saturation in magnetic activity with rotation from these systems is due to one (or a combination of) the five effects outlined above or due to some form of stellar analogue of the results found by Neukirch (1993a). However, whilst this the parallel rotator model is generally valid for considering magnetospheres such as those of the Earth and Jupiter, there are notable exceptions in the form of the gas giants Uranus and Neptune where their is evidence of oblique and off-axis dipole-like fields.

1.2 Kinetic theory

A full theoretical description of a magnetised rotating plasma system requires the solution of all of the equations of motion of all of the plasma particles together with the solution of Maxwell's equations. Such an approach could not be practically realised and it is therefore necessary to adopt an approximation that will be both physically relevant and computationally expedient. A full account of the hierarchy of the different plasma descriptions, their full derivations, applications in different physical environments and of the different forms of these descriptions, may be found in a number of standard texts (e.g Krall & Trivelpiece (1973) and Sturrock (1994)). In kinetic theory the thermal motion of the electrons and ions is accounted for by the introduction of a distribution function $f_s(\mathbf{x}, \mathbf{v}, t)$ defined on a six-dimensional phase space (with seven independent variables) for each particle species, s, present in an element of plasma with volume x_1 to $x_1 + dx_1$, x_2 to $x_2 + dx_2$, x_3 to $x_3 + dx_3$ and with velocities v_1 to $v_1 + dv_1$, v_2 to $v_2 + dv_2$ and v_3 to $v_3 + dv_3$

$$\begin{aligned} d^6N &= f(\mathbf{x}, \mathbf{v}, t) dx_1 dx_2 dx_3 dv_1 dv_2 dv_3 \\ &= f(\mathbf{x}, \mathbf{v}, t) d^3\mathbf{r} d^3v. \end{aligned} \tag{1.2}$$

This is under the condition that the spatial and velocity gradients (characterised by some dimension Δx and Δv respectively) are not too large, i.e.

$$f(\Delta x)^3 (\Delta v)^3 >> 1 \tag{1.3}$$

If f is normalised so that

$$\int_{-\infty}^{\infty} \hat{f}\,(\mathbf{x},\mathbf{v},t)\,d^3r d^3v = 1 \tag{1.4}$$

where $f(\mathbf{x},\mathbf{v},t) = N\hat{f}(\mathbf{x},\mathbf{v},t))$, then the distribution function $\hat{f}$ may be thought of as representing the probability of finding a particle in a specified element of the phase space and may then be used to average over that space to describe the following bulk plasma quantities (in the following discussion we will drop the hat-notation):

- particle density

$$n(\mathbf{x},t) = \int d^3v f(\mathbf{x},\mathbf{v},t)$$

- average velocity or particle flux

$$< \mathbf{v} > (\mathbf{x},t) = n^{-1} \int d^3v f(\mathbf{x},\mathbf{v},t)\mathbf{v}$$

- pressure tensor

$$< \underline{\underline{\mathrm{p}}} > (\mathbf{x},\mathbf{v},t) = m \int (\mathbf{v} - < \mathbf{v} >) : (\mathbf{v} - < \mathbf{v} >) f d^3v$$

- current density

$$\mathbf{j} = \sum_s q_s \int d^3v f_s(\mathbf{x},\mathbf{v},t)\mathbf{v} = \sum_s q_s n_s(\mathbf{x},\mathbf{v},t) < \mathbf{v} >_s$$

- charge density

$$\rho = \sum_s q_s \int d^3v f_s(\mathbf{x},\mathbf{v},t) = \sum_s q_s n_s(\mathbf{x},\mathbf{v},t)$$

for electric charges q_s. Furthermore, it is assumed that the domain has an overall neutral electric charge , i.e. $\int \rho d^3r = 0$.

In the non-relativistic limit (where $v << c$ for the speed of light c) the equation of motion of a given particle species may be written in terms of an acceleration vector field,

$$\mathbf{a}(\mathbf{x}, \mathbf{v}, t) \equiv \frac{d\mathbf{v}}{dt} = \frac{q_s}{m_s}\mathbf{E} + \frac{q_s}{m_s}\mathbf{v} \times \mathbf{B} \tag{1.10}$$

for an electric field E and magnetic field B. The magnetic induction $\boldsymbol{B}$ is not distinguished from the magnetic field $\mathbf{H} = \mathbf{B}/\mu$ in order to remain consistency with the literature. Choice of a normalisable distribution function, where the total number of particles, N, in the domain, Ω, is constrained to remain finite

$$\int_\Omega n(\mathbf{x}, \mathbf{v}, t) d^3r = \int f(\mathbf{x}, \mathbf{v}, t) d^3r d^3v = N$$

then allows the equation of motion for a non-relativistic collisionless plasma (where the time between collisions is considerably greater than the dynamical time scales of the system) to be rewritten as

$$\frac{df_s}{dt} = \frac{\partial f_s}{\partial t} + \mathbf{v} \cdot \nabla_r f_s + \frac{q_s}{m_s}(\mathbf{E} + \mathbf{v} \times \mathbf{B}) \cdot \nabla_v f_s = 0 \tag{1.12}$$

where ∇_r represents the spatial gradient and ∇_v gives the velocity space gradient. Equation (1.12) is known as either the *collisionless Boltzmann equation* or as the *Vlasov equation.* The description of the plasma is now completed by considering the Vlasov equations together with the phase space averaged Maxwell's equations

$$\nabla \cdot \mathbf{E} = \frac{1}{\varepsilon_0}\rho \tag{1.13}$$

$$\nabla \times \mathbf{B} = \mu_o \mathbf{J} + \frac{1}{c^2}\frac{\partial \mathbf{E}}{\partial t} \tag{1.14}$$

$$\nabla \cdot \mathbf{B} = 0 \tag{1.15}$$

$$\nabla \times \mathbf{E} = -\frac{\partial \mathbf{B}}{\partial t} \tag{1.16}$$

where μ_o is the magnetic permeability and ε_0 is the permittivity of free space. Equation (1.13) is Poisson's equation and implies the generation of electric fields by spatial distributions of electric charge, equation (1.14) is Ampère's law and implies that magnetic fields may be produced by currents. In Ampére's law the second right hand term gives the displacement current. Equation (1.15) is the solenoidal condition or Gauss's law and reflects the fact that no magnetic monopoles have been found to date. Equation (1.16) is Faraday's law and implies that time-varying magnetic fields may give rise to electric fields.

The Vlasov approximation therefore allows the description of collisionless plasmas with an appropriate distribution function for each particle species satisfying equations (1.12) to (1.16). This approach has been successfully applied to the geomagnetic tail, to the solar wind, to the solar corona and has also found galactic and extra-galactic applications.

1.3 The MHD approximation

The bulk of this thesis work is carried out within the framework of the single-fluid approximation of magnetohydrodynamics (hereafter abbreviated to MHD) wherein the density and velocity of ions and electrons are combined such that the variables of the

fluid (total density, electric current, charge-density and centre-of-mass velocity) may be readily obtained. The fluid is an electrically conducting medium threaded with magnetic field lines which may arise from being applied externally, from the current flow or from some combination of the two. The MHD formalism is established from a number of assumptions which limit the range and domain of applicability to physical systems. However, the formalism is internally self-consistent and has been very successfully applied to a wide-range of laboratory and astrophysical plasmas. The single fluid approximation rests on the condition that the plasma is collisionally dominated and that the distribution functions of the plasma particle species are locally Maxwellian. If a uniform magnetic field is applied to a plasma then a charged plasma particle will rotate with a helical trajectory perpendicular to the field at the *gyro-frequency*

$$\omega_c = \frac{qB}{m} \tag{1.17}$$

where q, B and m are the particle charge, the magnetic field and particle mass respectively. The radius of rotation is the *Larmor radius* or *gyro radius*

$$a_L = \frac{v_\perp}{\omega_c} \tag{1.18}$$

and where $v_\perp$ is the perpendicular component of the particle velocity. The orbiting particles drift freely along the field line until they undergo a Coulomb collision with another particle. For the collisonally dominated single-fluid MHD approximation to be valid, it is required that the MHD length scale ℓ, be large compared to the mean free path

$$\ell_m = \frac{1}{n\sigma} \tag{1.19}$$

(with collision cross-section σ) between collisions and large with respect to the *Debye length*,

$$\lambda_D = \left(\frac{\varepsilon_0 k_B T}{2nq^2}\right)^{\frac{1}{2}} \tag{1.20}$$

where n is the electronic or ionic density (in cm^{-3}), T is the temperature (in Kelvin) and k_B is Boltzmann's constant and ε_0 is the permittivity of free space. The Debye length is the scale beyond which the potential of a test charge in the plasma is exponentially attenuated below its vacuum value and any particles within this sphere are considered to be in collision. If slow moving plasma elements of size $\ell >> \lambda_D$ are considered then the plasma may be assumed to be globally quasi-neutral. i.e., $N_+ - N_- << n$, where N_+ and N_- are the number of positive and negative ions respectively and where $n = n_+ + n_-$ is the total number of ions present in the plasma. Ionised fluids for which $\ell >> \lambda_D$ are considered to be a plasma. In the case of solar and stellar coronae these plasmas are usually fully ionised. Furthermore, the scale length ℓ must be much greater than the Larmor radius a_L, to allow the electron diamagnetic and Hall effect terms to be neglected from the electron momentum equation. The electron inertia may then be incorporated into the ion momentum equation to yield a single-fluid momentum equation. Whenever local charge concentrations arise in (or external potentials are introduced into) the system, these potentials will be shielded out in a distance short compared with ℓ thereby leaving the bulk of the plasma free of large electric potentials or fields. The large scale dynamics of the plasma are therefore influenced chiefly by the magnetic field.

A concomitant condition to that of the length scale is that of the MHD time scale which allows the displacement current term in equation (1.14) to be neglected by considering

the restriction of the formalism to the non-relativistic limit. The acoustic speed ($c_s = \gamma p/\rho$, for a ratio of specific heats at constant pressure and volume $\gamma = c_p/c_v$), Alfvén speed ($v_A = B/\sqrt{\mu\rho}$) and rotational velocity of the plasma are all much less than that of the speed of light, c, allowing a sufficient number of collisions between plasma particle species for the plasma to be considered to be collisionally dominated. The collisions are assumed to be sufficiently frequent as to keep the system isotropic at all times and allowing the gradient terms to be small with respect to the field terms. The assumption of an isotropic pressure gradient follows from the stipulation that (together with quasi-neutrality) the charged particle species have identical temperatures and therefore possess identical pressures. This assumption would neglect viscosity effects and would require the energy equilibrium time to be short compared to the characteristic MHD timescale t, i.e.

$$\left(\frac{m_i}{m_e}\right)^{\frac{1}{2}} \frac{v_{Ti}\tau_{ii}}{\ell} << 1 \tag{1.21}$$

where m_i and m_e are the ion and electron masses respectively, where v_{Ti} is the ion thermal speed and where τ_{ii} is the collision time between ions. A final assumption is that the values of magnetic permeability, μ, and electric permittivity ε, are equal to their values *in vacuo*. Together with equations (1.13) to (1.16) the final form of the MHD equations that we will be using is as follows

$$\frac{\partial \rho}{\partial t} + \nabla \cdot (\rho \mathbf{v}) = 0 \tag{1.22}$$

$$\rho(\frac{\partial \mathbf{v}}{\partial t} + (\mathbf{v} \cdot \nabla)\mathbf{v}) = -\nabla p + \mathbf{J} \times \mathbf{B} + \rho \nabla \psi + \rho \nu \nabla^2 \mathbf{v} \tag{1.23}$$

$$\frac{\rho^\gamma}{\gamma - 1} \frac{D}{Dt}\left(\frac{p}{\rho^\gamma}\right) = -L \tag{1.24}$$

$$\mathbf{E} + \mathbf{v} \times \mathbf{B} = \eta \mathbf{J} \tag{1.25}$$

$$p = \frac{k_B}{m} \rho T \tag{1.26}$$

Equation (1.22) describes mass continuity or conservation of mass at all points of the fluid where the quantities are continuous functions of position to the effect that there are no mass sources or sinks. The equation of momentum conservation in the plasma (or the fluid inertia, also known as the equation of motion) is described by equation (1.23) and is the equation that will be of most interest and study in this work as it couples the fluid to the fields. The Lorentz force $\mathbf{J} \times \mathbf{B}$, plasma pressure gradients, gravitational force (for a gravitational potential ψ) and viscous forces (for a constant coefficient of an isotropic kinematic viscosity ν with an incompressible flow $\nabla \cdot \mathbf{v} = 0$, where the density is not affected by pressure changes in the fluid see Braginskii (1965), Spitzer (1962)) are in balance in accordance with Newton's second law of motion when the plasma system is in a state of equilibrium. It is the Lorentz force which couples the fluid equations to the electromagnetic equations and combines the magnetic tension force, $\frac{1}{\mu_o}(\mathbf{B} \cdot \nabla)\mathbf{B}$ and magnetic pressure force, $-\nabla \left(\frac{B^2}{2\mu_o} \right)$ (for a magnetic field strength $B = \mid \mathbf{B} \mid$), of the field lines. The equation of energy conservation of the plasma is given by equation (1.24) with a convective time derivative

$$\frac{D}{Dt} = \frac{\partial}{\partial t} + \mathbf{v} \cdot \nabla \tag{1.27}$$

describing the time derivative following the motion of the fluid. The energy loss function, L, specifies the net effect of all sources and sinks of energy such as heat flux, radiative losses, Ohmic heating and other terms which must sum to zero in the case of the adi-

abatic equation of state. The resistive Ohm's law is given by equation (1.25) with the scalar plasma electrical resistivity η and is given in its most simple form (an extended discussion of the different forms which this may take, is given in Spitzer (1962)). The assumption that our plasma particles are in non-relativistical motion, implies that both the current density and the magnetic field are related to the total electric field in a frame of reference that moves with the plasma. Finally, it is necessary to specify an equation of state (equation (1.26)) to close the set of equations by relating the plasma pressure to the plasma density. In this case, the most simple choice is that of the perfect gas law. It is worth noting that there are a number of different forms of MHD which may be distinguished from each other by the different approximations and limits that may be made. In particular it is ideal MHD which will be used in this work as it leads to more simple and tractable problems without significantly impairing the applicability of the results to real astrophysical systems.

Combining equations (1.14) and (1.16) with Ohm's law (equation (1.25)) and applying some simple vector algebra allows us to write the induction equation

$$\frac{\partial \mathbf{B}}{\partial t} = \nabla \times (\mathbf{v} \times \mathbf{B}) + \eta \nabla^2 \mathbf{B} \tag{1.28}$$

where $\eta = 1/\mu_o \sigma$ is the magnetic diffusivity. The first term on the right-hand side represents the advection of magnetic field lines whilst the second term represents their diffusion. To measure the relative importance of these terms we take their ratio which then gives the dimensionless magnetic Reynold's number, $R_m = vL/\eta$, for some typical length scale L and some typical plasma speed, v. In the case of most astrophysical plasmas (particularly stellar coronae), the length scales are large so that the time scale, $\tau_d = l_o^2/\eta$,

is long and therefore the diffusion of the plasma may be neglected. An exception to this is in the case of some small regions where the magnetic field gradients may become large and it may be necessary to account for dissipative effects such as current sheets, which is important for the study of a wide range of phenomena, e.g flares, planetary magnetotails, heating of stellar coronae etc. Equation (1.28) now becomes

$$\frac{\partial \mathbf{B}}{\partial t} = \nabla \times (\mathbf{v} \times \mathbf{B}) \tag{1.29}$$

in the ideal MHD or perfectly conducting limit ($\sigma \rightarrow \infty$) in which the plasma behaves as if it is frozen into the field according to Alfvén's frozen-in-flux theorem (see Alfvén (1950) and standard works on MHD, e.g. Roberts (1967), Parker (1979)). If one were to consider a closed loop C of surface area S in the fluid, then the magnetic field that the loop encompasses would have a magnetic flux ϕ linking the loop, $\phi = \int_s \mathbf{B} \cdot d\mathbf{S}$. The theorem holds that if the loop moves with the fluid then the flux ϕ is conserved and so fluid elements that are initially located on the same field line will remain so and are therefore 'frozen' into the field. Ohm's law may then be rewritten as the ideal Ohm's law

$$\mathbf{E}' = \mathbf{E} + \mathbf{v} \times \mathbf{B} = \mathbf{0} \tag{1.30}$$

so that there is no electric field, $\mathbf{E}'$, in the rest frame of the fluid due to the high conductivity of the fluid. This is equivalent to stating that the reference frame of the magnetic field is the reference frame in which the electric field is zero. An alternative consideration of equation (1.25) is that for the plasma to be sufficiently collisional to be considered to be a single fluid and yet sufficiently collisionless for the resistivity to be neglected or in the case where the length scale ℓ is large such that the resistive diffusion time $\eta/\ell^2 << t$

then

$$\left(\frac{m_e}{m_i}\right)^{\frac{1}{2}} \frac{a_L^2}{\ell v_{Ti}\tau_{ii}} << 1 \tag{1.31}$$

which then leads to equation (1.30).

1.4 Magnetohydrostatic equilibria

In stellar coronae, a number of different physical phenomena are observed to occur over different timescales e.g., quiescent solar prominences have been observed to last for several months although their eventual eruption may occur over a course of minutes. However, in many coronal structures the evolution timescale is considerably longer than the Alfvén crossing time $T_A = \ell/v_A$ (for an Alfvén speed $v_A = B_0/\sqrt{\mu_0\rho_0}$) during quiet phases of activity). This allows us to assume that the plasma system evolves through a series of equilibrium states quasi-statically and thence to model the slow evolution of the plasma system. The fundamental assumption is that

$$\frac{T_A}{t_0} = \frac{v_0}{v_A} = \varepsilon << 1 \tag{1.32}$$

and so for small ε we may expand the MHD equations to obtain the lowest order form of the MHD equations in ε. Additional to the quasi-static approximation is the restriction that we do not consider flows i.e., $\mathbf{v} = 0$. Equilibria with flows ($\mathbf{v} \neq 0$) tend not to be as stable to small perturbations as stationary equilibria. This is due to the fact that additional kinetic energy from the flows may be tapped by instabilities. The solution of ideal magnetohydrostatic (MHS) equilibria of the MHD equations (for which $\mathbf{v} = \mathbf{0}$

and $\partial/\partial t = 0$) gives the stationary states of the plasma system. Time appears in the MHS equations now as a parameter and it now follows that in this formulation, the MHS equations become

$$\begin{aligned} \mathbf{J} \times \mathbf{B} - \nabla p - \rho \nabla \psi &= \mathbf{0} \\ \nabla \times \mathbf{B} &= \mu_0 \mathbf{J} \\ \nabla \cdot \mathbf{B} &= 0 \end{aligned} \tag{1.33}$$

together with an equation of state, such as one of the form given by equation (1.26). This is a highly nonlinear system of partial differential equations, the solution of which poses a formidable problem. In the energy equation (1.24) the energy loss function, L vanishes and this equation is no longer used for the purpose of our models. The electric field, E also vanishes and Faraday's law

$$\nabla \times \mathbf{E} = \mathbf{0} \quad \Longrightarrow \quad \mathbf{E} = \nabla \Phi \tag{1.34}$$

may be written in terms of a scalar potential Φ. However, Ampère's law (equation (1.14)) with no displacement currents) remains unchanged and the continuity equation (1.22) is automatically satisfied. The momentum conservation equation has now become a force-balance equation and is the fundamental equation that we consider. Finally, it should be noted that equilibrium sequences must satisfy the constraints imposed by the other equations. However, given that our interest is in rotating, magnetized plasma systems, it is clear that the static assumption $\mathbf{v} = \mathbf{0}$ does not hold and so we are not considering MHS equilibria in its strictest sense. This will become more apparent from the following discussion of the isorotation theorem where the effect of steady rotation is to introduce

an additional centrifugal force term to the force-balance equation. Whilst recent work (Fleck , 1997) has shown that in the case of the solar atmosphere, plasma flow is relatively common (and there is a body of work available for the consideration of equilibria with flows, e.g. Chandrasekhar (1961)) the inclusion of such flows would be beyond the scope of this work.

1.5 Model magnetospheres

In order to address the question of modelling the emission and structure of rapidly rotating magnetospheric systems it is necessary to impose restrictions that will allow us to recover mathematically tractable and pliant equations without loss of physical credibility. The work of this thesis has been motivated by results and calculations from both stellar and planetary magnetospheric physics. In the stellar case, part of the motivation for this work arises from observations of young F-M spectral type dwarfs which have exhibited a saturation of their coronal X-ray emission over a range of rotational velocities (in the case of M-dwarfs there has also been a suggestion of a supersaturation of emission with rotation, see for example, Randich (1998), Hempelmann et al. (1995), James et al. (2000)). It is reasonable therefore, to consider some of the more basic aspects of these stellar coronae. Firstly, the data is taken principally for single stars. Given that binary star systems are as common as single star systems it would also be desirable to undertake an investigation of the magnetospheric structure and behaviour of these systems. However, to undertake an investigation of binary star system magnetospheres would neither be

straightforward nor would it be appropriate at this stage of the development of the models. Therefore we choose not to consider the magnetospheres of these systems in this work (this choice is mitigated by the observation that, in the case of M-dwarfs, the authors of James et al. (2000) believe that there is little difference in the X-ray behaviour between single and binary star systems). Our intention is to proceed from the simplest, physically plausible model and then work to refine these models. This does not mean to say that there is no research conducted on the subject of MHD in binary systems (e.g. Ferreira (1998) and the comprehensive review of the subject Campbell (1997)), however much of the work is related to questions of viscosity in discs which we do not consider within an ideal MHS framework. The simplest point from which to proceed constructing stellar coronal models is to firstly assume that the background magnetic field is that of a simple dipole, that is aligned with and parallel to the rotation axis of the star. It should be noted, however that in studies of the conditions for stable centrifugal support of sheet-like prominences in rapidly rotating coronae (see Ferreira , 2000) it has been demonstrated that the coronal magnetic field must exhibit a complex multipolar topology at distances of two or more stellar radii above the photosphere if the clouds are to be stably supported at the locations they have been seen to occupy in well-observed stars such as the rapidly rotating star AB Doradus (e.g., Collier Cameron & Robinson , 1989).

In the case of the Sun, it has been known since Skylab that the X-ray bright regions have closed magnetic field lines and are therefore not carrying solar wind whereas the open field lines, (such as in coronal holes) are dark in X-rays. Given that we are attempting to model the coronae and the coronal emission of stars that are bright in X-rays, we

will choose to neglect treatment of the open field line regions and make the assumption that X-rays are only emitted from plasma that is trapped by closed-field lines. This has the additional advantage of absolving us from the problem of handling the more complicated question of incorporating stellar winds into our models, which should only be addressed once the more simple models have been investigated and refined. The poloidal component of the magnetic field would be important were we to include stellar winds in our models but as we have temporarily discarded this consideration, we may also neglect consideration of the poloidal flows and so we confine our attention to the X-ray emitting closed field line regions of the surface. The above argument is the basis for one of our principal model assumptions, that of axisymmetry wherein we only allow rotation around the symmetry axis and therefore all our gradients in the azimuthal direction may be neglected, i.e., $\frac{\partial}{\partial \phi} \rightarrow 0$ in our equations. The system is considered to be axisymmetric as long as it is not disturbed by non-axisymmetric forces. Neglecting the poloidal component of the flow field so that it is described purely by a toroidal component will give us a velocity at all points and is of the form

$$\mathbf{v} = v_\phi \mathbf{e}_\phi = \Omega r \sin\theta \mathbf{e}_\phi \tag{1.35}$$

where v_ϕ and Ω may be arbitrary functions of the coordinates r and θ, but not of the azimuthal coordinate ϕ because of rotational symmetry. At this point we should make clear what we mean by use of the term 'stellar surface.' Stellar physics does not share the luxury of the detailed observations of atmospheric structure that are available to solar physicists (in that they cannot be structurally resolved). A broader discussion of the difficulties of measuring the extent of stellar coronae and of taking coronal measurements in

general may be found in Schrijver & Zwaan (2000). Consequently, we are constrained to consider our surface as the base of the stellar corona, i.e. the height of the atmosphere above which there is significant X-ray emission (soft and hard) and where the temperatures significantly exceed photospheric and chromospheric temperatures. This definition will be of use for the necessary scaling and boundary considerations of our models.

1.5.1 The isorotation principle

The magnetic field is represented by

$$\mathbf{B} = \frac{1}{r \sin\theta}(\nabla A \times \mathbf{e}_\phi) + B_\phi \mathbf{e}_\phi \tag{1.36}$$

where the function A is a scalar function and such that the solenoidal condition, equation (1.15), is automatically satisfied and the natural coordinate system is that of spherical polars (r, θ, ϕ). The scalar function is also known as the flux function and measures the amount of magnetic flux between field lines. The directional derivative

$$\mathbf{B} \cdot \nabla A = 0 \tag{1.37}$$

implies that lines of constant A are magnetic field lines or equivalently, A is constant along magnetic field lines. The divergence-free constraint on the magnetic field lines may be re-written in terms of a magnetic vector potential, $\mathcal{A}$ such that

$$\mathbf{B} = \nabla \times \mathcal{A} \tag{1.38}$$

so that under the assumption of axisymmetry , the two functions $\mathcal{A}$ and A may be related using equations (1.36) and (1.38)

$$A = r \sin\theta \mathcal{A}_\phi \tag{1.39}$$

where $\mathcal{A}_\phi$ is the toroidal component of the magnetic vector potential.

Returning to consider Ohm's law (equation(1.30)) and substituting in the model forms of electric field (from equation (1.32)), plasma velocity (equation (1.35)) and magnetic field (equation (1.36)) allows it to be rewritten

$$\begin{aligned} -\nabla\phi + v_\phi e_\phi \times \left\{ \frac{1}{r\sin\theta} \nabla A \times \mathbf{e}_\phi + B_\phi \mathbf{e}_\phi \right\} &= 0 \\ \implies -\nabla\phi + \frac{v_\phi}{r\sin\theta} \nabla A &= 0 \end{aligned} \tag{1.40}$$

so that when the scalar product of this equation is taken with the magnetic field (from equation 1.36) we find that the electric field potential, ϕ, is constant along magnetic field lines.

$$\mathbf{B} \cdot \nabla\phi = 0 \quad \implies \quad \phi = \phi(A) \tag{1.41}$$

This property is shared by with the angular velocity, Ω, as may be seen by substitution of $\phi(A)$ into equation (1.40) and is known as Ferraro's theorem of isorotation

$$\begin{aligned} -\frac{d\phi}{dA}\nabla A + \frac{v_\phi}{r\sin\theta}\nabla A &= 0 \\ \implies \qquad \Omega = \Omega(A) &= \frac{d\phi}{dA} \end{aligned} \tag{1.42}$$

so that the angular velocity of the plasma is constant along a field line or equivalently, each field line may be considered to be labelled by a different value of A and to be rotating at a certain constant angular velocity, $\Omega(A)$. The principle advantage of incorporating

isorotation into the physical model is that the closed field lines will rotate at the same angular velocity as the angular velocity at the stellar surface where $\Omega(A) = \Omega_\star$ so that if $\Omega_\star$ is known then the angular velocity at all points along a field line is also known for every field line touching the surface at least once. Ferraro's isorotation theorem places significant restrictions on the angular velocity, Ω, for rigidly rotating bodies because $v_\phi = \Omega_\star r \sin\theta$ becomes very large for field lines that stretch very far out into the magnetosphere and so the centrifugal force may also become very large leading to accelerating plasma flowing outwards along field lines. In general, this may lead to the opening of field lines and the more complicated considerations of a stellar wind, however discussion of this question will be postponed until we discuss specific model details and their boundary conditions.

1.5.2 Rigid rotation

It is necessary to assume that the stellar plasma at the coronal base is held in rigid rotation because were this not to be the case then instead there would be differential rotation of the plasma (and consequently toroidal shearing of field line foot points). The rate of surface shear due to differential rotation on AB Doradus was determined by Donati & Collier Cameron (1997) to be very similar to that of the Sun in that significant shearing to the loop footpoints only occurred on timescales of weeks to months and they inferred that the coronal geometry evolved on timescales much faster than either surface differential rotation or than the growth and decay of small-scale magnetic field concen-

trations on the stellar surface. In the context of the timescales for calculating quasi-static MHS equilibria it is therefore quite acceptable for us to only consider rigid rotation of the surface. Other considerations are clearly not within the scope of the basic structure of our models as we do not attempt to consider differentiation of structure or distributions of angular velocity across the stellar surface which would entail a more involved consideration of photospheric processes and sub-photospheric dynamo processes. Instead, we simply consider the emission from the stellar surface to be integrated and homogeneous, i.e., undifferentiated by structures such as loops. Furthermore, it should be noted that a plasma system that is not rotationally symmetric will be time-dependent unless we transform our equations into a corotating frame of reference such that the azimuthal coordinate ϕ is replaced by

$$\phi' = \phi - \Omega t$$

and it may be readily verified that the MHS equations are satisfied in this frame of reference. In particular, when we have only toroidal flows then the left hand side of equation (1.23) becomes

$$\rho(\frac{\partial \mathbf{v}}{\partial t} + (\mathbf{v} \cdot \nabla)\mathbf{v}) = -\rho\nabla\left(\frac{1}{2}\Omega_\star^2 \sin^2\theta\right) \tag{1.44}$$

which is the centrifugal force arising from the rotation of the system. This is incorporated into the effective potential term of the force-balance equation in (1.33) as shown in the following discussion. Treating the stellar surface in this manner is comparable to treating the surface of the star as a large active region, the magnetic field of which would be approximately dipolar, which is consistent with our initial assumption for the magnetic field line configuration.

1.6 Mathematical formulation

Under the assumptions of our model, the MHD equations are all fulfilled and it only remains to discuss the continuity equation (equation (1.22)), and the equations of MHS (equations (1.34)). The continuity equation is automatically fulfilled because we are considering equilibria, $\frac{\partial \rho}{\partial t} = 0$ and because of the axisymmetry of the system then the second term also vanishes

$$\nabla \cdot (\rho \mathbf{v}) = \frac{1}{r \sin\theta} \frac{\partial}{\partial \phi} [\rho v_\phi] = 0 \tag{1.45}$$

The remaining equations to consider are those that give rise to the force-balance equation in the form of the *Grad-Shafranov equation.* As we cannot consider purely static equilibria for rotating bodies, we use the force-balance equation (1.23) with only the $\frac{\partial}{\partial t}$ term set to zero, rather than the MHS form. In MHS, there are many different symmetric solutions where the solutions are invariant in at least one coordinate direction because the force-balance equation reduces to a single elliptic differential equation, (the Grad-Shafranov equation). Similarly, there are many different classes of MHS solutions that are characterised by their different symmetry configurations and geometries so that our axisymmetric equilibria merely take the form of one of these classes. Indeed, it is possible to find a generalised Grad-Shafranov equation (Grad , 1960) which is elliptic for incompressible fluids where $\nabla \cdot \mathbf{v} = 0$ but when the flow is steady and compressible then the PDE changes between being an elliptic equation and being a hyperbolic equation, at certain points (Heinemann & Olbert , 1978). An extensive review of MHS equilibria may be found in Neukirch (1998).

1.6.1 The Grad-Shafranov equation

For a magnetic field of the form of (equation (1.36)), we can use the MHS equation for the current density (1.33) to rewrite it as

$$\mu_o \mathbf{J} = \frac{1}{r\sin\theta}\nabla\left[r\sin\theta B_\phi\right]\times\mathbf{e}_\phi - \frac{1}{r}\left[\frac{\partial}{\partial r}\left(\frac{1}{\sin\theta}\frac{\partial A}{\partial r}\right)+\frac{1}{r^2}\frac{\partial}{\partial\theta}\left(\frac{1}{\sin\theta}\frac{\partial A}{\partial\theta}\right)\right]\mathbf{e}_\phi \tag{1.46}$$

and if we adopt the abbreviated notation that $b_\phi := r\sin\theta B_\phi$ then the Lorentz force may be more conveniently written

$$\mathbf{J}\times\mathbf{B} = \frac{1}{\mu_o}\left\{-\frac{1}{r^2\sin^2\theta}\left(\nabla b_\phi\times\mathbf{e}_\phi\cdot\nabla A\right)\mathbf{e}_\phi \right.$$
$$\left. -\frac{1}{r^2\sin^2\theta}\left[\frac{\partial}{\partial r}\left(\frac{1}{\sin\theta}\frac{\partial A}{\partial r}\right)+\frac{1}{r^2}\frac{\partial}{\partial\theta}\left(\frac{1}{\sin\theta}\frac{\partial A}{\partial\theta}\right)\right]\nabla A - \frac{1}{r\sin\theta}B_\phi\nabla b_\phi\right\} \tag{1.47}$$

Considering the left hand side of equation (1.23) in terms of the radial and poloidal vector components (the first term on the left hand side is zero) then we may use the vector relation $(\mathbf{v}\cdot\nabla)\,\mathbf{v} = \nabla\left(\frac{\mathbf{v}\cdot\mathbf{v}}{2}\right) - \mathbf{v}\times(\nabla\times\mathbf{v})$ so that we have

$$\begin{aligned}\mathbf{v}\times(\nabla\times\mathbf{v}) &= 2\Omega_\star^2 r\sin\theta(\cos\theta\mathbf{e}_\theta+\sin\theta\mathbf{e}_\theta)\\ &= \nabla(\Omega_\star^2 r^2\sin^2\theta)\end{aligned} \tag{1.48}$$

It then follows that the full form of the velocity derivative term in equation (1.23) will appear in the force-balance equation as the centrifugal force resulting from the rotation of the system

$$-\rho(\mathbf{v}\cdot\nabla)\mathbf{v} = \rho\left[\nabla\left(\frac{1}{2}\Omega_\star^2 r^2\sin^2\theta\right)-\nabla\left(\Omega_\star^2 r^2\sin^2\theta\right)\right] \tag{1.49}$$

$$= -\rho\nabla\left(\frac{1}{2}\Omega_\star^2 r^2\sin^2\theta\right) \tag{1.50}$$

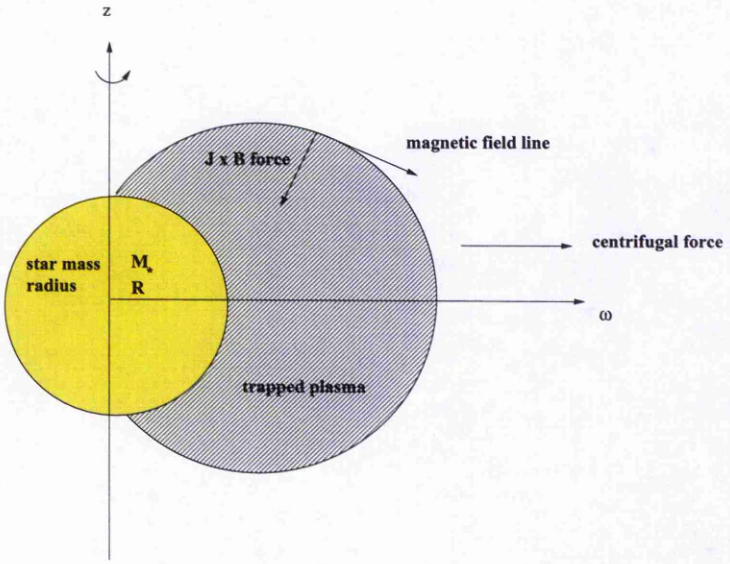

Figure 1.4: Schematic diagram of force balance on the trapped plasma, where gravity is directed inwards.

and may therefore be included together with the gravitational potential in a term representing the effective potential or effective gravity, U, in which the plasma moves. The force-balance equation then takes the following form

$$\mathbf{j} \times \mathbf{B} - \nabla p - \rho \nabla U = \mathbf{0} \tag{1.51}$$

where

$$U = \psi - \frac{1}{2}\Omega_\star^2 r^2 \sin^2\theta \tag{1.52}$$

for a gravitational potential $\psi = -GM_\star / r$. The balance of forces on plasma associated with a given field line and the geometry of these forces is illustrated in figure (1.4).

The Lorentz force only acts across the field so that plasma pressure gradients along the field are balanced by the combined gravitational and centrifugal effective potential gra-

dients for field lines that are in quasi-static equilibrium. Indeed Ferreira (1998) demonstrated that for the observed support of stellar filaments (e.g., Collier Cameron & Robinson , 1989) to be possible, the component of the effective gravity along the direction of the field line must vanish and give rise to a stable equilibrium. Inspection of the toroidal component of the above equation reveals that it is only the Lorentz force term (equation 1.47) that will have a non-vanishing ϕ component because the assumption of axisymmetry dictates that the other components must vanish, i.e. $\frac{\partial p}{\partial \phi} = 0$ and $\frac{\partial U}{\partial \phi} = 0$. We also find that

$$(\nabla A \times \nabla b_\phi) \cdot \mathbf{e}_\phi = 0 \tag{1.53}$$

and upon application of some simple vector algebra it follows that the first term from the Lorentz force expression must also vanish. An additional consequence of the assumption of axisymmetry is that of eliminating the toroidal field gradient term, $\frac{db_\phi}{d\phi} = 0$, which then allows the remaining component to be rewritten in the form of a directional derivative

$$\mathbf{B} \cdot \nabla b_\phi = 0 \tag{1.54}$$

in a similar manner to the earlier discussion of the flux function, A, (in equation 1.37) and the isorotation theorem (equation 1.42). The implication is that the b_ϕ form of the toroidal magnetic field is also dependent on the flux function

$$b_\phi = r \sin\theta B_\phi = b_\phi(A) \tag{1.55}$$

The last term in the expression for the Lorentz force may therefore be expressed in terms of a gradient of the flux function rather than that of the field

$$b_\phi \nabla b_\phi = b_\phi \frac{db_\phi}{dA} \nabla A \tag{1.56}$$

allowing the force balance equation to be written as a sum of gradient terms

$$-\nabla p - \rho\nabla U - \frac{1}{\mu_o r^2 \sin^2\theta}\left\{ b_\phi \frac{db_\phi}{dA} + \frac{\partial^2 A}{\partial r^2} + \frac{\sin\theta}{r^2}\frac{\partial}{\partial\theta}\left[\frac{1}{\sin\theta}\frac{\partial A}{\partial\theta}\right]\right\}\nabla A = 0 \qquad (1.57)$$

each of which will have only two components, namely those in the the radial and latitudinal (θ) directions. It follows that only two of these vector fields can be linearly independent and so we make the assumption that the ∇A and ∇U fields are linearly independent apart from sets of measure zero when the field $\mathbf{B}$ is perpendicular to the potential field, U. The latter configuration is clearly a special case and will not be considered in the more general outlook of this work. Given that the ∇A and ∇U fields are now generally considered to be linearly independent, it is useful to consider them as coordinates rather than the spherical polar quantities r and θ. We are now able to regard the plasma pressure p as a function of A and U, from which it follows that

$$\nabla p = \left.\frac{\partial p}{\partial A}\right|_U \nabla A + \left.\frac{\partial p}{\partial U}\right|_A \nabla U \qquad (1.58)$$

where the first term is held at a constant U and the second held at a constant A. Since we have linear independence of the fields ∇A and ∇U, it follows that the coefficients in the force balance equation (1.57) must now vanish to give us the final form of the equation that we wish to solve in terms of the flux function A

$$-\frac{\partial^2 A}{\partial r^2} - \frac{\sin\theta}{r^2}\frac{\partial}{\partial\theta}\left(\frac{1}{\sin\theta}\frac{\partial A}{\partial\theta}\right) = \mu_o r^2 \sin^2\theta\left(\frac{\partial p}{\partial A}\right)_U + b_\phi\frac{db_\phi}{dA} \qquad (1.59)$$

$$\left(\frac{\partial p}{\partial U}\right)_A = -\rho \qquad (1.60)$$

where equation (1.59) derives from the first term of equation (1.57) and is the derivative

of the pressure p taken at a constant U whereas equation (1.60) derives from the second term of equation (1.57) and is the derivative of p taken at constant A. This is the Grad-Shafranov equation (also known as the Grad-Shafranov-Schlüter equation) for which it remains to consider the boundary conditions as well as to either specify a physically sensible and mathematically convenient form of b_ϕ and a form of the plasma pressure $p(A, U)$ (see Neukirch (1998) for a further discussion of this point) to relate it to the plasma density, ρ, (thereby closing the set of equations) or to fix these quantities given some additional information. These equations are the fundamental equations to be solved and take the form of a nonlinear elliptic partial differential equation, which must be solved numerically to construct sequences of equilibria from the calculated flux function, A. The role of the Grad-Shafranov equation in MHS equilibria and the different forms that it may take under different symmetry invariance (such as rotational invariance in our case) and coordinate constraints has been discussed and summarised at length in Neukirch (1998).

1.6.2 Surface pressure distributions

Many models of the global or large scale magnetic fields in a stellar MHS atmosphere have confined their attention to the magnetic field of either a force-free dipole-like field (where $\mathbf{J} \times \mathbf{B} = \mathbf{0}$, e.g. Browning & Priest (1984)) or that of a potential field configuration (where $\nabla \times \mathbf{B} = \mathbf{0}$, e.g. Jardine & Collier Cameron (1991)). However, Hundhausen et al. (1981) begun to allow deviations from the potential field and in the isothermal case,

MHS solutions were found for pressure of the form

$$p = p_o(A) \exp\left(\frac{GM\mu}{k_B T r}\right) \tag{1.61}$$

where μ is the average molecular weight of the plasma, but none were found for the cases where the plasma was rotating or had a toroidal field component. One feature of the force-balance equation (equations (1.59) and (1.60)) is that it essentially describes the toroidal component of the magnetospheric current density as being driven by both pressure and magnetic field gradients. There are a number of approaches available to consider the question of the prescription of the stellar surface plasma pressure distribution and its solution for the consequent density. One approach for our models is that of fixing the plasma density as a function of A and U to recover the plasma pressure as a function of A and U, such as would be the case were we to deploy a polytropic equation of state with $p = K\rho^{\gamma}$ with K and γ held constant. Substitution of this form into equation (1.60), integrating and solving for p (at a constant U and assuming that Ω does not depend on A) gives a form of the pressure which clearly contains both mathematical and physical difficulties when the term sum inside the brackets becomes negative

$$p\,(A,U) = K\left[\left(\frac{p_o(A)}{K}\right)^{\frac{\gamma-1}{\gamma}} - \frac{\gamma-1}{\gamma}\frac{U-U_o}{K}\right]^{\frac{\gamma}{\gamma-1}} \tag{1.62}$$

A second option is to consider an equation of state together with an energy equation. Whilst being the most physically realistic option this is a more difficult case and $T(A,U)$ will remain unknown until the energy equation is solved. Lastly, it is possible to simply assume a specific equation of state and specify the temperature as a function of A and of U. The simplest approach is to make the assumption that the plasma behaviour is that of

an ideal gas

$$p = R\rho T \tag{1.63}$$

with the gas constant, R and for a given temperature profile $T = T(A, U)$. It immediately follows that

$$\frac{\partial p}{\partial U} = -\frac{p}{RT}. \tag{1.64}$$

A single integration of equation (1.60) then yields

$$p = p_0\,(A) \exp\left(-\int_{U_o}^{U} \frac{dU'}{RT(A, U')}\right) \tag{1.65}$$

so that in the more special case of an isothermal ideal gas the form of the pressure is that of the barometric law

$$p = p_0\,(A) \exp\left(-\frac{U - U_0}{RT}\right) \tag{1.66}$$

with different base pressure $p_0(A)$ for each field line. In our models we chose to adopt the assumption that the behaviour of the plasma is ideal and isothermal as the most simple starting point from which to proceed to more realistic models. In these models the choice of the form of the pressure $p(A, U)$ and of the toroidal magnetic field component B_ϕ will be the key distinguishing features between the models.

1.6.3 Boundary considerations

The mathematical formulation of the physical problem has to be complete with the specification of the boundary conditions. Given that we are dealing with a nonlinear elliptic PDE, the usual types of boundary conditions are Dirichlet or homogeneous von

Neumann boundary conditions. In the case of the former, the flux function, A is specified on the boundary ($A|_{boundary}$) to be some known function of space. The physical interpretation of imposing this boundary condition is that it fixes the point where a given field line A crosses the boundary so that specifying A on the boundary is equivalent to specifying the magnetic flux distribution through that boundary. In the case of the von Neumann conditions, the normal derivative, $\frac{\partial A}{\partial n}$ is specified as a known function of space. If this condition is imposed on all boundaries then it is necessary to impose an additional condition in order to make the solutions unique. It is this boundary condition which determines the angle of intersection of a given field line A with the boundary because in a Cartesian geometry

$$|\mathbf{B} \times \mathbf{n}| = |\left(\mathbf{n} \cdot \nabla A\right) \mathbf{e}_y| = |\mathbf{B}| \sin\theta \tag{1.67}$$

where θ is the angle between $\mathbf{B}$ and the normal vector $\mathbf{n}$. It follows that the field will be perpendicular to the boundary when the normal derivative is zero

$$\frac{\partial A}{\partial n} = 0 \Longrightarrow \mathbf{B}||\mathbf{n} \tag{1.68}$$

In the case of our models it will be (mostly) natural to adopt a spherical polar coordinate system. Figure (1.5) shows the basic configuration of our general magnetospheric boundary conditions where the boundaries are on the stellar surface, the rotation axis, the equatorial plane and some outer boundary chosen to satisfy the requirement that the mathematical problem is to be well-posed. This condition will be satisfied if the boundary is at infinity but given that we are solving our equations numerically, we are constrained to choose a finite radius of sufficient extent that the influence of this boundary does not perturb the solution too much. Considering firstly the stellar surface boundary condition (at

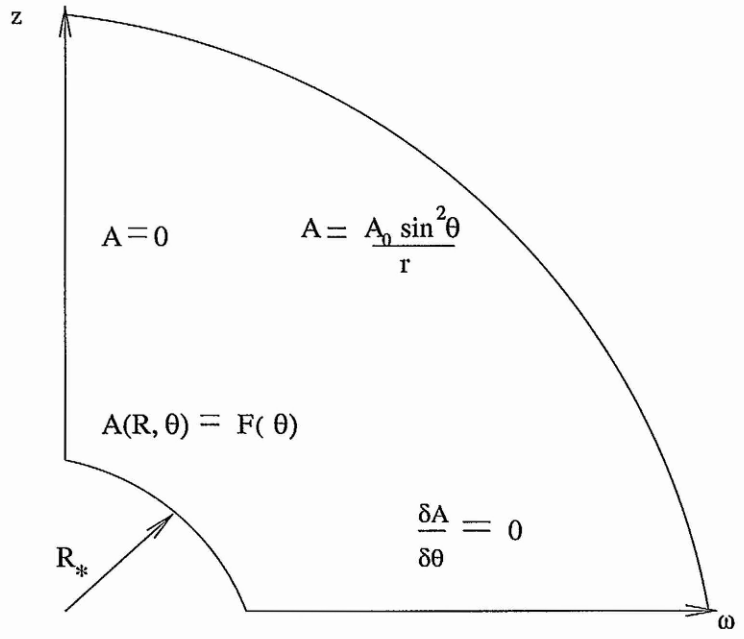

Figure 1.5: Magnetospheric boundary conditions in a spherical geometry

some radial $r = R_\star$) we prescribe the Dirichlet boundary condition that the flux function, A, is dependent only on the latitudinal coordinate θ

$$A\left(R_\star, \theta\right) = F(\theta) \tag{1.69}$$

thereby fixing the radial component of a magnetic dipole flux distribution on the stellar surface. Secondly, in the case of the axial boundary we again prescribe a Dirichlet boundary condition but in this case we choose to set the flux to a constant, $A = 0$ (i.e., there is a field line on the axis). This also ensures that the coordinate singularity at $\theta = 0$ in equation (1.36) does not cause any numerical difficulties. Thirdly, we have equatorial symmetry and so $\frac{\partial A}{\partial \theta} = 0$. This symmetry is apparent from consideration of equation (1.59) which may be seen to be invariant under the variable transformation $\theta \rightarrow -\theta$. Together with the assumption of axisymmetry this reduces the problem from a three di-

mensional sphere to that of a two dimensional quadrant. Any calculated bulk plasma quantities (such as the stellar emission measure) may then simply be integrated over the whole volume (a number of authors have, however, begun to tackle the different problem of constructing fully three dimensional MHS atmospheres, e.g. with applications to the solar corona, see Low (1985), Bogdan & Low (1986), Low (1991), Neukirch (1995)).

Finally we must consider the position of the outer boundary. Given that our primary interest is in that of the behaviour of plasma trapped by closed field lines (as we are not considering stellar winds) we must choose the extent of the boundary to be such that the outer boundary does not significantly affect those regions where the bulk of the current density is concentrated. The decision as to the extent of this box should also be influenced by the practical considerations of implementing the numerical problem, however the choice of the extent of the box should primarily be such that the additional dipole field at the outer boundary (induced by the plasma) is considered to be 'weak' compared to that of the star. We have checked this criterion for the solutions presented later and have found it to be satisfied for our choice of outer boundary which we usually place at $r = 50R_{\star}$.

1.7 Thesis outline

In this thesis we will construct simple models of rotating stellar and planetary magnetospheres within the framework of ideal MHD. These models will take the basic outline of a stellar magnetosphere that we have outlined above as a starting point from which to

proceed further. In summary, this simple magnetosphere will be that of a single, rapidly rotating star with an axisymmetric dipole magnetic field at the base of its corona and with an axis that is in alignment with that of the rotation axis. It is the isothermal plasma associated with this field that will give rise to the magnetospheric emission and which is held in strict corotation with the stellar surface. Equatorial and rotational symmetry reduce the domain to one quarter of a two dimensional quadrant. We will consider timescales that are much longer than the typical time scales of the system, which will allow us to model the evolution of the system quasi-statically by calculating sequences of MHS equilibria. This is achieved by numerical solution of the Grad-Shafranov equation (in terms of the flux function, A) which requires us to specify a suitable surface pressure distribution and specify the toroidal component of the magnetic field as a function of A. The second chapter will outline the numerical procedure that will be employed to calculate these equilibrium sequences, and the practical realisation of this procedure. The third chapter will discuss different models which will be characterised by different surface pressure distributions but all of which will lack a toroidal magnetic field component. The fourth chapter will discuss results from a model which includes a toroidal magnetic field component. The models successfully reproduce the observed saturation and supersaturation of stellar emission with rotation. The fifth chapter will address the question of analytically constructing three dimensional equilibria that may be of use in the modelling of magnetospheres with magnetic field geometries that are not in alignment with their rotation axes or which are displaced from the centre of the rotating body, such as the giant gas planets Uranus and Neptune. The last section of the thesis will be a brief discussion of our

conclusions, a review of the work of the thesis and will consider the outlook for further development, extension and refinement of our models.

Chapter 2

Numerical method

The studies of rotating magnetospheric systems that have, to a degree, motivated this work, yield nonlinear elliptic partial differential equations which require a numerical method for their solution. In the MHD formulation of such problems, these equations describe the stationary states (equilibria) of the continuous system and often display bifurcation, limit or catastrophe points which may be associated with some change in the stability of the equilibrium. In the absence of any available general unique, analytical theory to solve the nonlinear equations a numerical method must be applied. One such method that has been successfully applied to a number of magnetospheric systems (e.g., Neukirch (1993a), Neukirch (1993b), Becker (1999)), is that of Keller's (Keller , 1977) numerical continuation method (developed by Zwingmann (1987)) which has been used to follow sequences of different classes of equilibria through bifurcation points obtaining entire bifurcation branches and is applicable to a general class of differential operators.

2.1 Numerical continuation methods

2.1.1 Keller's method

The numerical continuation method developed by Keller (see Allgower & Georg (1990) for a comprehensive review of such methods) is a predictor-corrector based scheme which may be applied to any general nonlinear, elliptic partial differential equation

$$G(u, \lambda) = 0 \tag{2.1}$$

$$u|_{\partial\Omega} = f(\mathbf{r}, \lambda) \tag{2.2}$$

where $u = (u_1(\mathbf{r}), u_2(\mathbf{r}), ..., u_N(\mathbf{r}))$ is a vector function such that $u \in \mathbb{B}$ for a Banach space $\mathbb{B}$, G is an elliptic differential operator such that G: $\mathbb{B} \times \mathbb{R} \rightarrow \mathbb{B}$, λ is an intrinsic real parameter of the system and $f = (f_1, f_2, ...f_N)$ are defined on a continuous domain $\Omega \in \mathbb{R}^n$. Considering the boundary conditions, we note that instead of a Dirichlet boundary condition on the complete outer boundary, we may use a combination of both Dirichlet and von Neumann boundary conditions

A one parameter family of solutions (i.e. a solution branch) of equation (2.1)

$$\Gamma_{ab} : [u(\sigma), \lambda(\sigma)] \quad , \quad \sigma_a \leq \sigma \leq \sigma_b \tag{2.3}$$

is defined with λ depending on the parameter $\sigma \in [\sigma_a, \sigma_b]$ continuously with derivatives up to second order. This arclength parameterisation is arbitrary on each branch and is employed because most continuation methods will have significant difficulties upon encountering solutions at some point $u = u_c$ and $\lambda = \lambda_c$ on the branch where the Fréchet

derivative $D_u G(u_c, \lambda_c)$ is singular (the subscript denoting differentiation with respect to u) or where there are limit points and the solution branch bends back. Such difficulties can be avoided by the imposition of an additional constraint that is equivalent to replacing equation (2.1). In the abstract function space, the arclength σ along the branch is defined in the usual manner

$$< \frac{du}{d\sigma} \mid \frac{du}{d\sigma} > + \left(\frac{d\lambda}{d\sigma}\right)^2 = 1 \tag{2.4}$$

for every point (u, λ) along the equilibrium sequence and where $< \bullet \mid \bullet >$ denotes a suitable scalar product such as the L_2 norm. Each of these points correspond to a unique σ and vice versa. If some solution at $(u = u_0, \lambda = \lambda_0)$ to equation (2.1) is already known then a new solution (u_1, λ_1) may now be computed by a predictor-corrector scheme using a steplength s along the solution branch in the projected subspace. As with σ, the steplength s may be arbitrarily large or small along the curve in this space.

The step is given by

$$u_1(r) = u_o(r) + s\dot{u}_o(r) \tag{2.5}$$

$$\lambda_1 = \lambda_0 + s\dot{\lambda}_0 \tag{2.6}$$

where the dot indicates differentiation with respect to the arclength of the solution curve. Figure (2.1) shows that if s is not too large then (u_1, λ_1) lies near the solution curve and is a good point to start a Newton iteration to determine $(\dot{u}_0, \dot{\lambda}_0)$, the tangent to the curve at (u_0, λ_0).

The introduction of a tangential condition gives rise to an additional condition that

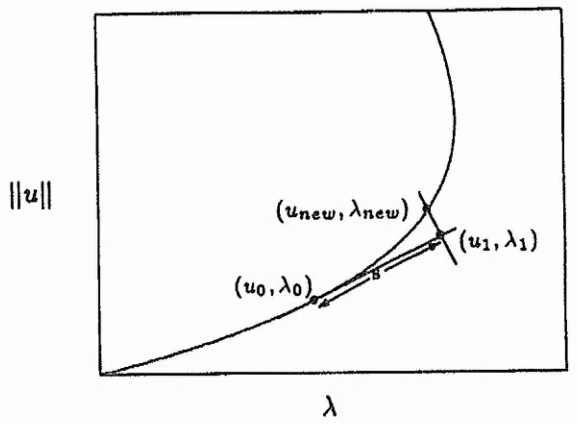

Figure 2.1: Sketch of method for calculating solution branches

allows equation (2.1) to be replaced by

$$G(u, \lambda) = 0 \tag{2.7}$$

$$N(u, \lambda, s) = 0 \tag{2.8}$$

where $N : \mathbb{B} \times \mathbb{R}^2 \rightarrow \mathbb{R}$. The form of equation (2.8) is different in the predictor and corrector steps. The linearised equations (in terms of $(\dot{u}_0, \dot{\lambda}_0)$) which have then to be solved are found upon differentiating equations (2.7) and (2.8) with respect to the arclength σ

$$D_u G(u_0, \lambda_0)\, \dot{u}_0 + \frac{\partial G}{\partial \lambda}(u_0, \lambda_0)\, \dot{\lambda}_0 = 0 \tag{2.9}$$

$$D_u N(u_0, \lambda_0)\, \dot{u}_0 + \frac{\partial N}{\partial \lambda}(u_0, \lambda_0)\, \dot{\lambda}_0 + \frac{\partial N}{\partial s}\dot{s} = 0 \tag{2.10}$$

together with the arclength condition (equation (2.4)), where $D_u G\bullet$ denotes the Fréchet derivative (or linearisation of operators on vector function spaces) of G. It remains to impose the Dirichlet boundary condition

$$\dot{u}_0 \mid_{\partial\Omega_D} = -\frac{\partial U_b}{\partial \lambda}\dot{\lambda}_0 \tag{2.11}$$

on elements of the boundary of the domain $\partial\Omega_D$ and prescribe von Neumann conditions on the complement $\partial\Omega_N$. The space perpendicular to the tangential space is determined by solutions of

$$< \dot{u_0} \mid u - u_1 > + \dot{\lambda}_0 (\lambda - \lambda_1) = 0. \tag{2.12}$$

A Newton-Raphson iteration is to be carried out from the point (u_1, λ_1). The $n+1$ th such iteration is

$$u^{n+1} = u^n + \delta u \tag{2.13}$$

$$\lambda^{n+1} = \lambda^n + \delta\lambda \tag{2.14}$$

and the simultaneous equations

$$D_u G(u^n, \lambda^n)\, \delta u + \frac{\partial G}{\partial \lambda}(u^n, \lambda^n)\, \delta\lambda = -G(u^n, \lambda^n) \tag{2.15}$$

$$< \dot{u_0} \mid \delta u > + \dot{\lambda}_0 \delta\lambda = 0 \tag{2.16}$$

are then solved at each step under the boundary conditions

$$\delta u \mid_{\partial\Omega_D} - \frac{\partial u_b}{\partial \lambda}\delta\lambda = -u^n \mid_{\partial\Omega} + u_b \tag{2.17}$$

Equation (2.17) derives from the expansion of the boundary conditions

$$u^{n+1} \mid_{\partial\Omega_D} = u_b\left(\mathbf{r}, \lambda^{n+1}\right).$$

This is expanded in terms of $\delta\lambda$ to give

$$u^{n+1} \mid_{\partial\Omega_D} \approx u_b(\mathbf{r}, \lambda^n) + \frac{\partial u_b}{\partial \lambda}(\mathbf{r}, \lambda^n)\, \delta\lambda \tag{2.18}$$

Now given that equation (2.13) holds everywhere, it follows that

$$u^{n+1} \mid_{\partial\Omega} = u^n \mid_{\partial\Omega} + \delta u \mid_{\partial\Omega}$$

$$= u_b(\mathbf{r}, \lambda^n) + \frac{\partial u_b}{\partial \lambda}(\mathbf{r}, \lambda^n)\delta\lambda \tag{2.19}$$

Equation (2.17) then follows upon equating equation (2.18) with equation (2.19). Using this notation we can consider that at each iteration of the corrector steps, a system of linear equations is to be solved

$$\begin{pmatrix} D_u G\left(u^n, \lambda^n\right) \circ & \frac{\partial G}{\partial \lambda}\left(u^n, \lambda^n\right) \\ < \dot{u}_0 \mid \circ > & \dot{\lambda}_0 \end{pmatrix} \begin{pmatrix} \delta u \\ \delta\lambda \end{pmatrix} = - \begin{pmatrix} G\left(u^n, \lambda^n\right) \\ N\left(u^n, \lambda^n, s\right) \end{pmatrix} \tag{2.20}$$

To calculate $(\dot{u}_{new}, \dot{\lambda}_{new})$ we take the derivative of the equilibrium conditions (equations (2.7) and (2.8) at (u_{new}, λ_{new}) with respect to the arc length σ that we defined in equation (2.4)

$$\frac{dG}{d\sigma} = D_u G(u_{new}, \lambda_{new})\dot{u}_{new} + \frac{\partial G}{\partial \lambda}(u_{new}, \lambda_{new})\dot{\lambda}_{new} = 0 \tag{2.21}$$

$$\frac{dN}{d\sigma} = D_u N(u_{new}, \lambda_{new})\dot{u}_{new} + \frac{\partial N}{\partial \lambda}(u_{new}, \lambda_{new}, s)\dot{\lambda}_{new} + \frac{\partial N}{\partial s}\dot{s} = 0 \tag{2.22}$$

and $\dot{s}$ may then be eliminated by dividing these equations through by $\dot{s}$ and using the relation between the arc-length and the steplength

$$\frac{d}{ds} = \frac{d\sigma}{ds}\frac{d}{d\sigma} = \frac{1}{\dot{s}}\frac{d}{d\sigma} \tag{2.23}$$

together with the definition of the arclength (2.4) and the more convenient relations

$$u_s = \frac{\dot{u}_{new}}{\dot{s}} \tag{2.24}$$

$$\lambda_s = \frac{\dot{\lambda}_{new}}{\dot{s}} \tag{2.25}$$

finally allows us to calculate $(\dot{u}_{new}, \dot{\lambda}_{new})$

$$\dot{u}_{new} = \dot{s}u_s = \frac{u_s}{\sqrt{\langle u_s \mid u_s \rangle + \lambda_s^2}} \tag{2.26}$$

$$\dot{\lambda}_{new} = \dot{s}\lambda_s = \frac{\lambda_s}{\sqrt{\langle u_s \mid u_s \rangle + \lambda_s^2}} \tag{2.27}$$

2.1.2 Alternative formulation

A considerably simpler implementation of the above formulation is possible when we write the system of equations to be solved in terms of a matrix operator M

$$M \begin{pmatrix} \hat{u} \\ \hat{\lambda} \end{pmatrix} = \begin{pmatrix} R_1 \\ R_2 \end{pmatrix} \tag{2.28}$$

where $M = \begin{pmatrix} D_u G(\bullet) & \frac{\partial G}{\partial \lambda} \\ < \dot{u} \mid \bullet > & \dot{\lambda} \end{pmatrix}$. At the predictor step, this is of the form $\hat{u} = \dot{u}_0, \hat{\lambda} = \dot{\lambda}_0, R_1 = 0$ and $R_2 = 1$ whereas in the corrector step it takes the form $\hat{u} = \delta u, \hat{\lambda} = \delta\lambda, R_1 = -G\left(U^n, \lambda^n\right)$ and $R_2 = -N\left(u^n, \lambda^n, s\right)$.

Predictor step

The approach that we take to this problem is to rewrite $\hat{u}$ as a function that is split and depends on two other arbitrary functions u, v and upon an arbitrary real number $\alpha \in \mathbb{R}$

$$\hat{u} = w + \alpha v \tag{2.29}$$

so that in the predictor step we have

$$D_u G w + \alpha D_u G v + \frac{\partial G}{\partial \lambda}\hat{\lambda} = R_1 \tag{2.30}$$

Comparing this with the general matrix form given by equation (2.28) it follows that the natural choices to make are

$$D_u G w = R_1 = 0 \tag{2.31}$$

and for $\alpha = \hat{\lambda}$ we have

$$D_u G v = -\frac{\partial G}{\partial \lambda} \tag{2.32}$$

The second row of the matrix allows us to calculate $\hat{\lambda}$

$$\langle \dot{u}_o \mid w \rangle + \hat{\lambda} \langle \dot{u}_o \mid v \rangle + \lambda_o \hat{\lambda} = R_2 = 1 \tag{2.33}$$

$$\Longrightarrow \hat{\lambda} = \frac{1 - \langle \dot{u} \mid w \rangle}{\langle \dot{u} \mid v \rangle + \dot{\lambda}_o} \tag{2.34}$$

and given that w and v are known functions (from the solution of the equations (2.30) and (2.31)) then we are able to calculate $\hat{u}$ from

$$\hat{u} = w + \hat{\lambda} v \tag{2.35}$$

Before calculating $\hat{u}$ it is necessary to reconsider the Dirichlet boundary condition for the solution on the branch, u in the predictor step, that is given by equation (2.11). To ensure a unique solution of equation (2.30) and to decouple the problem we must tailor the boundary conditions accordingly

$$\begin{aligned} u_s &= \frac{\dot{u}}{\dot{s}} = w + \lambda_s v = w + \frac{\dot{\lambda}}{\dot{s}} v \\ u_s \mid_{\partial\Omega_D} &= \frac{1}{\dot{s}} \dot{u} \mid_{\partial\Omega_D} = \frac{1}{\dot{s}} \frac{\partial u_b}{\partial \lambda} \dot{\lambda} = w \mid_{\partial\Omega_D} + \frac{1}{\dot{s}} \dot{\lambda} v \mid_{\partial\Omega_D} \end{aligned} \tag{2.36}$$

so that the choice of $w \mid_{\partial\Omega_D} = 0$ and $v_{\partial\Omega_D} = \frac{\partial u_b}{\partial \lambda}$ for which $D_u G_v = -\frac{\partial G}{\partial \lambda}$. Given v we may therefore readily find λ_s and thence u_s which take the same form as equations (2.26) and (2.27).

Corrector step

For the corrector step in the matrix ((2.20) or (2.28) we have

$$\hat{u} = \delta u = w + \delta \cdot \lambda v \tag{2.37}$$

with the corresponding equations to be solved, which are given by

$$D_u G\left(u^n, \lambda^n\right) w = -G\left(u^n, \lambda^n\right) \tag{2.38}$$

$$D_u G\left(u^n, \lambda^n\right) v = -\frac{\partial G}{\partial \lambda}\left(u^n, \lambda^n\right) \tag{2.39}$$

The boundary conditions were discussed in the earlier section but the equation for v and its boundary condition are the same as in the predictor step, the difference between the two steps being in the form of the $D_u G w$ equation. However, for numerical purposes it is better to use

$$\hat{w} = \hat{u} + w \tag{2.40}$$

which gives the equation for w and its boundary condition as

$$\begin{aligned} D_u G(u^n, \lambda^n)\hat{w} &= -G(u^n, \lambda^n) + D_u G(u^n, \lambda^n) u^n \\ \langle \dot{u}_0 \mid \delta u \rangle + \dot{\lambda}_0 \delta\lambda &= -N(u^n, \lambda^n, s) \\ \hat{w} \mid_{\partial\Omega_D} &= w \mid_{\partial\Omega_D} + u^n \mid_{\partial\Omega_D} = u_b(\mathbf{r}, \lambda^n) \end{aligned} \tag{2.41}$$

Combining equation (2.37) with equation (2.40) and substituting into equation (2.41) allows us to calculate $\delta\lambda$

$$\delta\lambda = \frac{\langle \dot{u}_0 \mid u_0 - \hat{w} \rangle + \left(\lambda_0 - \hat{\lambda}\right) + s}{\langle \dot{u}_0 \mid v \rangle + \dot{\lambda}_0} \tag{2.42}$$

and thence $u^{n+1} = \hat{w} + \delta\lambda v, \lambda^{n+1} = \lambda^n + \delta\lambda$ completes one corrector iteration step which we repeat until we have satisfied the equilibrium conditions to sufficient accuracy and have iterated back onto the solution branch.

2.2 The Finite element method

The method that is adopted to discretise the domain to facilitate the solution of our nonlinear equations using Keller's method is that of finite elements rather than that of finite differences (an introduction to these methods may be found in Wait & Mitchell (1985) and Braess (1997)). One of the principle reasons for this is that for physical systems such as rotating magnetospheres, it will often be useful and convenient to be able to refine the computational grid locally to enable study of those parts of the system that are of most interest in greater detail (e.g., Becker , 1999).

2.2.1 The Ritz-Galerkin method

The Ritz-Galerkin method (Ritz , 1908) exploits the fact that many elliptic problems may be formulated as a variational problem using the characterisation theorem (see Braess (1997) for further details) which states that a linear functional J defined over a suitable abstract function space attains its minimum over that space. This variational principle may be considered to be equivalent to a general differential equation which we may wish

to solve of the form

$$D_u G\phi = R \tag{2.43}$$

where G is a general linear second order differential operator on a set of functions ϕ. The variational principle and the differential equation above, are equivalent in the sense that the equation is the condition that makes the functional stationary with respect to a set of N free parameters $a_1, ...a_N$

$$\frac{\partial J\left[\phi_{ap}\right]}{\partial a_i} = 0 \tag{2.44}$$

when the function $J[\phi]$ is approximated by $J[\phi_{ap}]$ for some approximating function $\phi_{ap} = \phi_{ap}\left(\mathbf{r}, \mathbf{a}\right)$ which is a known function of space. The dependence on $\mathbf{a}$ will usually take the form of a set of N nonlinear equations for the a_i which we discretise in the function space rather than in the domain Ω. A useful choice of representation for the desired ϕ is to represent it by an expansion in the following manner

$$\phi = \phi_o(x, y) + \sum_{i=1}^{\infty} a_i \phi_i(x, y) \tag{2.45}$$

where the ϕ_i are a complete set of functions defined on the domain and which vanish on the boundary and where the ϕ_0 is the function satisfying the boundary conditions. The set of a_i are then determined to satisfy (2.44). The problem is made accessible to numerical solution by approximating the solution by the finite sum

$$\phi = \phi_{ap}(x, y) + \sum_{i=1}^{N} a_i \phi_i(x, y) \tag{2.46}$$

which is linear in a_i. It follows that if we have a functional that depends quadratically on ϕ (as is the case for linear partial differential equations) then the functional of ϕ_{ap} will be

a quadratic function of the a_i. A more concise form of the function $J_{ap}[a_1, ...a_N]$ may be introduced as follows.

The most general form of a second-order differential operator L is given by

$$L = -\nabla \cdot \left[\underline{\underline{D}}(x, y) \cdot \nabla\right] \tag{2.47}$$

For our purposes, we can (without loss of generality) assume that the matrix $\underline{\underline{D}}$ is symmetric. The appropriate functional $J[\phi]$ is then given by

$$J[\phi] = \int_\Omega \left[\frac{1}{2}\left(\nabla\phi \cdot \underline{\underline{D}} \cdot \nabla\phi\right) - R\phi\right] dxdy \tag{2.48}$$

Substitution of equation (2.46) into the above expression will now yield the approximate form of the functional $J_{ap}[\mathbf{a}]$ in the form

$$J_{ap}[\mathbf{a}] = \frac{1}{2}\mathbf{a}^T \cdot \underline{\underline{A}} \cdot \mathbf{a} - \mathbf{a}^T \cdot \mathbf{b} + \mathbf{c} \tag{2.49}$$

where $\mathbf{a}^T = (a_1, ..., a_N)$ and for which

$$A_{ij} = \int_\Omega \nabla\phi_i \cdot \underline{\underline{D}} \cdot \nabla\phi_j dxdy \tag{2.50}$$

$$b = -\int_\Omega \nabla\phi_0 \underline{\underline{D}} \cdot \nabla\phi_i dxdy + \int_\Omega R\phi_i dxdy \tag{2.51}$$

$$c = \frac{1}{2}\int_\Omega \nabla\phi_0 \cdot \underline{\underline{D}} \cdot \nabla\phi_0 dxdy - \int_\Omega R\phi_0 dxdy \tag{2.52}$$

We are now able to write the problem in the form of a system of linear equations for $\mathbf{a}$. The Ritz method that we have just described, will only work if the differential operator L is self-adjoint. In more general cases we would have to use Galerkin's method which reduces Ritz's method for self-adjoint differential operators.

$$\underline{\underline{A}} \cdot \mathbf{a} = \mathbf{b} \tag{2.53}$$

Unfortunately, the matrix $\underline{\underline{A}}$ in (2.53) is generally not sparse and so considerable numerical effort would be required to find its solutions. The linear differential equation from which we proceed, is of the form

$$D_u G \cdot \hat{u} = \hat{r} \tag{2.54}$$

for an elliptic operator G on a real-valued function $u(x, y)$ defined on the domain Ω and subject to the boundary conditions. Upon discretisation of the domain we may then approximate $\hat{u}$ in a subspace by

$$\hat{u}_{ap}(x, y) = \phi_o(x, y) + \sum_{i=1}^{N} a_i \phi_i(x, y) \tag{2.55}$$

where the ϕ_i are a complete set of functions (not necessarily orthogonal) which form a basis on the function space in which we seek solutions for $\hat{u}$ and which are linearly independent with respect to a suitable scalar product defined on the function space. Also, the ϕ_i have the property of vanishing on the boundary of the domain $\partial\Omega_D$. The set of ϕ_0 satisfies the boundary conditions for $\hat{u}$ and the a_i are a set of real free parameters for which we require an optimum choice to give the best approximation to actual solution of the original differential equation (2.54). Substitution of equation (2.55) into the equation (2.54) gives us a residual R

$$R(\phi_0, a_1, ..., a_i, x, y) = D_u G \cdot \hat{u}_{ap} - \hat{r} = D_u G \cdot \phi_0 + \sum_{i=1}^{N} a_i D_u G \cdot \phi_i - \hat{r} \tag{2.56}$$

The above residual is usually non-zero and is a known function of space (given the calculated ϕ_i and $D_u G \phi_i$) and is linear in terms of the coefficients a_i. The 'closest' approximation of $\hat{u}_{ap}$ to u is found from the N equations for the a_i, for which R has no

non-zero components in the subspace spanned by the set of ϕ_i functions and in which the approximation will exactly satisfy the original equation (2.54), i.e.

$$< \phi_i \mid R >= \int_\Omega \phi_i R d\Omega = 0 \qquad\qquad i = 1, ...N \tag{2.57}$$

This linear algebraic system of N equations for the coefficients a_i allows us to calculate the optimal $\hat{u}_{ap}$ such that the original equation (2.54) is satisfied in the subspace orthogonal to the residuum R.

Defining a matrix $\underline{\underline{A}}$ by forming inner products with ϕ_i in the space spanned by the ϕ_i

$$A_{ij} =< \phi_i \mid D_u G \cdot \phi_j > \tag{2.58}$$

with a vector $\mathbf{b}$

$$b_i =< \phi_i \mid \hat{r} > - < \phi_i \mid D_u G \cdot \phi_0 > \tag{2.59}$$

where only the second term will contribute to the boundary conditions because application of Gauss's theorem shows that surface integrals will not contribute as the ϕ_i are vanishing on the boundary. The approximated equation may now be rewritten in the form of a matrix equation of the same form as given by (2.53) which is usually not sparse. The Ritz-Galerkin method does not yield a sparse matrix unless it is applied together with the finite element method. A partial integration and application of Green's first identity on the above integrals demonstrates that it is possible to replace these integrals with a form whereby the operators contain lower order derivatives than in the original integrand.

2.2.2 Finite element domain discretisation

A rectangular domain $D \subset \mathbb{R}^2$ is partitioned into a finite number of subdomains in the form of non-overlapping triangles where the set of triangles $\triangle_j \subset D, j = 1, ..., n_T$ (for a total number of triangles, n_T) is ordered such that neighbouring triangles share two corners as shown in figure (2.2). The function, $\hat{u}$ that we wish to determine by

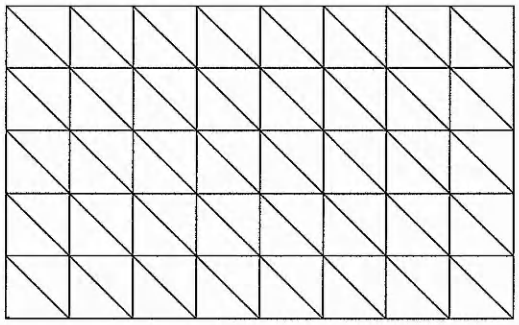

Figure 2.2: Discretisation of a rectangular domain into finite elements

the Ritz-Galerkin approximation ($\hat{u}_{ap}$) is represented by a polynomial function of the coordinates of the domain. Our choice for the shapes which we will use to partition the domain and our choice for the form of the polynomial with which we choose to make our representation of $\hat{u}$ is based on the need for computational practicality and upon prior successful implementations of the method. We choose a fixed triangle (see figures 2.3 (a) and (b)) within which we will make our evaluation for u by means of an interpolation that is expressed in the form of local "shape functions", e.g.

$$\hat{u}_{ap}(x, y) = a_1 + a_2 x + a_3 y \tag{2.60}$$

$$\hat{u}_{ap}(x, y) = a_1 + a_2 x + a_3 y + a_4 x^2 + a_5 y^2 + a_6 xy \tag{2.61}$$

where (2.60) is the linear shape function appropriate to the element (a) in figure (2.2) and (2.61) is the quadratic polynomial appropriate to the element (b) in figure (2.2) as the degree of the polynomial determines the number of nodal points that we need to uniquely determine the set of unknown a coefficients.

Figure 2.3: Nodes of the nodal basis for a) linear and b) quadratic elements

Each node of the triangles fixes the value of the a coefficients (and therefore of $\hat{u}_{ap}$) and a value of the shape function is assigned to each node. The choice for these shape functions is such that the interpolations are continuous (but not necessarily continuously differentiable) across element boundaries resulting in so-called "Lagrangian triangles". This continuity of the shape functions follows from the property that for a given set of points the local shape function, σ_{jk}, for a particular node, p_{jk} is defined a s a polynomial which is determined from

$$\sigma_{jk}(x,y) = \begin{cases} 1 \quad for \quad (x,y) = p_{jk} \\ 0 \quad for \quad (x,y) = p_{jl}, \quad l \neq k \end{cases} \tag{2.62}$$

(It should be noted that when we use the term "finite element" then we are referring to both the geometrical subdomain or the shape of the region on which we are interpolating plus the choice of the polynomial representation on that space). To ensure that all the shape

functions that have been defined on the triangles are polynomials of the same degree and to allow us to conveniently number all our nodal points in a consecutive manner, we must impose the condition that the number of nodal points $p_{jk} \in \triangle_j, k = 1, ..., n_P$ on each triangle is the same (this makes our elements "conformal"). As we discussed earlier, one of the principal considerations with constructing our domain is that we must construct a set of basis functions ϕ_i for the space of approximate solutions. Once we have taken all the nodal points in the domain, D, and numbered them consecutively, i.e., $p_i, i = 1, ..., N$ then we the basis functions, ϕ_i may then be constructed as global shape functions for the nodes p_i

$$\phi_i(x,y) = \begin{cases} 1 \quad \forall \quad (x,y) \in \triangle_i \quad \text{with k from} \quad p_i = p_{ik} \\ 0 \qquad\qquad\qquad\qquad\quad \text{elsewhere} \end{cases} \tag{2.63}$$

If there is any point which lies on the boundary of two neighbouring triangles then only one of the triangles is chosen for the evaluation of the basis function ϕ_i. In the case where there is more than one function to be approximated it is worth noting that the degree of the local shape functions can be chosen independently for each of these functions whilst still using the same triangulation, however in this thesis we will only be approximating one function at our nodes so we will not expand any further on this point. The basis functions now have the property that they take the value of unity at a particular nodal point and are zero at the others, i.e., $\phi_i(p_j) = \delta_{ij}$ so that the value of the coefficients a_i take on the value of $u_a(p_i)$ and the a_i are now known as nodal variables. Another important property of our choice of basis functions for the finite element discretisation is that they have compact spatial support so that the integral over the domain that has to be performed

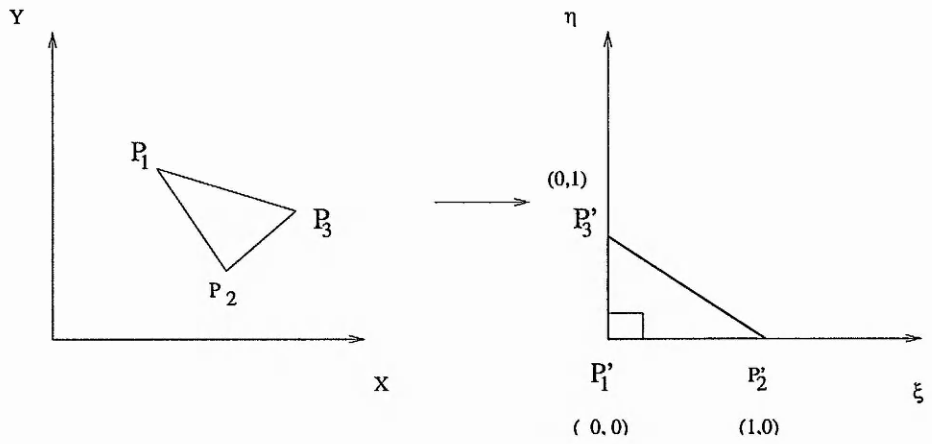

Figure 2.4: Transformation of a general triangle to a unit triangle

in (2.57) is reduced to an integral over the support of the particular basis functions which in turn breaks the integral up into the sum of integrals over the triangles that define this support. One consequence of this is that the system of linear equations that we have to solve for the nodal variables may be solved element by element. It also follows from our restriction of the integral to the support of the basis functions of a node that only neighbouring nodes will contribute to our summation so that the matrix of the linear system (2.60) will be sparse (given a suitable numbering of nodes it may be banded).

The shape functions take on a particularly convenient and easy to use form if we express the basis functions in terms of a unit triangle in some $\xi - \eta$ space. A suitable transformation of the coordinates then allows the result from a particular point to be transferred back to a particular triangle in the (x, y) space. Figure (2.4) shows a standard 6-node triangle (as in figure (2.3 b) with nodes numbered as in figure (2.5)) $P_1P_2P_3$ in the x-y plane for which we use the form of the quadratic interpolating polynomial as given in

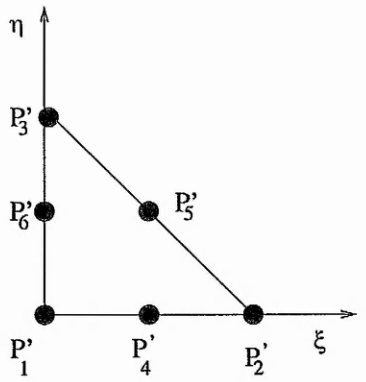

Figure 2.5: $\xi - \eta$ space triangle in figure (2.5)

(2.61) but in terms of ξ and η

$$N_i = c_1 + c_2\eta + c_3\xi + c_4\eta^2 + c_5\eta\xi + c_6\xi^2 \tag{2.64}$$

We will now determine six sets of the six c_i coefficients which will be obtained using the simple properties of the shape functions. For example for the N_1 function that is assigned to the node P_1 in figure (2.5) we will have

$$\begin{aligned}
1 &= c_1 && (P_1)\\
0 &= c_1 + c_2 + c_4 && (P_2)\\
0 &= c_1 + c_3 + c_6 && (P_3)\\
0 &= c_1 + \tfrac{c_3}{2} + \tfrac{c_4}{4} && (P_4)\\
0 &= c_1 + \tfrac{c_2}{2} + \tfrac{c_3}{2} + \tfrac{c_4}{4} - \tfrac{c_5}{4} + \tfrac{c_6}{4} && (P_5)\\
0 &= c_1 + \tfrac{c_3}{2} + \tfrac{c_6}{4} && (P_6)
\end{aligned}$$

for which we see that we have six equations of for six unknowns and for which it follows

that we may readily obtain the solutions for the coefficients that $c_1 = 1, c_2 = -3, c_3 = -3, c_4 = 2, c_5 = 4$ and $c_6 = 2$. The first shape function N_1 in equation (2.64) now takes the form

$$N_1(\xi, \eta) = 1 - 3\xi - 3\eta + 2\eta^2 + 4\xi\eta + 2\eta^2 = (1 - \eta - \xi)(1 - 2\xi - 2\eta) \tag{2.65}$$

which equals one at P_1 and zero elsewhere. In a similar manner we may recover the other five shape functions

$$\begin{aligned} N_2 &= \xi(2\xi - 1) \\ N_3 &= \eta(2\eta - 1) \\ N_4 &= 4\xi(1 - \xi - \eta) \\ N_5 &= 4\xi\eta \\ N_6 &= 4\eta(1 - \xi - \eta) \end{aligned}$$

A more convenient coordinate system is that of the "natural coordinates" where the triangle is subdivided into 3 smaller triangles T_1, T_2 and T_3 as shown in figure (2.6) defined by drawing lines from any point, P to the corners P_1, P_2 and P_3.

This allows us to introduce three new coordinates ζ_1, ζ_2 and ζ_3 which are geometrically defined as the ratio of the relative area of the subtriangle with respect to the full triangle, i.e.,

$$\zeta_i = \frac{F_i}{F}, \qquad i = 1, 2, 3 \tag{2.66}$$

where F_i are the area of the subtriangles T_i, and F is the area of the whole triangle, thereby

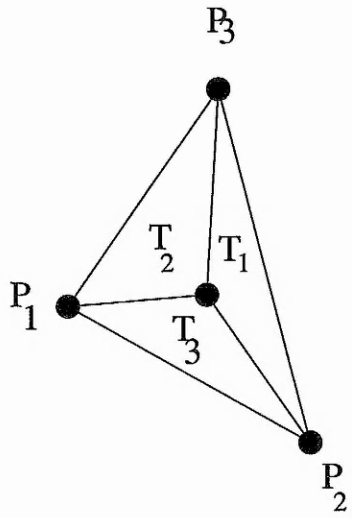

Figure 2.6: Subdivision of a general triangle in terms of the natural coordinate system

allowing us to uniquely define the point P and given that

$$\zeta_1 + \zeta_2 + \zeta_3 = 1. \tag{2.67}$$

We may now calculate x and y in terms of ζ_1, ζ_2 and ζ_3 which yields

$$\begin{aligned} x &= x_1\zeta_1 + x_2\zeta_2 + x_3\zeta_3 \\ y &= y_1\zeta_1 + y_2\zeta_2 + y_3\zeta_3 \end{aligned} \tag{2.68}$$

where x_1, x_2 and x_3 are the x coordinates of P_1 and y_1, y_2 and y_3 are the y coordinates of P_1. In the unit triangle we have to replace x by ξ which gives us $\xi = \zeta_2$ and similarly we have to replace the y coordinate with η which gives us $\eta = \zeta_3$ which then allows us to relate these quantities

$$\zeta_1 = 1 - \xi - \eta \tag{2.69}$$

and thereby rewrite the shape functions in terms of our new natural coordinates

$$
\begin{aligned}
N_1 &= \zeta_1(2\zeta_1 - 1) \\
N_2 &= \zeta_2(2\zeta_2 - 1) \\
N_3 &= \zeta_3(2\zeta_3 - 1) \\
N_4 &= 4\zeta_1\zeta_2 \\
N_5 &= 4\zeta_2\zeta_3 \\
N_6 &= 4\zeta_1\zeta_3
\end{aligned}
$$

If for example, the point P is at the corner of the triangle, P_1 then $\zeta_1 = 1, N_1 = 1$, the other quantities $N_2 - N_6$ must then all vanish and so F_1 is the area of the whole triangle and the areas of the subtriangles F_2, F_3 vanish. These coordinates allow us to freely manipulate the shape functions as no preferred direction has been introduced. This may be readily seen by the fact that the introduction of a cyclic permutation on the ordering of the numbering of the element, recovers the same set of shape functions $N_1 - N_6$. The shape functions are now known as functions of ξ and of η so that in every single triangle element we may represent the required solution u_a as a quadratic polynomials over the triangle as

$$u_a = \sum_{1=1}^{6} u_i N_i(\eta, \xi) \tag{2.70}$$

so that we may calculate derivatives with respect to ξ and η and then transform back and find the derivatives with respect to x and to y on each element. If we have continuity then we could construct global shape functions from the contributions of all the elements in the domain with nearest neighbour element contributions as discussed earlier. Returning to

the method of transformation to the unit triangle, we have a linear transformation between (x, y) and (ξ, η)

$$\begin{aligned} x &= c_1 + c_2\xi + c_3\eta \\ y &= c_4 + c_5\xi + c_6\eta \end{aligned} \tag{2.71}$$

and then calculate the coefficients c_i. For point P_1 at (x_1, y_1) in the (x, y) general triangle (in figure (2.5)) mapping to the point P_1' at $(0, 0)$ in the (ξ, η) unit triangle, we have $\xi = 0$ and $\eta = 0 \Rightarrow x_1 = c_1$ and $y_1 = c_4$. Similarly for the mapping of the other points we have $P_2(x_2, y_2) \mapsto P_2'(1, 0)$ gives $x_2 = c_1 + c_2$ and $y_2 = c_4 + c_5$ and $P_3(x_3, y_3) \mapsto P_3'(0, 1)$ gives $c_3 = x_3 - x_1$ and $c_6 = y_3 - y_1$. Substitution of these coefficients back into equation (2.71) gives us the general transformation for any point in the triangle

$$x = x_1 + (x_2 - x_1)\xi + (x_3 - x_1)\eta \tag{2.72}$$

$$y = y_1 + (y_2 - y_1)\xi + (y_3 - y_1)\eta \tag{2.73}$$

This allows us to transform between the (x, y) and (ξ, η) spaces given the appropriate Jacobian which will allow us to calculate integrals

$$\begin{aligned} dxdy = |J|\, d\xi d\eta &= \begin{vmatrix} \frac{\partial x}{\partial \xi} & \frac{\partial y}{\partial \xi} \\ \frac{\partial x}{\partial \eta} & \frac{\partial y}{\partial \eta} \end{vmatrix} d\xi d\eta \\ &= \begin{vmatrix} x_2 - x_1 & y_2 - y_1 \\ x_3 - x_1 & y_3 - y_1 \end{vmatrix} d\xi d\eta \\ &= \left((x_2 - x_1)(y_3 - y_1) - (x_3 - x_1)(y_2 - y_1)\right) d\xi d\eta \end{aligned} \tag{2.74}$$

It is worth noting that the choice of mapping to a unit triangle ensures that the above determinant remains non-zero for each element which guarantees that our transformation

is invertible as required. To calculate the derivatives $\frac{\partial u_a}{\partial x}$ and $\frac{\partial u_a}{\partial y}$ for this transformation, we will consider u_a as a known function of η and ξ and consider the quantities η and ξ as functions of x and of y. On the unit triangle we will know the values of $\frac{\partial u_a}{\partial \xi}$ and $\frac{\partial u_a}{\partial \eta}$ and are then able to perform an invertible linear transformation

$$\frac{\partial u_a}{\partial x} = \frac{\partial u_a}{\partial \xi}\frac{\partial \xi}{\partial x} + \frac{\partial u_a}{\partial \eta}\frac{\partial \eta}{\partial x} \tag{2.75}$$

$$\frac{\partial u_a}{\partial y} = \frac{\partial u_a}{\partial \xi}\frac{\partial \xi}{\partial y} + \frac{\partial u_a}{\partial \eta}\frac{\partial \eta}{\partial y} \tag{2.76}$$

The factors $\frac{\partial \xi}{\partial x}$, $\frac{\partial \xi}{\partial y}$, $\frac{\partial \eta}{\partial x}$ and $\frac{\partial \eta}{\partial y}$ are then found by differentiating the transformation equations (2.73) with respect to x and to y which gives two sets of two linear equations for two unknowns. For example in the case of the x coordinate

$$1 = (x_2 - x_1)\,\xi_x + (x_3 - x_1)\,\eta_x \tag{2.77}$$

$$0 = (y_2 - y_1)\,\xi_x + (y_3 - y_1)\,\eta_x \tag{2.78}$$

where $\xi_x = \frac{\partial \xi}{\partial x}$ and $\eta_x = \frac{\partial \xi}{\partial x}$. These equations are readily expressed in the form of a system of linear equations

$$\begin{pmatrix} x_2 - x_1 & x_3 - x_1 \\ y_2 - y_1 & y_3 - y_1 \end{pmatrix} \begin{pmatrix} \frac{\partial \xi}{\partial x} \\ \frac{\partial \eta}{\partial x} \end{pmatrix} = \begin{pmatrix} 1 \\ 0 \end{pmatrix} \tag{2.79}$$

so we are now able to invert this matrix to give us

$$\frac{\partial \xi}{\partial x} = \frac{y_3 - y_1}{(x_2 - x_1)(y_3 - y_1) - (x_3 - x_1)(y_2 - y_1)} \tag{2.80}$$

$$\frac{\partial \eta}{\partial x} = -\frac{y_2 - y_1}{(x_2 - x_1)(y_3 - y_1) - (x_3 - x_1)(y_2 - y_1)} \tag{2.81}$$

similarly for the y derivatives

$$\frac{\partial \xi}{\partial y} = -\frac{x_3 - x_1}{(x_2 - x_1)(y_3 - y_1) - (x_3 - x_1)(y_2 - y_1)} \tag{2.82}$$

$$\frac{\partial \eta}{\partial y} = \frac{x_2 - x_1}{(x_2 - x_1)(y_3 - y_1) - (x_3 - x_1)(y_2 - y_1)} \tag{2.83}$$

the denominators for these four quantities are merely the Jacobian of the transformation, J, used in (2.74).

2.2.3 Implementation of the differential operator and integration method

The most general form of the linearised Fréchet differential operator $D_u G u_a$ which we need to solve in the Keller method is given by

$$-\frac{\partial}{\partial x}\left[a_1 \frac{\partial u_a}{\partial x}\right] - \frac{\partial}{\partial y}\left[a_2 \frac{\partial u_a}{\partial y}\right] - \frac{\partial}{\partial x}\left[a_3 \frac{\partial u_a}{\partial y}\right] - \frac{\partial}{\partial x}\left[a_4 \frac{\partial u_a}{\partial x}\right] + a_5 u_a - a_6 \frac{\partial u_a}{\partial x} - a_7 \frac{\partial u_a}{\partial y} = R \tag{2.84}$$

where $a_i = a_i\left(x, y, u_{ao}, \frac{\partial u_{ao}}{\partial x}, \frac{\partial u_{ao}}{\partial y}\right)$ for known solutions u_{ao} and where the coordinates x, y may be generalised to other coordinate systems such as the spherical polar system. The index i runs from one to seven. The R_i are given by $R_i = b_i - \frac{\partial b_2}{\partial x} - \frac{\partial b_3}{\partial y}$ where $b_i = b_i\left(x, y, u_{ao}, \frac{\partial u_{ao}}{\partial x}, \frac{\partial u_{ao}}{\partial y}\right)$. It remains to solve the system of linear algebraic equations of the form (2.53) that results from the finite element discretisation procedure that we have outlined above. The matrix A takes the form of a banded matrix together with an augmented matrix which incorporates the information that arises from the boundary conditions. Firstly, $\hat{u}$ is represented by the finite elements and substituted into the linearised

differential operator and we sum over all the elements and over all the integration points of each triangle. The integrations must be of the form $\int_{\triangle} a_j N_j N_k dxdy$ where the a_j are functions of space that have been determined numerically. These numerical integrations can be carried out reliably and accurately using the method of Gaussian integration. As we are using triangular finite elements then we will use the formula appropriate for the unit triangle

$$\int_{\triangle} f(\xi, \eta) = \sum_{1=1}^{7} w_i f(\xi_i, \eta_i) \tag{2.85}$$

where the seven integration points are shown in figure (2.7) and where the values of the coordinates are given in table (2.1). Equation (2.85) gives exact integrals for polynomia up to degree five. More comprehensive details of these methods may be found in standard textbooks on the subject (e.g., Wait & Mitchell , 1985, Braess , 1997).

i	ξ_i	η_i	w_i
1	$1/3$	$1/3$	0.225
2	$\frac{6+\sqrt{15}}{21}$	$\frac{6+\sqrt{15}}{21}$	$\frac{155+\sqrt{15}}{2400}$
3	$\frac{9-2\sqrt{15}}{21}$	$\frac{6+\sqrt{15}}{21}$	$\frac{155+\sqrt{15}}{2400}$
4	$\frac{6+\sqrt{15}}{21}$	$\frac{9-2\sqrt{15}}{21}$	$\frac{155+\sqrt{15}}{2400}$
5	$\frac{6-\sqrt{15}}{21}$	$\frac{6-\sqrt{15}}{21}$	$\frac{155-\sqrt{15}}{2400}$
6	$\frac{9+2\sqrt{15}}{21}$	$\frac{6-\sqrt{15}}{21}$	$\frac{155-\sqrt{15}}{2400}$
7	$\frac{6-\sqrt{15}}{21}$	$\frac{9+2\sqrt{15}}{21}$	$\frac{155-\sqrt{15}}{2400}$

Table 2.1: The coordinates and weights for Gaussian integration where seven points were used to integrate fifth order polynomials exactly and where quadratic shape functions have been used on the unit traingle.

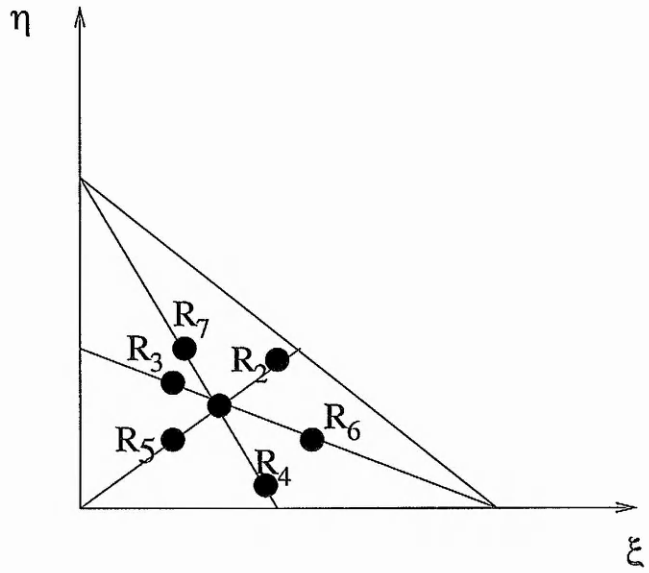

Figure 2.7: Schematic illustration of integration points in an element centred on a point R_i

Chapter 3

Physical models

3.1 Constant pressure models

In the work of Mestel & Spruit (1987) the effect of the variation of angular velocity (and therefore of the centrifugal forces) on the magnetic field structure was investigated. The authors were then able to estimate the dependence of the rate of magnetic braking (of the field on the plasma) on the rotation of the star. The structure of a magnetic field B that may be resolved into toroidal ($\mathbf{B_t}$) and poloidal ($\mathbf{B_p}$) components

$$\mathbf{B} = \mathbf{B_p} + \mathbf{B_t} \tag{3.1}$$

is supposed to be such that the poloidal component is given and therefore such that the pressure at the coronal base is fixed. In axisymmetric systems such as these, it may be shown that the angular momentum loss rate of the plasma is equivalent to that carried by gas kept in strict corotation with the star out to an Alfvénic surface S_A where the wind

speed becomes Alfénic which is defined by

$$v_p = v_A = \frac{B_p}{(4\pi\rho)^{\frac{1}{2}}} \tag{3.2}$$

for a poloidal plasma velocity v_p and Alfvénic velocity v_A (for a detailed review of magnetic stellar wind theory see Collier Cameron et al. (1991) and Mestel (1999)). By parameterising the dynamo relation between the pole strength B_o of the dipolar component of the field and the stellar rotation rate Ω by

$$B_o \propto \Omega^p \tag{3.3}$$

for some value p, the authors were able to construct a simply parametrised field model that gives rise to a multi-component corona wherein the Alfénic surface moves further outwards from the star with increasing field (which results from the increasing activity of the dynamo driven by the increasing rotation). The stronger field then tends to trap more gas within a so-called, 'coronal dead-zone' the extent of which is limited by the magnetic pressure required to balance the higher centrifugal force and which does not contribute to the magnetic braking. If the local plasma pressure at the summits of the tallest loops exceeds the magnetic pressure then the loops may be blown open and the extent of the closed corona would thereby be reduced. It is clear then that deep within the Alfvénic surface (where the field is relatively strong and where $v_p << v_A$) the thermal and centrifugal forces that drive the stellar wind are insufficient to distort the magnetic field significantly. A schematic illustration of this model is given in figure (3.1) where the field line ABC shows the extent of the dead-zone. With a dipole aligned with the stellar rotation axis and with an assumed dipole flux distribution over the stellar surface,

the authors derived an expression for denisty using the field-aligned equation of MHS equilibrium. This density is chosen to be constant with θ at the coronal base. However, if the appropriate $p_0(A)$ for such a constant coronal base density is chosen, it turns out that the current density deriving from such a $p_0(A)$ will be incorrectly directed, i.e., it acts to stretch field lines. The pressure gradient on the other hand, is acting inwards so that the forces will be balancing in a counterintuitive manner for such a model. We will show this in more detail below. The conclusions of the authors are in no significant way affected by this detail as their attention is focused on the braking-rates for which other terms are more significant.

The effective potential, U, in which the plasma moves includes both gravitational and centrifugal terms. It is given in equation (1.51) and appears in the simple isothermal surface pressure distribution discussed in the introduction (equation (1.66)) where it was noted that the pressure and field quantities $p_o(A,U)$ and B_ϕ remained to be specified. In this chapter, we set the toroidal component to zero whilst for $p_0(A)$, the most simple point from which to proceed is to assume a constant base pressure. It is then convenient to collect the physical constants of the system together by normalising the radial coordinate r to the stellar radius $R_\star$, yielding two parameters in the pressure exponent

$$\xi_1 = \frac{GM_\star m_p}{k_B T_\star R_\star} \tag{3.4}$$

$$\xi_2 = \frac{\Omega_\star^2 R_\star^2 m_p}{k_B T_\star} \tag{3.5}$$

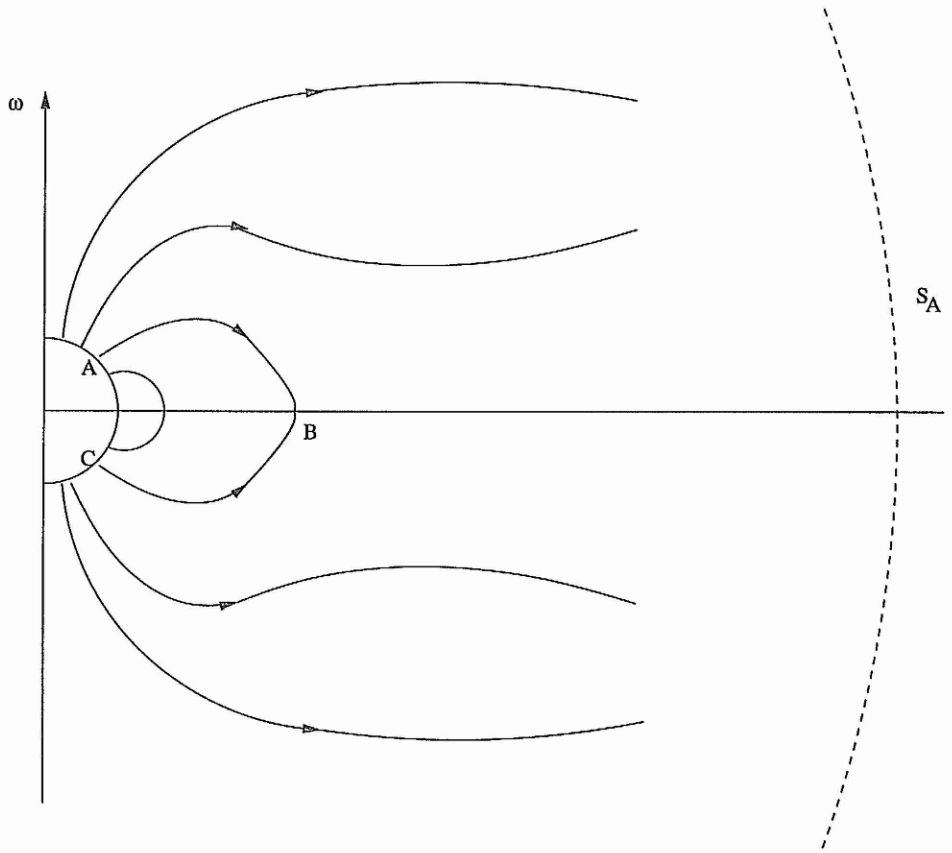

Figure 3.1: Schematic illustration of the magnetic field model developed by Mestel & Spruit (1987). S_A is the Alfvén surface and ABC indicates the extent of the coronal "dead-zone".

where the symbols have their usual meanings and m_p is the mass of a proton. The first parameter, ξ_1 (equation(3.4)), represents the ratio of the gravitational energy of a proton at a distance $R_\star$ from the centre of a star of mass $M_\star$ to the thermal energy of a gas with temperature $T_\star$, whereas the second parameter ξ_2 (equation(3.5)), gives the rotational kinetic energy of a proton at the stellar surface to the thermal energy that the proton would possess. For a surface dipole field, the pressure takes the form

$$p\left(A,U\right) = \bar{p}\exp[\xi_1\left(\frac{1}{\tilde{r}}-1\right)-\frac{\xi_2}{2}\left(\tilde{A}-\tilde{r}^2\sin^2\theta\right)] \tag{3.6}$$

where $\bar{p}$ is the coronal base pressure, $\tilde{A}$ is the normalised flux function and where $\tilde{r}$ is a suitably normalised radial coordinate (the normalisation will be discussed later in this chapter). In the manner outlined in our discussion of appropriate boundary conditions in the introduction we impose a magnetic dipole field on the stellar surface that will satisfy the Grad-Shafranov equations (1.59) and (1.60) nontrivially (i.e. where $\frac{\partial p_o}{\partial A} \neq 0$)

$$A = A_o \sin^2\theta \tag{3.7}$$

at $r = R_\star$ and at the outer boundary condition at 50 stellar radii (or $r = r_{out}$). Normalising the scalar flux function,

$$\tilde{A} = \frac{A}{A_o} \tag{3.8}$$

allows the force balance equation to be written in terms of a normalised pressure

$$-\frac{\partial^2\tilde{A}}{\partial\tilde{r}^2}-\frac{\sin\theta}{\tilde{r}^2}\frac{\partial}{\partial\theta}\left(\frac{1}{\sin\theta}\frac{\partial\tilde{A}}{\partial\theta}\right) = \lambda\tilde{r}^2\sin^2\theta\frac{\partial\tilde{p}}{\partial\tilde{A}}. \tag{3.9}$$

where

$$\lambda = \frac{\mu_0 R_\star^4\bar{p}}{A_o^2}$$

However, one can immediately see that the cross-field pressure gradient

$$\left(\frac{\partial p}{\partial A}\right)_U = -\frac{\xi_2}{2} p < 0 \tag{3.10}$$

Since ∇A generally points outwards, the pressure increases outwards, which is certainly unphysical. This has been shown to be the case in our numerical calculations, in which we have demonstrated a shrinking of field lines instead of the expected expansion. We therefore have to dismiss this simple approach to fix $p_0(A)$ and must seek a different approach to choose p. Our discussion of this choice is postponed to chapter 3.3 with mathematical details provided in the appendix.

3.2 Inclusion of magnetic moment in the boundary conditions

In the first chapter, the boundary conditions for the simplest possible realistic physical model was broadly outlined. On the outer boundary the dipole flux, A was prescribed

$$A = \frac{\sin^2 \theta}{r_{out}} \tag{3.11}$$

for some suitable distance from the stellar surface, r_{out}. The presence of an additional magnetic dipole moment caused by the magnetospheric currents, is a relatively straightforward modification to the models and is one which considerably enhances the physical realism of the models. Furthermore, the form of the predictor-corrector method which we have chosen as a numerically convenient algorithm with which to solve the Grad-Shafranov equation (as outlined in the preceding chapter) has the additional advantage

that it may be readily tailored to the incorporation of an additional dipole moment in the outer boundary conditions. A generalized magnetic dipole moment may be described in terms of the distribution of a current density $\mathbf{J}(r,\theta)$ in a volume τ

$$\mathbf{m} = \frac{\mu_0}{8\pi}\int_\tau \mathbf{r}\times\mathbf{J}\ d\tau \tag{3.12}$$

In an axisymmetric system, the right hand side of the Grad-Shafranov equation (1.59) gives us the axial component of the current density (in spherical polar coordinates, (r,θ,ϕ)) so that the cross product in the integrand of equation (3.12) will result in a quantity directed in the opposite sense to the poloidal angle, θ. By use of simple coordinate geometry this may then be related to a more convenient form in terms of the cylindrical coordinates $(\varpi, \alpha, \mathrm{z})$

$$\mathbf{r}\times\mathbf{J} \ \propto\ \mathbf{r}\times\mathbf{e}_\phi \ =\ -\mathbf{r}\mathbf{e}_\theta \ =\ -\mathbf{r}\left(\cos\theta\mathbf{e}_\varpi - \sin\theta\mathbf{e}_\mathbf{r}\right) \tag{3.13}$$

In general, for an axisymmetric system, the axial component of the dipole moment in cylindrical coordinates may be readily related to the toroidal component of the current density in spherical coordinates

$$m_z \propto \int_0^{2\pi}\int_1^\infty\int_0^\infty \tilde{r}^4\sin^3\theta\frac{\partial\tilde{p}}{\partial\tilde{A}}d\phi dr d\theta. \tag{3.14}$$

The full form of the dipole moment is then expressed as a double integral over the domain where the constants have been gathered into the term in front of the integral and where the exponential term has been written more conveniently as the function $n = n(A,\lambda)$. In this model, the quantity λ is dependent upon various model parameters and we obtain

$$\mathbf{m} \propto \lambda\int_1^\infty\int_0^\pi \tilde{r}^4\left(sin^3\theta\mathbf{e}_\mathbf{r} - \cos\theta\sin^2\theta\mathbf{e}_\varpi\right)n(A,\lambda)dr d\theta \tag{3.15}$$

The second term in the brackets makes no contribution to the integral and will vanish upon consideration of its symmetry properties.

The final form taken by the dipole moment is one which will be readily seen to be particularly convenient as it is complementary to the numerical formulation that we have already adopted in order to calculate our sequences of MHS equilibria

$$\hat{m} = \frac{\lambda}{4}\int_1^{\infty}\int_0^{\pi} \tilde{r}^4 \sin^3\theta \, n(A,\lambda) d\tilde{r} d\tilde{\theta} \tag{3.16}$$

$$:= \frac{\lambda}{4} I \tag{3.17}$$

Introducing the more convenient quantity, I to denote the integral, it then follows that a simple first differentiation of equation (3.17) yields

$$\frac{d\hat{m}}{d\lambda} = \frac{1}{4} I + \frac{d\lambda}{4}\frac{dI}{d\lambda} \tag{3.18}$$

where

$$\frac{dI}{d\lambda} = \int_0^{\infty}\int_0^{\pi} \tilde{r}^4 \sin^3\theta \left[\frac{\partial n}{\partial \lambda} + \frac{\partial n}{\partial A}\frac{\partial A}{\partial \lambda}\right] d\tilde{r} d\tilde{\theta} \tag{3.19}$$

In the preceding chapter on the numerical methods that we have deployed, we discussed the implementation of a more convenient 'alternative formulation' to that which was originally developed by Zwingmann (1987). To calculate the Dirichlet boundary conditions, this method yields an equation (2.36) that is of the same structure as the above equation. This allows us to substitute $\frac{\partial A}{\partial \lambda}$ for v and to calculate v during the iteration. $\hat{m}$ then modifies the outer boundary conditions from that which it takes in the absence of a magnetic dipole moment (i.e. $A = \frac{\sin^2\theta}{r_{out}}$) to the new form

$$A = (1+\hat{m})\frac{\sin^2\theta}{r_{out}} \tag{3.20}$$

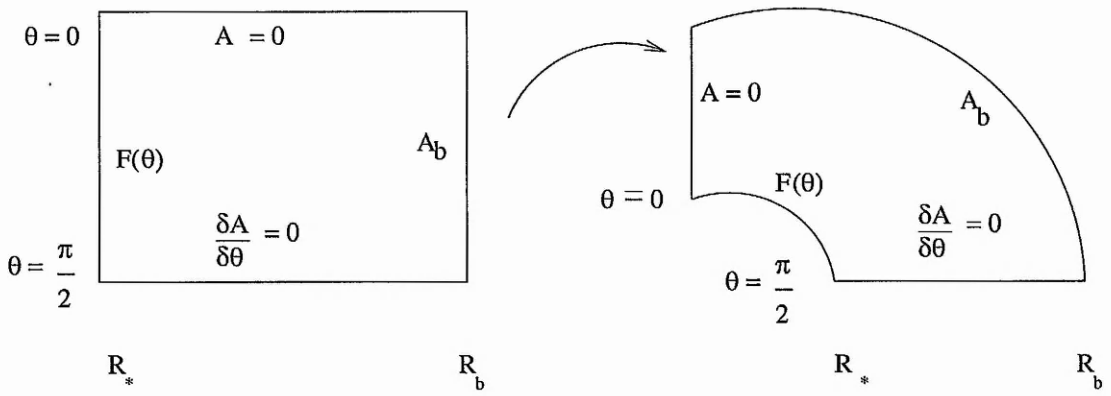

Figure 3.2: Transformation of the rectangular domain to the magnetospheric domain

which may be easily implemented in the numerical code. Once our boundary conditions have been formulated, we can transform our rectangular finite element discretised domain to that of the magnetospheric domain in the manner outlined in figure (1.5) and figure (3.2) in the introductory chapter.

3.3 Scaling models

In our introduction we reviewed magnetic activity in rotating stellar coronae with passing reference to the influence of the magnetic dynamo, particularly with respect to explaining the observed saturation of magnetic activity with increasing rotation. One explanation was offered by Jardine & Unruh (1999) in the form of so-called *centrifugal stripping* where the emission saturation is explained by a reduction in the volume of the X-ray emitting corona with increasing rotation. In theses models, the authors calculate densities, emission measures and radiative losses which can then be integrated over the

emitting volume. All the key quantities, namely the base pressure, magnetic flux and conductive flux (F), are scaled as a function of rotation rate, Ω, such that $p_0(\Omega) \propto \Omega^{2q}$, $B_0(\Omega) \propto \Omega^q$ and $F_0 \propto \Omega^{4q-1.5}$ where $-1 < q < 2$. However, it is the equation of motion for plasma associated with the *undistorted* magnetic (dipolar or quadrupolar) field lines of their closed-field pressure-limited coronae that they have considered. This form of scaling would seem to form a natural starting point with which to refine and advance our models so that we are able to solve not just for force-free ($\mathbf{J} \times \mathbf{B} \approx \mathbf{0}$) fields but for the full force-balance equation and allow for distortions of the field by pressure, gravitational and by centrifugal forces given an isothermal magnetosphere and a simple, physically plausible coronal surface pressure distribution.

To adapt such a system of scalings to our purposes we choose to scale the coronal (equatorial) surface quantities of temperature, $T_\star$, plasma density $\rho_\star$ and magnetic field $B_\star$ to the rotation rate, Ω in terms of the relevant well-observed solar quantities which have been denoted with the $\odot$ subscript. As we have already stated, we will begin by provisionally neglecting the azimuthal component of the magnetic field to allow us to make progress more readily. The scaling relations for $T_\star$, $\rho_\star$ and $B_\star$ are

$$T_\star = T_\odot \left(\frac{\Omega}{\Omega_\odot} \right)^n \tag{3.21}$$

$$\rho_\star = \rho_\odot \left(\frac{\Omega}{\Omega_\odot} \right)^m \tag{3.22}$$

$$B_\star = B_\odot \left(\frac{\Omega}{\Omega_\odot} \right)^q \tag{3.23}$$

These quantities are the fundamental physical variables which appear in the force-balance equation from which we construct our equilibria. It remains to specify a real-

istic form of surface pressure distribution. The barometric pressure is given in our introductory discussion of surface pressure distributions as equation (1.66) as $p(A,U) = p_0(A)\exp(-URT)$) and is the most useful option, although $p_0(A)$ remains to be specified as a free function. Through its dependence on U, (the effective potential in which the plasma is confined and which consists of the gravitational and centrifugal potentials as given by equation (1.52)) the pressure already contains the contribution of the centrifugal force to the balance of forces. Our choice for $p_0(A)$ is motivated by that which we have derived by assuming that the electron and ion distribution functions are given take the form of drifting Maxwellian distributions, i.e.

$$p_0 \propto \exp(A) \tag{3.24}$$

which is similar in form to that which we derived by considering a rotating isothermal magnetosphere within the framework of Vlasov theory and in a manner similar to that adopted by Neukirch (1993a) but incorporating the additional feature of a gravitational field. An outline of this derivation is given in Appendix A. Starting from an undisturbed dipole field at the coronal base we may then solve the force-balance equation and construct a sequence of equilibria, it will be a straightforward matter to calculate some form of emission measure proxy. Hundhausen (HAO Report, 1993) gives the total free-free collision emission measure integrated over all wavelengths as being proportional to the quantity $\int N^2 d\ell$ and so it is the density dependence which enters uniformly into the emission processes and which will allow us to use ρ^2 as the basis of our emission measure proxy

$$EM \propto \int_c \rho^2 dV \tag{3.25}$$

integrated over the closed-field line region. Once an equilibrium has been calculated, the density is readily recovered from the solution of the pressure gradient given by equation (1.65) but which will clearly depend on the form of assumed surface pressure distribution. Other factors such as the gaunt factor and temperature will be scaled out by considering the emission measure relative to the solar emission measure or to some other typical emission measure to the scalings of magnetic field, density and temperature. The former may be appropriate where $q = 1, m = 1$ and $n = 1$ but the latter might not necessarily be an appropriate scaling for stars defined by other sets of parameters. A more detailed discussion of the derivation, background and applicability of such forms of the emission measure is given in Hundhausen (HAO Report, 1993).

It remains to consider the closed-field coronal volume, from which most of the X-ray emission will originate. It follows then, that in order to determine the fraction of emitting closed magnetic flux it is necessary to introduce some form of cut-off criterion for the flux that will determine the extent of the emitting magnetosphere and therefore we are required to specify a cut-off field-line for each equilibrium solution that we have calculated. None of the plasma found beyond this field-line will therefore contribute to the integrated emission measure but instead the emission will only originate from that plasma associated with flux bound within this field-line. The absence of a contribution to the emission from plasma found beyond this last closed field-line (where the flux is open to the stellar wind) is concomitant with our assumed neglect of poloidal flows in the stellar corona, as discussed in the introductory formulation of model magnetospheres and which we justified by means of the solar-stellar paradigm. A means of constructing an

appropriate cut-off criterion may be found by considering the stressing of coronal fields as the current density in the magnetosphere increases as we evolve along the sequence of equilibrium solutions. The models of Jardine & Unruh (1999) were confined to potential fields with no electric currents, however the work of Wolfson & Dlamini (1999) cites observations of nonradial density variations (and therefore nonradial pressure gradients) in the solar corona as a motivation for considering the role of deviations from force-free conditions in coronal evolution with specific reference to the onset of coronal mass ejections. When coronal currents do contribute to the magnetic field then it is altered from the potential field with the same boundary conditions on the normal field at the coronal base. The field aligned current picture is adequate for the lower corona where the plasma beta is low, however the thermal pressure ($W_t \propto \int PdV$) will drop off more slowly than the magnetic energy density ($W_m \propto \int \frac{B^2}{2} dV$) so that the plasma beta will begin to rise in the outer corona where cross-field currents will begin to become more significant and distort the field-lines. The thermal pressure of the plasma must therefore roughly balance the pressure from the magnetic energy density at some point in the magnetosphere, as we move from the lower to the upper corona. At this point, where $\beta \approx 1$ we may consider the field to be sufficiently distorted as to allow us to choose to neglect the emission associated with any further flux that lies beyond the field-line where we have found the pressures to roughly balance. Equivalently we can state that the current density, $j_\phi = r \sin\theta \frac{\partial p}{\partial A}$ is zero on those field lines beyond the cut-off radius. For the purposes of computational practicality it is considerably more convenient to seek the "last closed field line" where $\beta \approx 1$ in the equatorial plane.

In terms of the above scalings of the magnetic field, density and temperature (equations (3.21)-(3.23)) the normalised force balance equation (3.9) now yields the following form of λ

$$\begin{aligned}\lambda &= \frac{\mu_0 R^4 p_\star}{A_0^2} = \frac{\mu_0 k_B T_\star \rho_\star}{B_\star^2} \\ &= \frac{\mu_0 k_B T_\odot \rho_\odot}{B_\odot^2} \left(\frac{\Omega}{\Omega_\odot}\right)^{n+m-2q} \\ &= \frac{1}{2}\beta_\odot \left(\frac{\Omega}{\Omega_\odot}\right)^{n+m-2q} \end{aligned} \tag{3.26}$$

where we have used the relation

$$p_\star = c_s^2 \rho_\star = \frac{k_B T_\star}{m_p} \rho_\star \tag{3.27}$$

for an isothermal corona, and where c_s denotes the acoustic speed. λ is a coefficient to the pressure gradient, $\frac{\partial p}{\partial A}$ in the force-balance equation which in turn is proportional to the toroidal component of the current density, j_ϕ. Advancing along the equilibrium sequence (for a given rotation rate) therefore increases the current density in the magnetosphere until the cut-off criterion is satisfied. While calculating sequences in λ, we formally keep ξ_1 and ξ_2 (normalised in the following section 3.3) and thus Ω, n and m, fixed. In order to be able to construct a sequence of solutions with varying Ω for a given set of parameters m, n and q, we will have to construct λ sequences for an array of Ω values. For a given $\beta_\odot$ and m, n, q we can then construct a sequence of emission measures with varying Ω. Since the required value of λ for a given parameter set will usually lie between two different solutions of a λ sequence ($\lambda_i < \lambda < \lambda_{i+1}$), it is necessary to use a linear interpolation to

extract the emission measure for the given parameters at a specific rotation rate as

$$EM(\lambda) = EM_i + \frac{\lambda - \lambda_i}{\lambda_{i+1} - \lambda_i}\left(EM_{i+1} - EM_i\right) \tag{3.28}$$

By changing the scaling parameters (n, m, q) within physically acceptable ranges we are able to consider the values which will match the observations most closely. Likely values for the exponent of the magnetic field B on the stellar surface with rotation rate (or the proxy for the relation between the dynamo and rotation) q are $0 < q < 2$. For the exponent of the scaling of the plasma density at the coronal base with rotation rate, m the likely values fall in the range $-1 < m < 1$ and for the exponent of the isothermal temperature scaling, n the values fall in the range $0 < n < 2$. Solar physics literature suggests that a reasonable value for quiet solar coronal base beta would be in the range $0.01 < \beta_\star < 0.3$. Furthermore, we are able to easily change our scalings from solar values to those of a different class of stars (such as M-dwarves) in order to compare our models with the observed saturation and super-saturation curves for those stars.

3.3.1 Normalisation

In the absence of an azimuthal component, the form of the magnetic dipole field is as given in equation (1.36) with $A = \alpha\frac{\sin^2\theta}{r}$ for some constant α. It then follows that the full form of the magnetic field may be given as

$$\mathbf{B} = \alpha\left(\frac{2\cos\theta}{r^3}\mathbf{e}_r + \frac{\sin\theta}{r^3}\mathbf{e}_\theta\right) \tag{3.29}$$

At the equator of the stellar surface, where $r = R_\star$ and $\theta = \frac{\pi}{2}$ the surface field will be $B_\star = \frac{\alpha}{R_\star^3}$ so that if we normalise the flux function A to one at $\theta = \frac{\pi}{2}$, $r = R_\star$ and

normalise r to $R_\star$ then α is also normalised to one. The form of the pressure distribution to be prescribed on the stellar surface has been motivated by our calculations for a model magnetosphere using Vlasov theory (given by equations (A.21) and (A.23) as discussed in the appendix) which then suggests that the pressure be prescribed as follows

$$p(A,U) = p_\star \exp\left[\xi_3 (A-1) - \frac{U}{k_B T}\right] \tag{3.30}$$

where ξ_3 is a free parameter which indicates the strength of the current density associated with the pressure gradients across the magnetic field and where the gravitational potential, U, is given by

$$U = -\left(\frac{GM_\star\mu}{r} - \frac{GM_\star\mu}{R_\star}\right) - \frac{1}{2}\mu\Omega^2\left(r^2\sin^2\theta - R_\star^2\right) \tag{3.31}$$

where μ is the mean atomic weight of the plasma (in the case of a hydrogen plasma, $\mu = \frac{m_p}{2}$ and which we may normalise to obtain

$$U = -\frac{GM\mu}{R_\star}\left(\frac{1}{r} - 1\right) - \frac{1}{2}\mu\Omega^2 R_\star^2\left(r^2\sin^2\theta - 1\right) \tag{3.32}$$

Upon defining the following dimensionless parameters

$$\xi_1 = \frac{GM_\star\mu}{R_\star k_B T} \tag{3.33}$$

$$\xi_2 = \frac{\mu\Omega^2 R_\star^2}{k_B T} \tag{3.34}$$

we arrive at the final forms of the pressure and of the density

$$p(A,U) = p_\star \exp\left[\xi_3 (A-1) + \xi_1\left(\frac{1}{r} - 1\right) + \frac{1}{2}\xi_2\left(r^2\sin^2\theta - 1\right)\right] \tag{3.35}$$

$$\rho = \rho_\star \exp\left[\xi_3 (A-1) + \xi_1\left(\frac{1}{r} - 1\right) + \frac{1}{2}\xi_2\left(r^2\sin^2\theta - 1\right)\right] \tag{3.36}$$

With physical constants taken from Zombeck (1990) the dependence of the constants ξ_1 and ξ_2 (equations (3.33) and (3.34 respectively) may be expressed in terms of their dependence upon the scaling parameters and their scaling dependence in terms of the fundamental stellar model variables of mass, temperature and of radius

$$\xi_1 = 11.5496 \left[\frac{T}{10^6 k}\right]^{-1} \left[\frac{M_\star}{M_\odot}\right] \left[\frac{R_\star}{R_\odot}\right]^{-1} \left[\frac{\Omega}{\Omega_\odot}\right]^{-n} \tag{3.37}$$

$$\xi_2 = 2.1279 \cdot 10^{-4} \left[\frac{R_\star}{R_\odot}\right]^{2} \left[\frac{T_\odot}{10^6 k}\right]^{-1} \left[\frac{\Omega}{\Omega_\odot}\right]^{2-n} \tag{3.38}$$

The isothermal corona condition (equation 3.27) allows us to determine $\rho_\star$ as $\rho_\star = \frac{\mu p_\star}{k_B T_\star}$ and thereby use the scaling relations of $T_\star$ and of $\rho_\star$ (equations (3.21) and 3.22) respectively) to show the scaling dependence of $p_\star$

$$p_\star = \frac{k_B T_\odot \rho_\odot}{\mu} \left(\frac{\Omega}{\Omega_\odot}\right)^{n+m} \tag{3.39}$$

from which it is apparent that $p_\star$ scales as Ω^{n+m} with the rotational velocity, Ω. Returning to consider the cut-off criterion for the last-closed field line ($\beta \ll 1$), we choose to evaluate this criterion in the equatorial plane where $\theta = \frac{\pi}{2}$, with

$$\mathbf{B} = -\frac{1}{r}\frac{\partial A}{\partial r}\mathbf{e}_\theta \tag{3.40}$$

for which all the field lines crossing the plane will experience the maximum distorting effect of centrifugal forces, in the case of a magnetic dipole field configuration. Using normalised coordinates, we now have the cut-off criterion written as a nonlinear equation for r

$$\frac{1}{2r^2}\left(\frac{\partial A}{\partial r}\right)^2 = p_\star \exp\left[\xi_3 (A-1) + \xi_1 \left(\frac{1}{r} - 1\right) + \frac{1}{2}\xi_2 \left(r^2 - 1\right)\right] \tag{3.41}$$

the solution of which gives identifies the location of the cut-off field line, which we must calculate numerically for each solution along the equilibrium sequence. The plasma beta associated with this field line is therefore equal to one in the equatorial plane. The cut-off criterion (from equation (3.41)) can be rewritten in normalised form in terms of our scaling parameters and in terms of corresponding solar variables, by noting that

$$\frac{2\mu_0 p_\star}{B_\star^2} = \frac{2\mu_0 p_\odot}{B_\odot^2}\left(\frac{\Omega}{\Omega_\odot}\right)^{n+m-2q} = \beta_\odot\left(\frac{\Omega}{\Omega_\odot}\right)^{n+m-2q}. \tag{3.42}$$

Once r_c and A_c have been determined, we can calculate the emission measure proxy (equation (3.25)) for $A > A_c$ by substituting in the plasma density, ρ, given by equation (3.36)

$$\begin{aligned} EM &= \int_{\bar{v}} \rho^2 d\bar{V} \\ &= 4\pi\rho_\star^2 \int\int_{A\geq A_c} r^2 dr \sin\theta d\theta \exp\left[2\xi_3 A + \xi_1\left(\frac{1}{r}\right)\right. \\ &\qquad \left. + \xi_2\left(r^2\sin^2\theta - 1\right)\right] \end{aligned} \tag{3.43}$$

where the condition $A \geq A_c$ determines the volume of the magnetosphere for which we have defined the field lines as being closed. The emission measure proxy now takes the form

$$\begin{aligned} EM &= \rho_\star^2 \int\int_{A\geq A_c} \widehat{EM} r^2 \sin\theta dr d\theta \\ &= \rho_\odot^2 \left(\frac{\Omega}{\Omega_\odot}\right)^{2m} \int\int_{A\geq A_c} \widehat{EM} r^2 \sin\theta dr d\theta \end{aligned} \tag{3.44}$$

which is calculated automatically by the numerical code. Given the fundamental solar parameters ($T_\odot, \beta_\odot, \Omega_\odot, R_\odot, M_\odot$) we therefore need to make appropriate choices for the model parameter, ξ_3, the plasma density, temperature and magnetic field scaling param-

eters, m, n, q and then to calculate ξ_1 and ξ_2 at a given stellar rotation rate, Ω, from equations (3.37) and (3.33) respectively. This will determine the position of the cut-off field line, r_c for a given λ (through equation(3.41)), whereby we can calculate the volume of the closed field corona and then integrate the emission measure proxy over that volume (equation(3.44)). By repeating this procedure for a range of different stellar surface rotation velocities we may then construct a curve showing the variation of emission measure with rotation and thence to compare our model results with observations such as those taken by Hempelmann et al. (1995). With a rescaling from solar mass and radius values to those appropriate for M-dwarf stars, we would also then be in a position to generate emission measure curves which could be compared with observations of supersaturation of emission for those stars (James et al. , 2000). The range of stellar rotation velocities for which we may generate these models will be informed by the range of velocities over which the saturation and supersaturation phenomena are observed to occur. Figure (1.3) shows that rotational velocities of up to approximately $180\Omega_\odot$ would be appropriate as our limit. As the rotational velocity of a star is increased, the corotation radius (equation (1.1)) will move inwards towards the stellar surface while the coronal density rises. For example, a star with $\Omega = 10\Omega_\odot$ has a corotation radius at $r_c = 8.0R_\odot$ whereas for a star with $\Omega = 30\Omega_\odot$, the corotation radius is located at $3.8R_\odot$. When the corotation radius has reached the stellar surface (i.e. $r_{corot} = R_\star$) then there will be no emission from the closed field line corona. For a star of solar mass and radius this breakup velocity occurs at $\Omega \approx 233.0\Omega_\odot$ which therefore represents an absolute upper limit on our range of velocities. Further freedom in our models arises through our choice of the scaling parameters

and of ξ_3. The ranges for the former (as given earlier) are informed by current observations whereas the latter may require experimentation. The model and method outlined above provides a natural link between observed stellar magnetic activity and the dynamo mechanism from which all such activity must ultimately originate.

3.3.2 Results

The normalised Grad-Shafranov equation is now in a form such that we can apply the general numerical continuation method (outlined in chapter 2) in order to generate sequences of equilibria. In each case we have fixed the angular velocity, Ω and other parameters in order to calculate equilibrium sequences with varying λ. In practice, this may involve calculating up to (and occasionally beyond) 1000 solutions along each sequence. Variation of the different model parameters (within limits) will distinguish the different equilibrium sequences from each other and will allow us to construct curves of model emission measure against rotation, in the manner described above. In order to compare our model results with recent observations, we have taken the results of Hempelmann et al. (1995) where the authors infer saturation in emission for single F through M spectral type dwarfs. For comparison of our models with observations of single M-dwarfs we have taken results from James et al. (2000) where the authors believe that they have identified evidence of supersaturation in these stars as well as for ultra-fast ($>\approx 100 kms^{-1}$) G and K spectral type dwarfs. When we calculate our emission curves, however, it is necessary to take into consideration the apparent under luminosity of the Sun as seen

from the Hertzsprung-Russell diagram. To normalize our calculated emission measures, we need to estimate an emission measure that would compensate for the observed solar under-luminosity or an emission measure that would be measured from a "solar-type" star in the comparison observations. Averaging of the emission measures of the stars in the comparison sample that possess roughly solar rotational velocities, shows that a suitable choice for normalization would be to take that of roughly twice the solar emission measure.

Figures (3.3), (3.4) and (3.5) show different solution curves for different combinations of model parameters, as compared with the data from Hempelmann et al. (1995). In this work, the authors analysed the coronal X-ray emission of single main sequence stars of spectral type F through to M with photometrically determined rotation periods, using X-ray data from the ROSAT all-sky survey. A qualitative change in behaviour was found for a Rossby number $\sigma \approx 1$. i.e. for $\sigma > 1$ they found that coronal activity dropped more rapidly with increasing Rossby number. From figure (3.3) it can be seen that for equilibrium sequences with the same stellar coronal surface plasma beta, same temperature and same plasma density scaling parameters (n and m), when the magnetic field scaling parameter, q is varied then the emission curves are lowered (comparing the solid and dashed curves) as might be expected because a weaker magnetic field is less effective at confining emitting plasma. Equivalently, equation (3.26) shows that in the exponent $(n + m - 2q)$, the larger q results in a larger Ω required to reach the same λ than for the solid curve. This in turn means that the relatively stronger pressure gradients and current densities (for smaller q) will lead to the cut-off criterion being satisfied at smaller radii

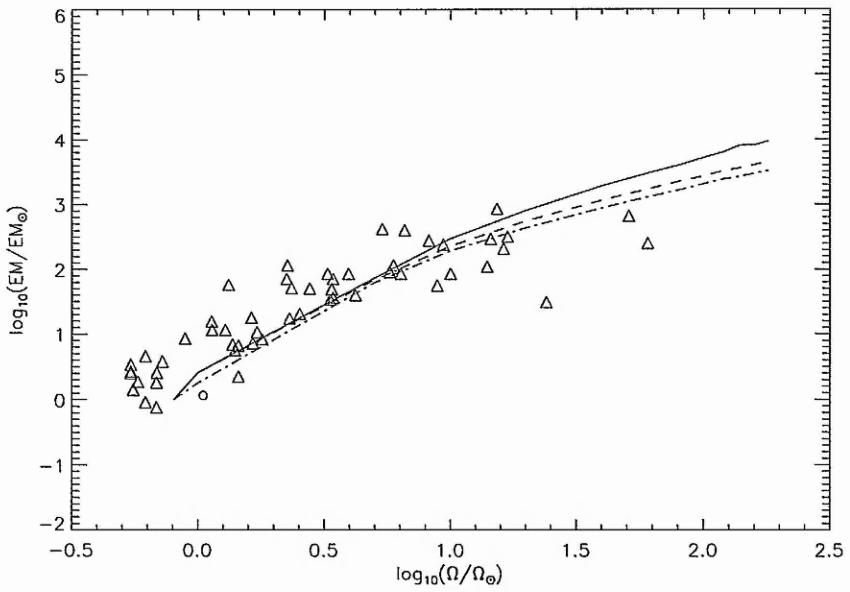

Figure 3.3: Emission measure vs. angular velocity. The triangles show data taken from Hempelmann et al. (1995). The solid line represents model results for $m = 0.5, n = 1.0, q = 0.75$ and $\beta_\odot = 0.005$, the dashed line represents results for $m = 0.5, n = 1.0, q = 0.6$ and $\beta_\odot = 0.005$ and the dash-dotted line represents results for which $m = 0.5, n = 1.0, q = 0.6$ and $\beta_\odot = 0.01$. The circle indicates the position of the Sun in the diagram.

and thence to a smaller volume of emitting plasma. A similar effect is seen when the dashed and dot-dashed curves are compared. This demonstrates the effect of changing the surface pressure (by changing the plasma beta, see equation (3.42)) whilst holding the other parameters constant and which again leads to a depression of solution curves for a higher plasma beta.

The saturation phenomenon is seen to be less pronounced in figure (3.3) due to the pa-

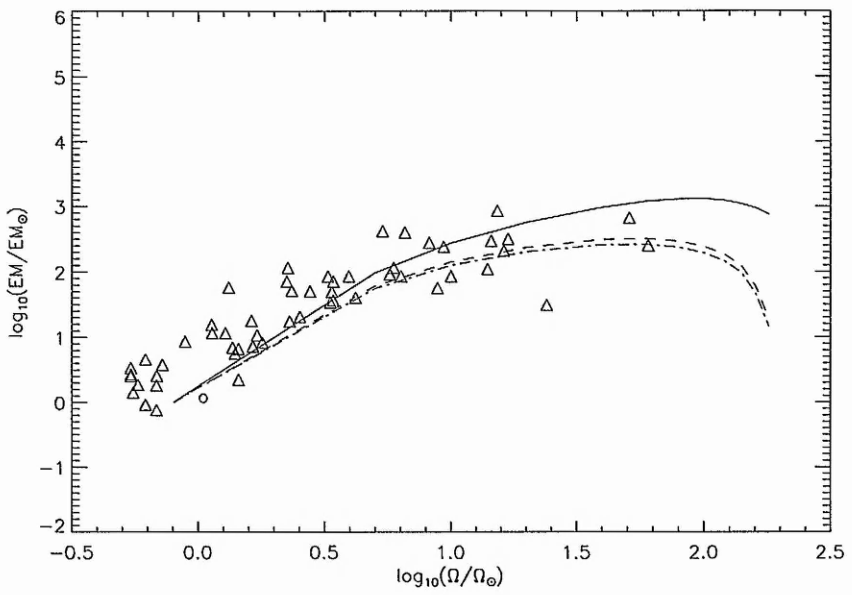

Figure 3.4: Emission measure vs. angular velocity. The triangles show data taken from Hempelmann et al. (1995). The solid line represents model results for $m = 0.7, n = 1.0, q = 0.5$ and $\beta_\odot = 0.02$, the dashed line represents results for $m = 0.579, n = 1.0, q = 0.418$ and $\beta_\odot = 0.02$ and the dash-dotted line represents results for which $m = 0.555, n = 1.0, q = 0.406$ and $\beta_\odot = 0.02$. The circle indicates the position of the Sun in the diagram.

rameter combinations leading to a stronger rotation scaling of Ω for λ in equation (3.26) because of the stronger increase in plasma beta with Ω. Figure (3.3) demonstrates a less "gradual" onset of saturation with the onset of saturation occurring at lower angular velocities than for the curves in figure (3.4) and which therefore shows a better fit to the observations. This set of curves also shows that when all model parameters other than the plasma density exponent m, are kept roughly constant then the lowering of m will have

the effect of depressing the solution curves. The reason for this is that by definition it is the plasma density which contributes most directly to the emission measure (equations (3.28) and (3.44)).

In the final set of solution curves (figure (3.5)) we show a different parameter combination which serves to demonstrate the sensitivity of these models to the choice of parameters. As an equilibrium sequence evolves and the current densities (and pressure gradients) increase, the cut-off radius must move inwards towards the stellar surface as the cut-off radius criterion is satisfied at progressively lower radii. This progression is shown for a single equilibrium sequence, at $\Omega = 0.8\Omega_{\odot}$, in the lower panel of figure (3.6). When the cut-off radius approaches the surface however, the flux-function for the cut-off field line will tend to one (equation (3.42)) and λ must tend to $\frac{1}{2}$. In practice, the choice of model parameters and their combinations will now be somewhat constrained because the equilibrium sequence will not evolve beyond $\lambda = \frac{1}{2}$ where the cut-off field line would be inside the surface of the star. Exactly how close the numerical code will evolve to $\lambda = \frac{1}{2}$ is a difficult matter which becomes important if we want to choose a combination of parameters which will give us a strong scaling with rotation, together with a realistic surface plasma beta. Some trade-off between the two is therefore required, as demonstrated in figure (3.5) where we have high plasma betas but only a weak rotation scaling and therefore we do not have the most ideal fit of our model results to the observations. Given this caveat, the fit may still be seen to be reasonably agreeable and all the emission curves shown in the figures, follow the steep rise in emission (up to angular velocities of around $20\mathrm{km}s^{-1}$ followed by the falling off in emission which is characteristic of the saturation

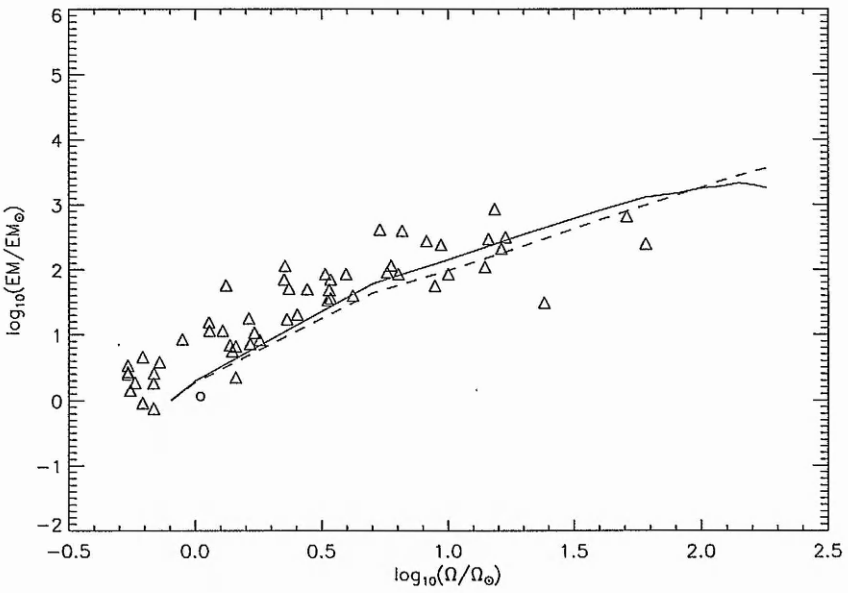

Figure 3.5: Emission measure vs. angular velocity. The triangles show data taken from Hempelmann et al. (1995). The solid line represents model results for $m = 1.0, n = 1.0, q = 0.938$ and $\beta_\odot = 0.5$, the dashed line represents results for $m = 0.882, n = 1.0, q = 0.895$ and $\beta_\odot = 0.5$. The circle indicates the position of the Sun in the diagram.

phenomenon. The inward progression of the cut-off field line is also shown in figure (3.7) and figure (3.8). In the case of the former, we show the progression of the cut-off field line varying with angular velocity and with respect to the position of the equatorial corotation radius (equation (1.1)) for three different combinations of model parameters. Our preceding discussion of the effects of changing these parameters on the position of the cut-off radius, ties in with the changes shown in this figure. Inside the equatorial corotation radius, it is gravitational forces which dominate over centrifugal forces whilst outside this radius, the reverse is the case. As the angular velocity increases, the corotation radius will move inwards and eventually move inside the stellar corona but it should be noted that the calculation of the position of the corotation radius is one which is purely kinematic. Where the corotation radius is greater than the cut-off radius, we will have a pressure dominated magnetosphere but once the angular velocity is increased, this position will reverse as the centrifugal force becomes more important. Figure (3.8) illustrates the field line contours as calculated from (equation (1.37)) for two different solutions along an equilibrium sequence of a star with a solar angular velocity. The field lines are shown in the projected $r - z$ plane and once again, the inward motion of the cut-off field line is evident. For such a slowly rotating star, it is not entirely unexpected that the field lines should be barely deformed by the weak current densities, from a dipolar geometry. The change in position of the cut-off radius over the course of an equilibrium sequence (i.e. the change with respect to λ) is one of a number of such diagnostic quantities that we are able to calculate. Figure (3.9) and figure (3.6) also show the variation of the thermal energy of the plasma, the poloidal magnetic energy and the variation of the emission. These

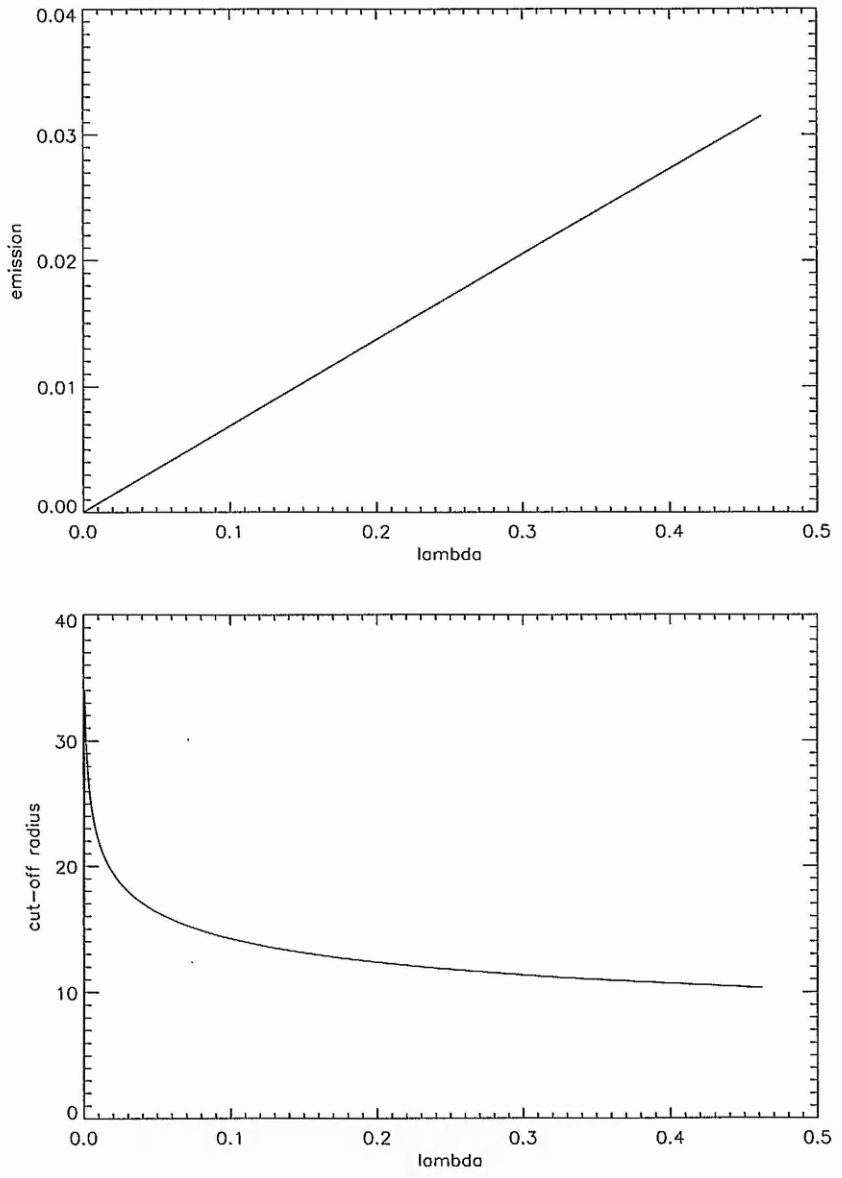

Figure 3.6: The top figure shows the variation in emission measure through one equilibrium sequence whilst the bottom figure shows the change in position of the cut-off radius through the sequence. Both figures are calculated for an equilibrium sequence where $n = 1.0$ and $\Omega = 0.8\Omega_{\odot}$.

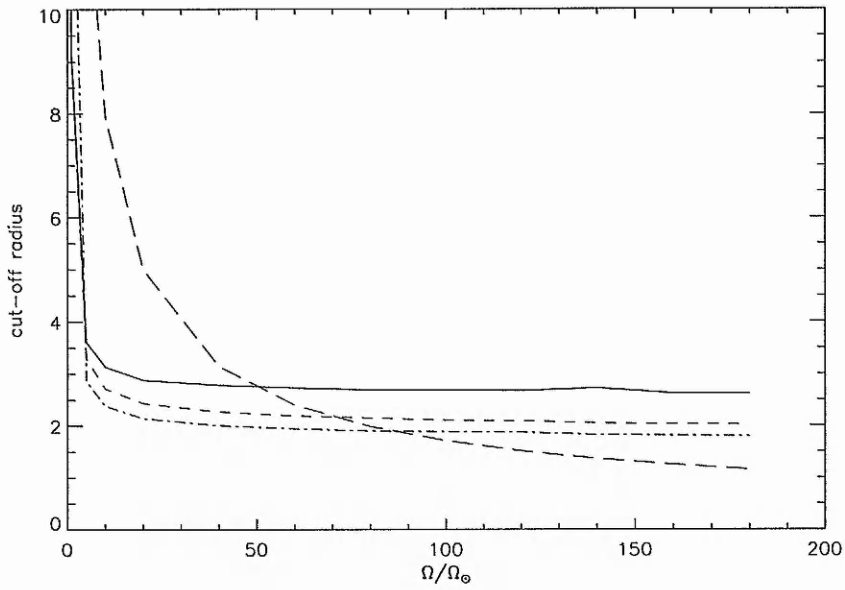

Figure 3.7: Position of cut-off field line vs. angular velocity in solar units. The long dashed line shows the variation of the corotation radius with rotation. The solid line represents model results for $m = 0.5, n = 1.0, q = 0.75$ and $\beta_\odot = 0.005$, the dashed line represents results for $m = 0.5, n = 1.0, q = 0.6$ and $\beta_\odot = 0.005$ and the dash-dotted line represents results for which $m = 0.5, n = 1.0, q = 0.6$ and $\beta_\odot = 0.01$.

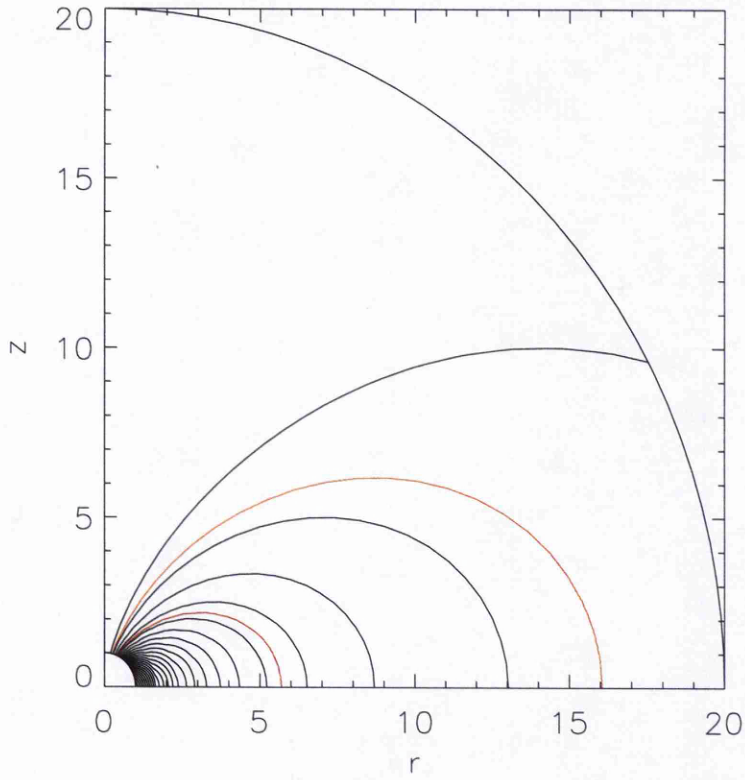

Figure 3.8: Magnetic field-lines in the $r - z$ plane. The position of the cut-off field line is shown for two different solutions along the equilibrium sequence and in the background of a relatively undeformed dipole field for a model with $n = 1.0$ and $\Omega = \Omega_{\odot}$. The outer orange line is taken from $\lambda \approx 0.44$ and the inner red line for $\lambda \approx 0.004$.

quantities are those which have been used in previous studies as bifurcation diagrams in order to discover information about the equilibrium and stability properties of plasma systems. However, in these figures it is evident that (over the range of λ appropriate to our models), the stresses and field line deformations are too weak to significantly affect the bifurcation properties of the plasma. So, in the upper panel of figure (3.9) we can see that the field barely changes from the dipolar value (the value of which corresponds exactly with the expected value which we may easily evaluate explicitly). Figure (3.6) shows a steady increase in emission as the equilibrium sequence evolves. Whilst these figures show the effect of a small amount of rotation on the plasma and on the magnetic field, figures (3.10) and (3.11) show the corresponding effects in the rapid rotation limit where $\Omega = 180.0\Omega_{\odot}$. Comparing the lower panel of figure (3.11) with the lower panel of figure (3.6) we see that in the presence of a significantly greater angular velocity, the fall off in the position of the cut-off radius is much sharper than would be the case at lower Ω, so that the cut-off radius clearly moves inwards much more rapidly, as one would expect. This then leads to a greater reduction in the extent of the more pressure-dominated emitting corona, which is reflected in the fall off in thermal energy, magnetic energy density and emission at much lower values of λ than would be seen in the curves for lower rotation.

Finally, it remains to discuss the comparison of our models results with the observations taken by James et al. (2000). In this work, the authors presented an analysis of rotation rates and X-ray luminosity for single and binary M-dwarf systems and demonstrate some evidence for the super-saturation phenomenon in a sample of ultra-fast rotating G

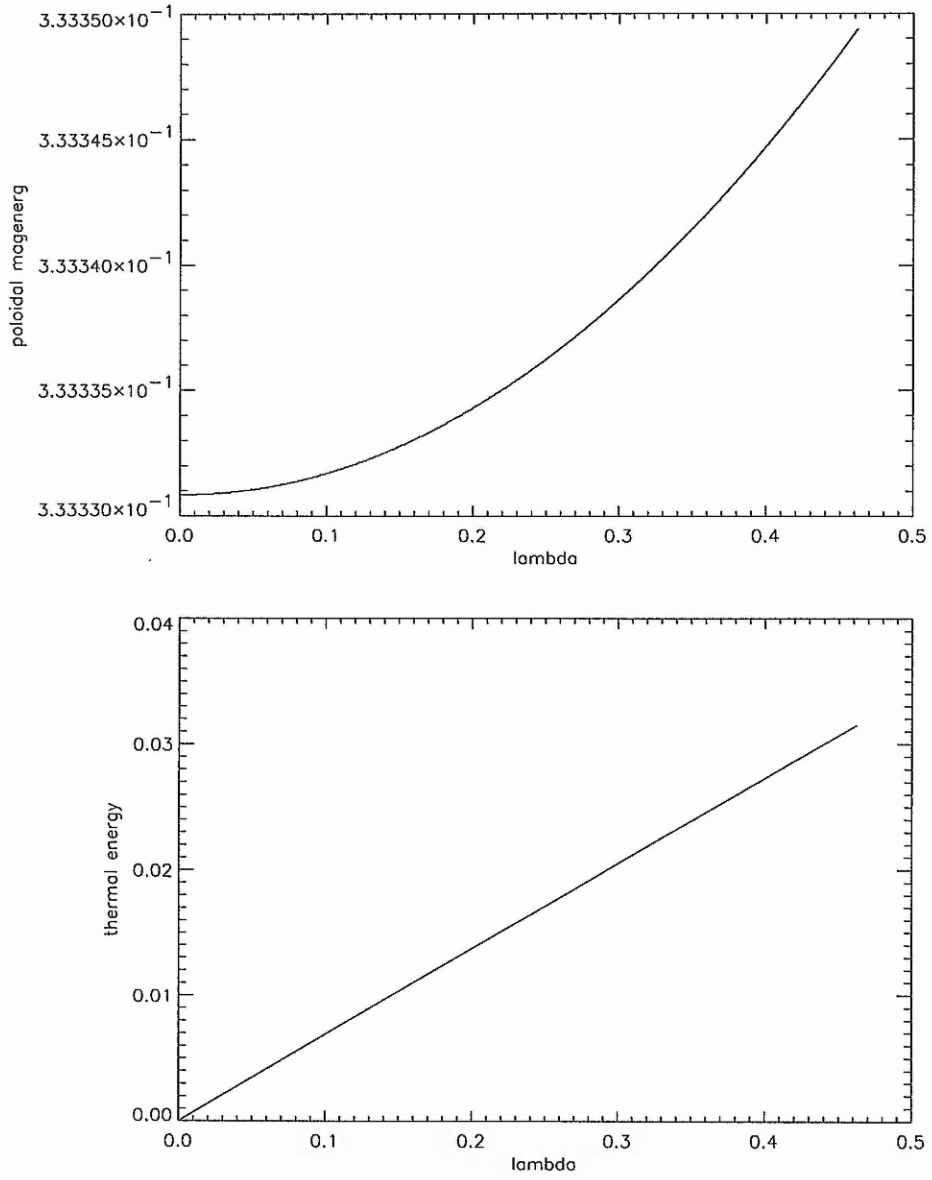

Figure 3.9: The top figure shows the deviation of the poloidal magnetic energy from an undeformed dipole field at $\lambda = 0$. The bottom figure shows the variation of the thermal plasma energy with λ. Both figures are calculated for an equilibrium sequence where $n = 1.0$ and $\Omega = 0.8\Omega_{\odot}$

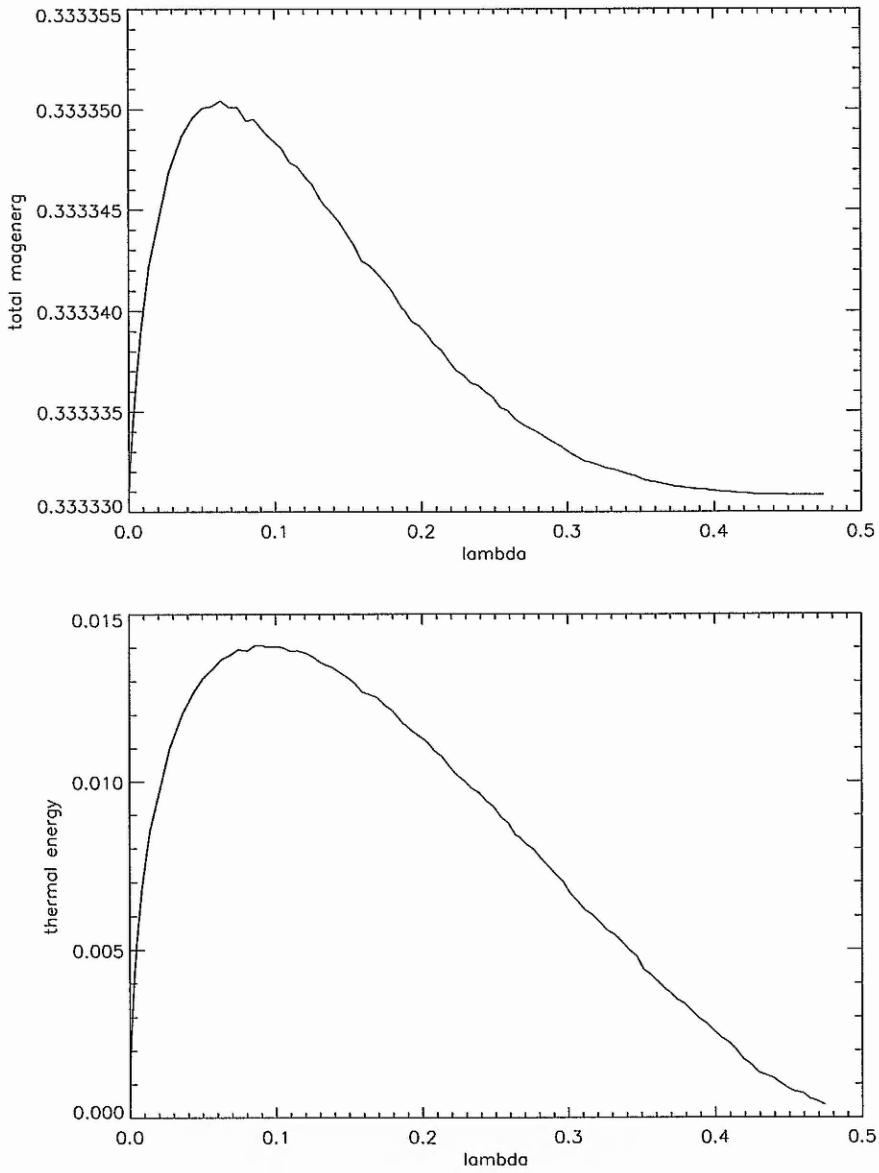

Figure 3.10: The top figure shows the variation in poloidal magnetic energy from an undeformed dipole field, with λ for an equilibrium sequence where $\Omega = 180.0\Omega_{\odot}$. The bottom figure shows the corresponding variation in the thermal energy of the plasma.

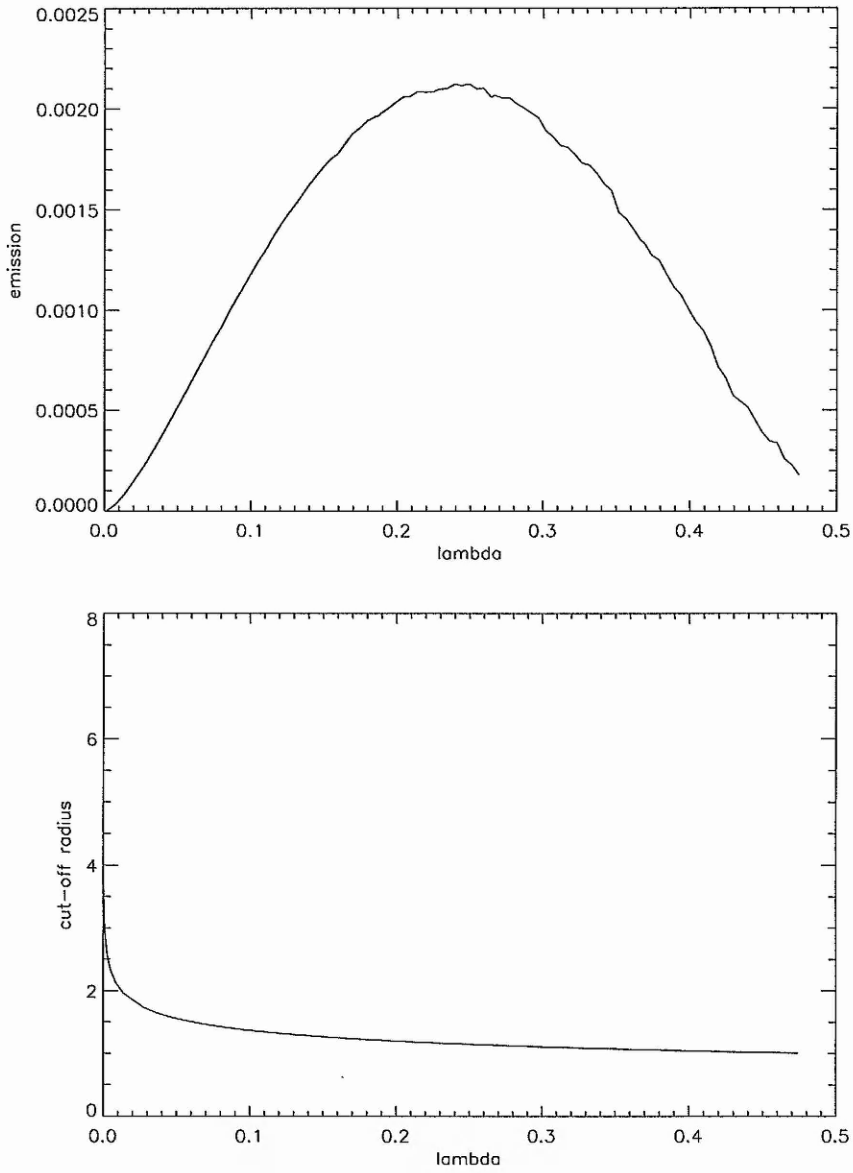

Figure 3.11: The top figure shows the variation in emission measure through one equilibrium sequence where $\Omega = 180.0\Omega_{\odot}$. The bottom figure shows the corresponding variation of the position of the cut-off radius for that equilibrium sequence.

and M dwarfs (with data taken from ROSAT PSPC X-ray observations). It is a simple matter to modify our scalings from the solar values of mass and radius ($M_\odot, R_\odot$) to those appropriate to M0 dwarfs by taking values of $M_\star = 0.47 M_\odot$ and $R_\star = 0.63 R_\odot$ quoted by Zombeck (1990) and by assuming that the stars would have a similar temperature scaling. The coronae of M-dwarfs are expected to be smaller and less luminous than their G spectral type counterparts (for the same magnetic field and temperature) with breakup velocities of around $320\Omega_\odot$ for an M0 dwarf. In addition, it is clear that we cannot scale our emission measures to those of a solar-type star so instead we have chosen to average the emission measures of those stars in the observations which have roughly solar angular velocities and to use that averaged emission as our scaling emission. Figure (3.12) shows some of the model results for one particular combination of model parameters and compares them with the observations. Once again, we see a good reproduction of the observed saturation but in addition to this, we have also been able to replicate the observed supersaturation. Whilst we are still able to consider different parameter combinations in a similar manner as before, the different scalings of the M-dwarfs mean that we must consider slightly different parameter sets. At this point it is worth commenting that there is a considerable body of both theoretical (including computational) and observational work that attempts to describe and discover the relationships between rotation, temperature, density, pressure and magnetic field in a stellar magnetosphere. If there was a clear and common consensus on this issue then we would have a guide to inform of us of an appropriate choice for our values of model parameters (m, n, q, β) but unfortunately this is not the case at present. However, we should make it clear that the choices that we have

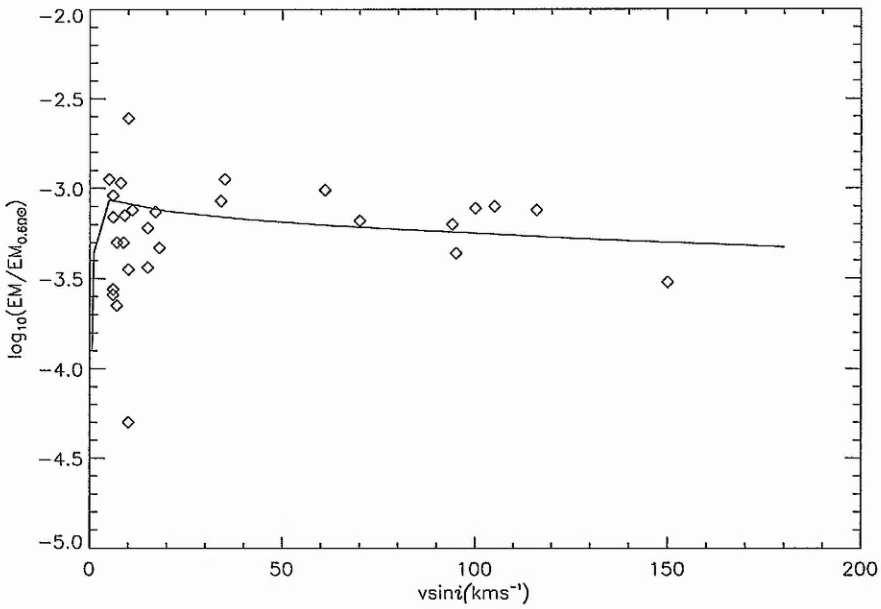

Figure 3.12: Emission measure vs. angular velocity. The diamonds show data taken from James et al. (2000). The solid line represents model results for $m = 1.0, n = 1.0, q = -0.75$ and $\beta_{\odot} = 0.005$. The data are best represented by the solid curve model.

made for our model parameters (and those that we can make) are all within the ranges of acceptable and physically plausible values. In general, we have shown that this relatively simple model that we have put forward is (in principle) capable of explaining the observed saturation and supersaturation phenomena in a satisfactory manner.

Chapter 4

Azimuthal field model

4.1 Model formulation

One of the key simplifying assumptions of the scaling models, which we discussed in the last chapter, was the neglect of the toroidal component of the magnetic field. Whilst this was a necessary simplification to allow us to proceed with our models, it is of course desirable to formulate the most physically realistic models that we can. In equation (1.59) we had set $b_\phi = r \sin\theta B_\phi = 0$ where $b_\phi(A)$ was a free function. In order to construct a model with a toroidal field component we need to choose an appropriate form for b_ϕ. There are many observational indicators and dynamo theory models of the form that this toroidal component should take (e.g., Kitchatinov et al. , 2000a,b) however we require a more simple, physically plausible form that will serve as a starting point from which to further develop these models.

Equation (1.59) may be written in the more abbreviated form

$$-\nabla \cdot \left(\frac{1}{r^2 \sin^2 \theta} \nabla A \right) = \mu_0 \frac{\partial p}{\partial A} + \frac{1}{r^2 \sin^2 \theta} b_\phi \frac{db_\phi}{dA} \tag{4.1}$$

The Grad-Shafranov equation with a toroidal field component included, may be treated in a similar manner to our treatment in the scaling models of the last chapter. We begin by considering a suitable normalisation scheme for the above equation where the flux function is normalised as in equation (3.8),

$$-\frac{\partial}{\partial r}\left[\frac{1}{\sin\theta}\frac{\partial \hat{A}}{\partial r}\right] - \frac{\partial}{\partial \theta}\left[\frac{1}{r^2 \sin\theta}\frac{\partial \hat{A}}{\partial \theta}\right] - \frac{\mu_0^2 p_0 R^4 r^2 \sin\theta}{A_0^2}\frac{\partial \hat{p}}{\partial \hat{A}}$$
$$-\frac{1}{\sin\theta}\frac{B_{\phi 0}^2 R^4}{A_o^2}\hat{b}_\phi \frac{d\hat{b}_\phi}{d\hat{A}} = 0. \tag{4.2}$$

We define λ_p as being equivalent to the λ in the scaling formulation and therefore it may be interpreted as being equal to one half of the plasma beta of the stellar coronal surface at the equator. An additional λ appears as the ratio of the azimuthal to the poloidal field strengths at the stellar coronal equatorial surface,

$$\lambda_\phi = \frac{B_{\phi 0}}{B_\star}$$

which allows us to rewrite equation (4.2)

$$-\frac{\partial}{\partial r}\left[\frac{1}{\sin\theta}\frac{\partial \hat{A}}{\partial r}\right] - \frac{\partial}{\partial \theta}\left[\frac{1}{r^2 \sin\theta}\frac{\partial \hat{A}}{\partial \theta}\right] - \lambda_p r^2 \sin\theta \frac{\partial \hat{p}}{\partial \hat{A}} - \frac{\lambda_\phi^2 \hat{b}_\phi}{\sin\theta}\frac{d\hat{b}_\phi}{d\hat{A}} = 0$$

To complete our model, we choose the simplest possible form of non-zero $\hat{b}_\phi$ which is one that is linear in terms of the flux function A.

$$\begin{aligned} \hat{b}_\phi &= \lambda_\phi \hat{A} \\ \implies \hat{b}_\phi \frac{d\hat{b}_\phi}{d\hat{A}} &= \lambda_\phi^2 \hat{A} \end{aligned} \tag{4.4}$$

The current density will now (after some simple manipulations) take the form

$$j_\phi = \mathbf{e}_\phi \cdot \nabla \times (\nabla A \times \nabla \phi) \tag{4.5}$$

$$= -\frac{1}{r}\left[\frac{\partial}{\partial r}\left(\frac{1}{\sin\theta}\frac{\partial A}{\partial r}\right) + \frac{\partial}{\partial \theta}\left(\frac{1}{r^2 \sin\theta}\frac{\partial A}{\partial \theta}\right)\right] \tag{4.6}$$

$$= \frac{1}{\hat{r}}\left[\lambda_p \frac{\partial \hat{p}}{\partial \hat{A}}\hat{r}^2 \sin\theta + \frac{1}{\sin\theta}\lambda_\phi^2 \hat{b}_\phi \frac{d\hat{b}_\phi}{d\hat{A}}\right] \tag{4.7}$$

Our previous calculation of the magnetic dipole moment on the outer boundary will now be modified in the presence of the additional current density. In the previous formulation we used the current density, $\frac{j_\phi}{\lambda} := \bar{j}_\phi$ to calculate the $z-$component of the magnetic dipole moment where $M_z = M_z(\lambda, A)$ because the current density allowed us to calculate

$$\frac{dM_z}{d\lambda} = \frac{\partial M_z}{\partial \lambda} + \frac{\partial M_z}{\partial A}\frac{\partial A}{\partial \lambda} \tag{4.8}$$

And as

$$M_z = \lambda \bar{M}_z \Longrightarrow \frac{\partial M_z}{\partial \lambda} = \bar{M}_z \tag{4.9}$$

we may use the form of our numerical method and calculate $\bar{M}_z$ in order to determine the magnetic dipole moment. However, M_z no longer has the above structure but must take the following form

$$m_z = \lambda_p \bar{M}_z^p + \lambda_\phi^2 \bar{M}_z^\phi \tag{4.10}$$

where the subscripts p and ϕ refer to the poloidal and toroidal components of the moment respectively. To calculate $\frac{\partial M_z}{\partial \lambda_p}$ we need not only $\bar{M}_z$ but the full form of M_z (including $\bar{M}_z^\phi$ and so we must make appropriate modifications to our numerical code to do this. Finally, we consider the change of the form of the magnetic energy density. Whilst the

poloidal component of the magnetic energy density will remain the same as it would be for those models and results discussed in the last chapter, there is now a toroidal component to the magnetic energy density which we may write with the aid of the above equation (4.4) together with equation (1.55) as

$$\begin{aligned} W_\phi &= \int_1^{r_c} \frac{1}{2} B_\phi^2 r^2 \sin\theta dr d\theta \\ &= \int_1^{r_c} \frac{b_\phi^2}{2\sin\theta} dr d\theta \\ &= \int_1^{r_c} \frac{\lambda_\phi^2 A^2}{2\sin\theta} dr d\theta \end{aligned} \tag{4.11}$$

Due to the symmetry properties of our models, all the above quantities are calculated over one quarter of a two-dimensional magnetosphere and must therefore be scaled appropriately if we wish to calculate their absolute values.

4.2 Results

In a similar manner to that outlined in the previous chapter, we are able to calculate sequences of MHS equilibria for sets of the different model parameters (the magnetic field scaling parameter q, the plasma density scaling parameter m, the temperature scaling parameter n and the surface plasma beta β) and to compare our results with those observations made by Hempelmann et al. (1995) for G-K stars.

Figure (4.1) shows the variation of our normalised emission measure proxy (normalised in the same manner as before) with angular velocity for four different model

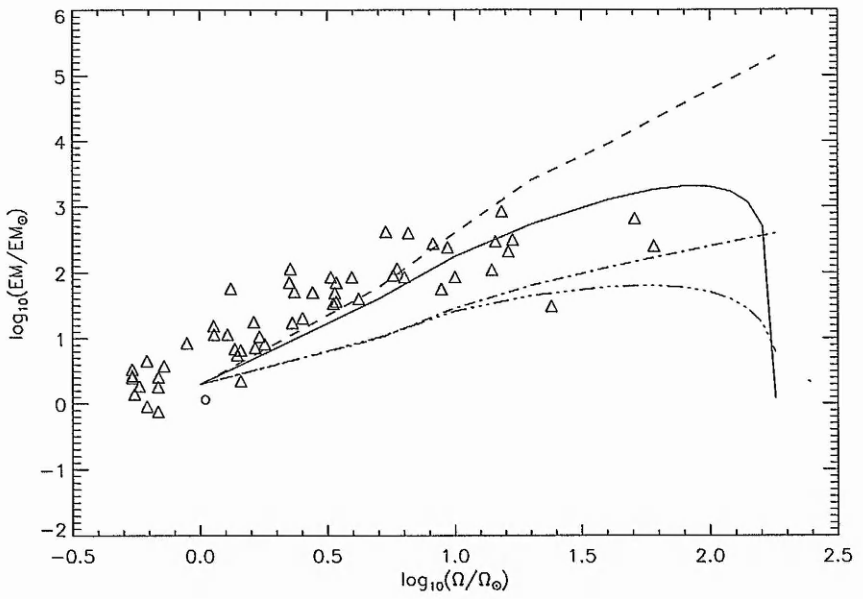

Figure 4.1: Emission measure vs. angular velocity. The triangles show data taken from Hempelmann et al. (1995). The solid line represents model results for $m = 1.0, n = 1.0, q \approx 0.558$ and $\beta_\odot = 0.01$, the dashed line represents results for $m = 1.0, n = 1.0, q = 1.0$ and $\beta_\odot = 0.01$, the dash-dotted line represents results for $n = 1.0, q \approx 0.558, m = 0.5$ and $\beta_\odot = 0.01$, the dash-double dotted line represents results for $m \approx 0.579, n = 1.0, q \approx 0.356$ and $\beta_\odot = 0.01$. All curves are for $\lambda_\phi = 0.005$. The circle indicates the position of the Sun in the diagram.

parameter combinations but for the same value of the plasma beta, $\beta = 0.01\beta_{\odot}$. For this set of results we have taken a simple $\lambda_{\phi} = 0.005$ for our form of $\hat{b}_{\phi}$, as given by equation (4.4). This value may be rather low but serves as a useful starting point for our models. Once again we see the same effects of varying the parameters m and q on the emission curves that we found for our earlier models with those combination of parameters that lead to a strong scaling of the angular velocity leading to a good fit of the models to the observations. In chapter 3 we recovered saturation of the emission with rotation for $G-K$ stars and super-saturation for M-dwarfs whereas here we can recover both phenomena for model scalings appropriate to $G-K$ stars. However, as super-saturation has not been reported to have been observed in stars of this spectral type then those model curves which display super-saturation clearly cannot constitute the best fit of the model results to the observations (but are included here for illustrative purposes). A reasonable fit of our model results to the observations is provided by the dash-dotted line in figure (4.1) where $n = 1.0, m = 0.5, q \approx 0.558, \beta = 0.01\beta_{\odot}$ but of course, other parameter combinations could be possible which might give better fits to the observations. Whilst the variation of the model parameters will influence the emission curves in the same manner as we discussed before, the presence of the toroidal field component will play a significant role in changing the profile of the emission curves. The effect of the additional contribution to the magnetic field given by the toroidal component is to provide an extra contribution to the current density which will, in general, increase the sensitivity of our models to our particular choice of parameter combination. The figure illustrates the fact that as the rotation scaling exponent $n + m - 2q$ for the determination of the cut-off λ, is increased,

the curves will in general move down (for the dashed curve, the parameters sum to zero) as was the case with our previous models. A different set of emission curves is shown in figure (4.2) and shows results for a higher plasma beta (the dashed line). This curve gives a reasonable fit to the observations and is encouraging because it was generated with a set of physically realistic model parameters.

The effects of the introduction of a toroidal component to the magnetic field are illustrated in figure (4.3) where an emission curves for an equilibrium sequence from a model without a toroidal component to its magnetic field (solid curve) is compared to the emission curve for an equilibrium sequence with $\lambda_\phi = 0.005$ (dashed curve). As one might expect, the additional current density (represented by the extra term in equation (4.7) acts to lower the emission density by causing further stressing of the field lines , forcing the cut-off criterion to be satisfied at smaller radii and thereby reducing the extent of the emitting closed-field corona. It should be noted that the form of the current density in equation (4.7) includes a quadratic dependence on λ_ϕ for a linear $\lambda_\phi - A$ relation so that weak λ_ϕ will lead to a weak contribution to the total current density. The changes in the total magnetic energy density and of its two components are shown in figures (4.4) and (4.5) respectively for a star with model angular velocity $\Omega = \Omega_\odot$. In the lower graph of figure (4.5) the change of toroidal magnetic energy density (given by equation (4.12)) with λ is shown to steadily decrease as the position of the cut-off field line moves inwards and this fall off will be more pronounced for the more rapid rotators. Combining the two components of the magnetic energy density from figure (4.5) will give us the total magnetic energy density from which we can see that the additional toroidal component to the

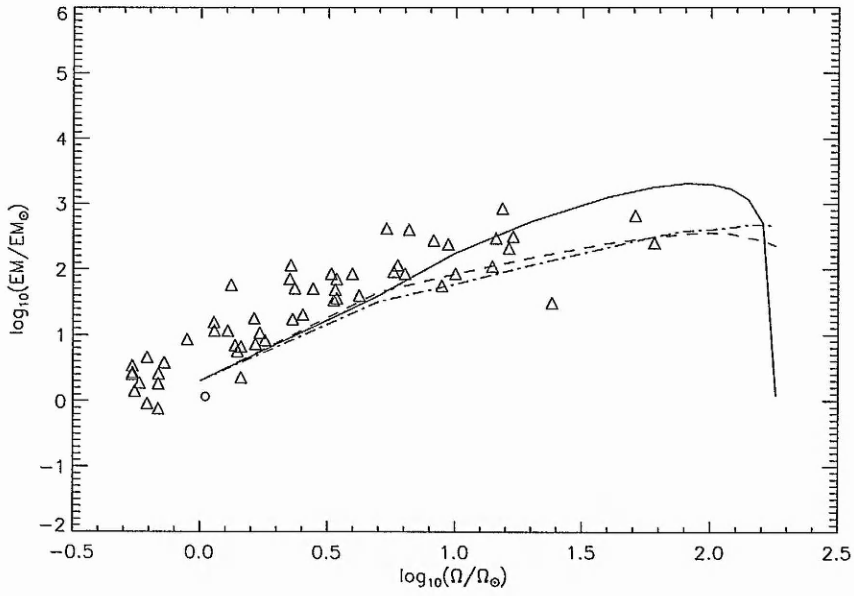

Figure 4.2: Emission measure vs. angular velocity. The triangles show data taken from Hempelmann et al. (1995). The solid line represents model results for $m = 1.0, n = 1.0, q \approx 0.558$ and $\beta_\odot = 0.01$, the dashed line represents results for $m \approx 0.724, n = 1.0, q \approx 0.756$ and $\beta_\odot = 0.3$, the dash-dotted line represents results for $n = 1.0, q \approx 0.840, m \approx 0.793$ and $\beta_\odot = 0.01$. All curves are for $\lambda_\phi = 0.005$. The circle indicates the position of the Sun in the diagram.

field raises the total energy density from $\lambda = 0$ since our equilibrium sequence does not begin from an undeformed dipole field. The total magnetic energy density falls off very slightly at first when the falling contribution of the toroidal component is significant but as the sequence progresses and the coronal volume is reduced, the poloidal component resumes its dominance over the total magnetic energy density.

Finally, we consider the effect of increasing λ_ϕ. Figure (4.6) shows model equilibrium solutions for $\lambda_\phi = 0.005$ (the solid curve) with those for $\lambda_\phi = 0.05$ (the dashed curve). Again, the effect (given similar model parameters) is to reduce the curves. Clearly whilst the curve for $\lambda_\phi = 0.05$ is broadly similar to the family of other curves shown earlier, there are still significant problems with this solution set. Larger values of λ_ϕ would be desirable in order to dove-tail our models more neatly with the state of current observations and to use the most physically realistic model parameters possible. Whilst we have some freedom with choosing our combinations of the parameters m, n and q, our numerical code does encounter difficulties with higher λ_ϕ. Currently we fix the value of λ_ϕ and calculate sequences of λ_p. Our method will face increasing difficulty calculating these sequences for higher λ_ϕ because the deviation from a dipole field at the start of each equilibrium sequence will be greater (through the flux function and due to the additional initial currents) and it will be more difficult for our numerical code to find an initial equilibrium from which to proceed. There are a number of alternative methods which we have begun investigating. One such method is to fix the λ_p and calculate sequences of λ_ϕ where we take an already generated equilibrium sequence (from $\lambda_\phi = 0$) and use this as a starting equilibrium for our new sequence. Both the sets of results discussed in chapters 3 and 4

have all been for a temperature scaling $n = 1.0$ and for $\xi_3 = 1.0$ in our surface pressure and density distributions (equations (3.35) and (3.36)). It remains for us to conduct a full search of the parameter space for the temperature scaling but in the case of ξ_3, its presence in the exponent means that we are necessarily restrained from investigating higher ξ_3 as this will result in very strong pressure gradients which may lead to numerical difficulties.

Despite these qualifying remarks, we have shown that the inclusion of a toroidal magnetic field component does not necessarily lead to a great change in the nature and in the form of our results. In turn, this shows that our model is relatively robust in its results and that the results do not depend crucially on any of the assumptions made in the formulation of the model.

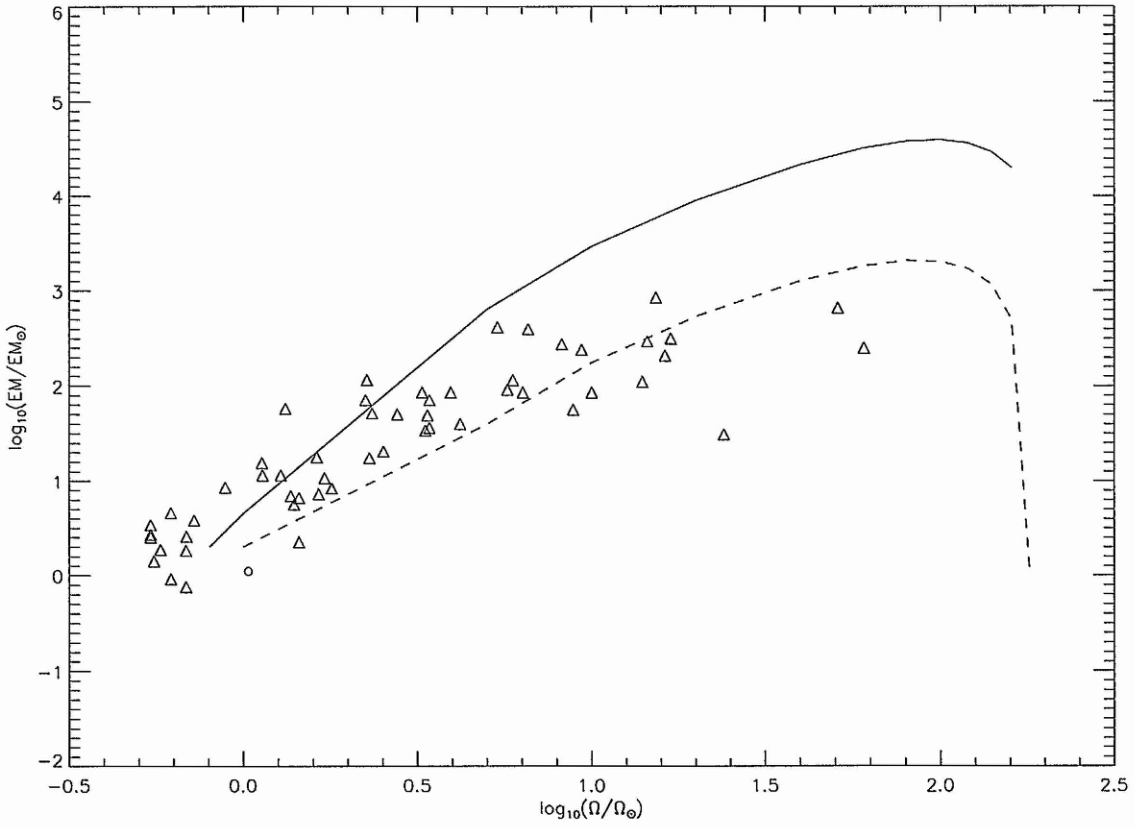

Figure 4.3: Emission measure vs.angular velocity. The solid line shows model results for an equilibrium sequence where $m = 1.0, n = 1.0, q = 0.567$ and $\beta = 0.01\beta_{\odot}$ for a magnetic field with no toroidal component. The dashed line shows model results for a sequence where $m = 1.0, n = 1.0, q \approx 0.558$ and $\beta = 0.01\beta_{\odot}$ for a magnetic field where $\lambda_{\phi} = 0.005$.

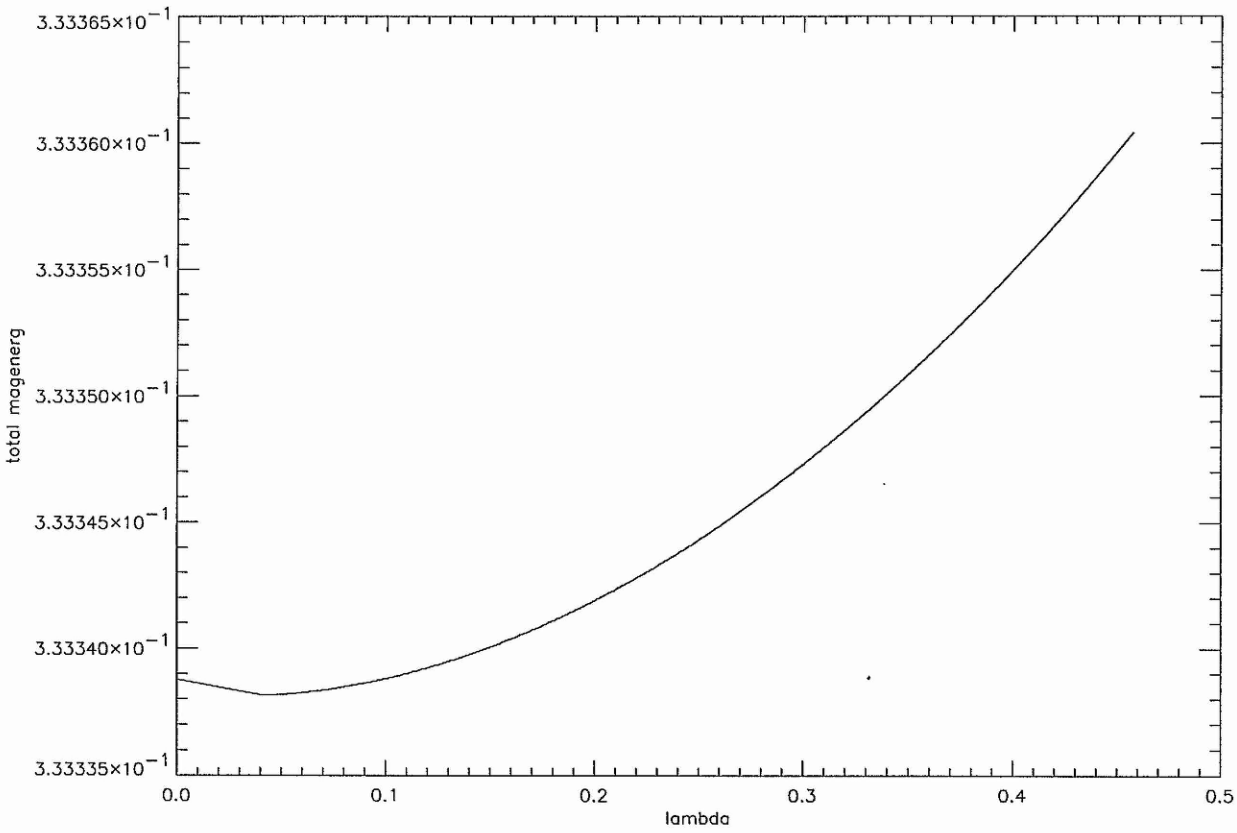

Figure 4.4: Total magnetic energy density vs. lambda for an equilibrium sequence where $\Omega = \Omega_{\odot}$ and $\lambda_{\phi} = 0.005$.

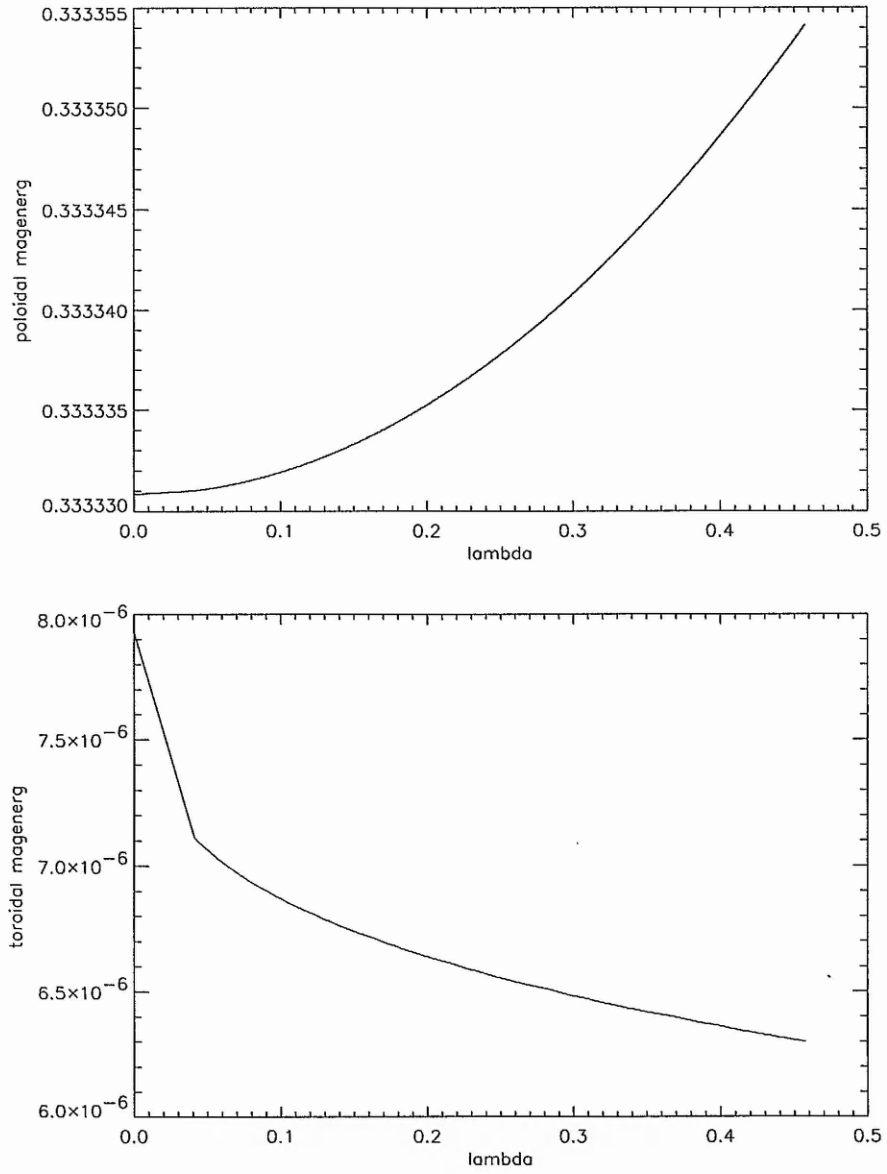

Figure 4.5: The top figure shows the variation of the poloidal component of the magnetic field with λ. The bottom figure shows the corresponding variation of the toroidal component of the field for an equilibrium sequence where $\Omega = \Omega_{\odot}$ and $\lambda_{\phi} = 0.005$.

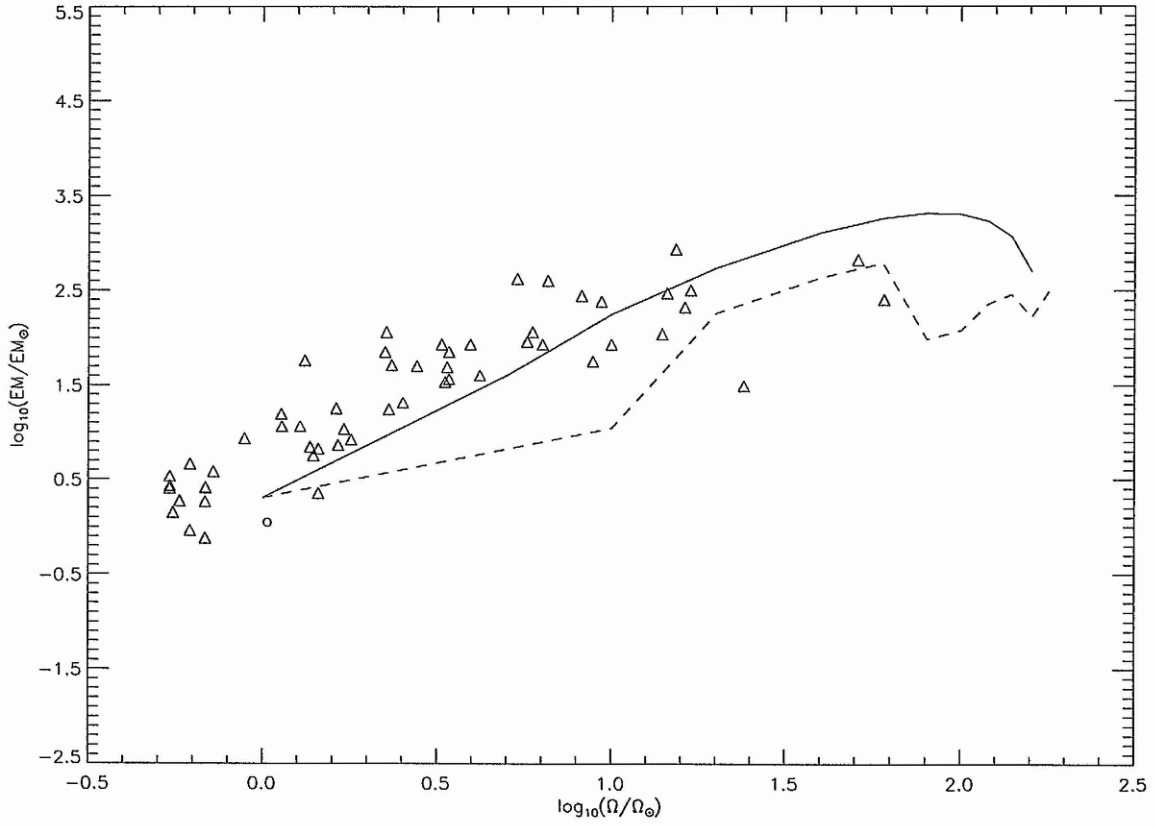

Figure 4.6: Emission measure vs.angular velocity. The solid line shows model results for an equilibrium sequence where $m = 1.0, n = 1.0, q \approx 0.567$ and $\beta = 0.01\beta_{\odot}$ for a magnetic field with $\lambda_{\phi} = 0.005$. The dashed line shows model results for a sequence with the same parameters but for a magnetic field where $\lambda_{\phi} = 0.05$.

Chapter 5

Three-dimensional models of rigidly rotating magnetospheres

5.1 Planetary magnetospheres

Our study of rotating magnetospheric plasma systems need not necessarily be confined to that of stellar magnetospheres. Whilst the models which we have developed in the previous chapters were specific to rigidly co-rotating, axisymmetric, rotationally aligned dipole-like stellar coronae, there is no reason why these models could not be applied and extended to the treatment of planetary magnetospheres (for more extensive reviews of the properties, observations and descriptions of planetary magnetospheres, see for example Bagenal (1992), Kennel & Coronti (1977), Parker (1979)). In the broadest sense, planetary magnetospheres are cavities that are carved out from interplanetary

space upon the encounter of a solar or stellar magnetised wind with a planetary magnetic field. Moreover, the plasma within this cavity is principally influenced by the properties of the particular planetary magnetic field. The planetary magnetic field strength, axial orientation with respect to the ecliptic plane together with the relative orientation of the planetary rotation axis with respect to the magnetic field axis are the most significant factors that determine the eventual size and extent of the magnetospheric cavity. This resultant magnetosphere is very often highly structured and time-dependent with planetary rotation. Within the solar-system there are two broad categories of magnetospheres, that of the symmetric and the asymmetric magnetospheres. These two classes are distinguished from each other by the requirement that the convection electric field (and thence the convective motions) is quasi-steady in the inertial frame of reference. This condition holds for symmetric magnetospheres (such as the earth, Jupiter and Saturn) but as soon as the angle between the planetary magnetic field axis and rotation axis becomes appreciable then the magnetosphere is asymmetric, as is the case for the outer planetary gas giants (Uranus and Neptune). A further complication to describing the structure of a planetary magnetosphere arises when the point of symmetry of the magnetic field is significantly displaced from the planetary centre as is the case with both Uranus and Neptune.

Uranus for example is highly unusual in that it is unique in the solar system for possessing an inclination of equator, ring system and satellite orbits at 98^o to its own orbital plane (see figure (5.1)) whilst Neptune also has its magnetic dipole axis misaligned from its planetary rotation axis and the solar-wind direction (see figure (5.2)). This means that both planets will exhibit very different magnetic field topologies over the course of a

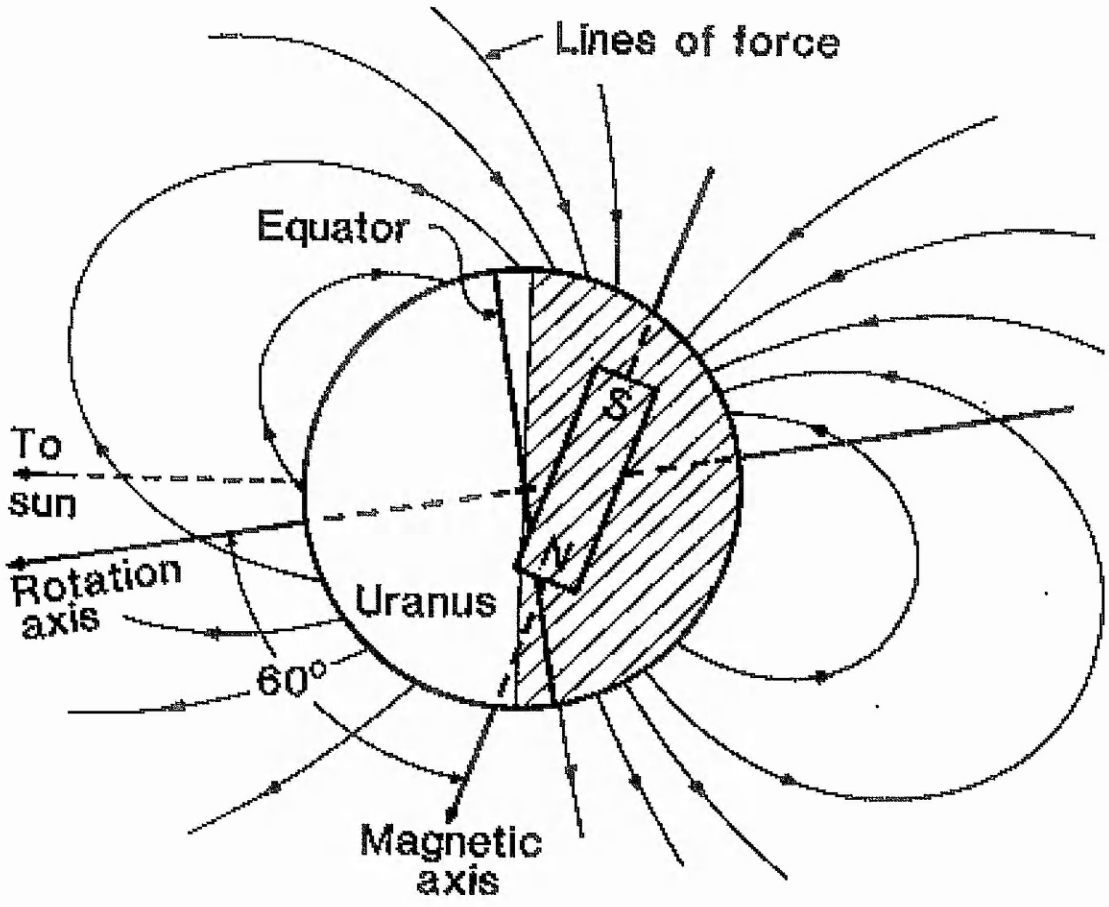

Figure 5.1: Magnetospheric geometry of Uranus as inferred from the 1986 Voyager 2 encounter. The equator, ring system and satellite orbits are all inclined at 98^o degrees to its orbital plane which leads to very different magnetic field topologies over a planetary rotation period. The figure is provided courtesy of Kopp (Homepage).

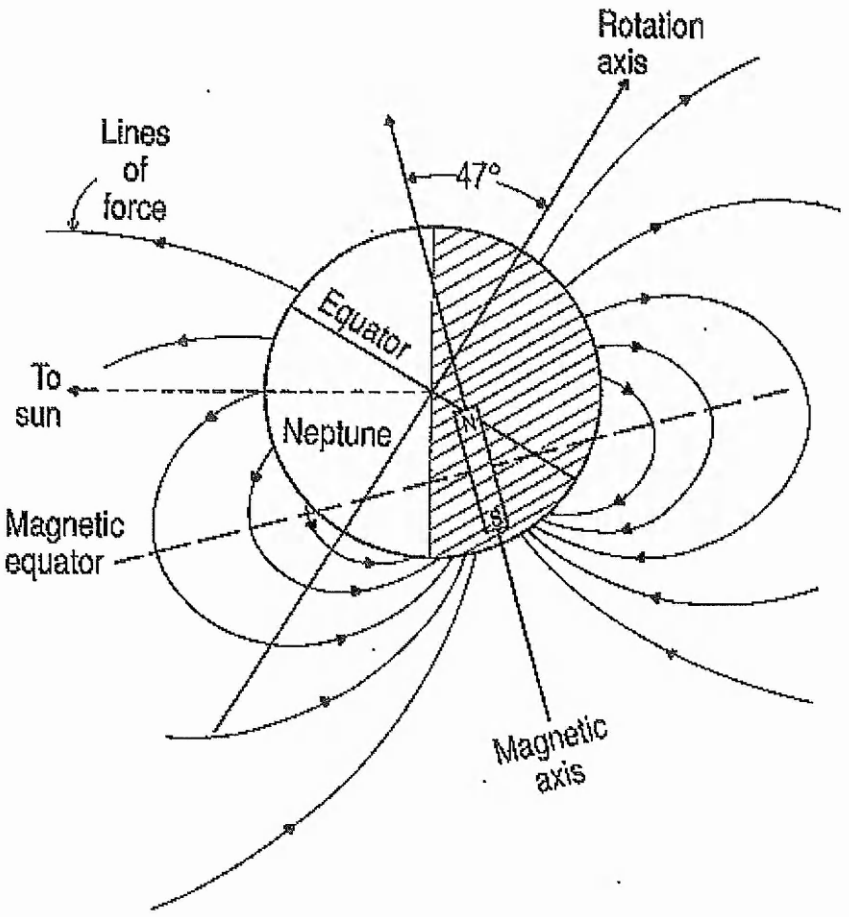

Figure 5.2: Magnetospheric geometry of Neptune as inferred from the 1989 Voyager 2 encounter. The planetary rotation axis is not approximately aligned with either the magnetic dipole axis or the ecliptic, which again leads to very different magnetic field topologies over a planetary rotation period. The figure is provided courtesy of Kopp (Homepage).

planetary rotation period and is part of the motivation for the work of this chapter.

The principal aim of this chapter is to formulate a mathematical framework which will allow us to be able to extend our models to the description of fully three-dimensional (but relatively simple) magnetospheres in a manner which should make it possible to address some of the problems associated with describing a planetary magnetosphere. In particular we will use the approach described in Low (1991) as our starting point. Similar examples of three-dimensional magnetohydrostatic equilibria in Cartesian (see Low , 1985, 1992, 1993a,b, Neukirch , 1997, Rastätter & Neukirch , 1999, Petrie & Neukirch , 2000) and spherical coordinates (see Bogdan & Low , 1986, Neukirch , 1995, Osherovich , 1985a,b) have been discussed by a number of authors. However whilst these papers describe three-dimensional solutions of the MHD equations in the presence of an external gravitational field, their models do not describe rotating MHD solutions. It should be noted that Low (1991) does include a discussion of a general theory of three-dimensional MHD equilibria in the presence of external forces wherein rigid rotation results in a centrifugal potential but the author does not discuss solutions for such a case. In this chapter we will consider the general theory discussed in Low (1991) and then seek analytical solutions of the basic equation of this theory for the specific case of a magnetized rigidly rotating massive cylinder. Clearly, this case does not represent the most physically realistic representation of a planetary magnetosphere, however it is found to be a useful case to analyze because it allows for more mathematically tractable separable solutions of the problem. Whereas such an advantage can not be gained in the more physically realistic case of a magnetised and rigidly rotating spherical body, in the case of the rotating cylinder model we

will be still considering the essential physical and mathematical properties of the general problem. The rotating cylinder case therefore presents us with a good, relatively simple approximation in order to begin to make progress with our problem. Nor would such a method be confined to the modelling of the closed field line regions of planetary magnetospheres but it could readily be applied to the treatment of stellar and other magnetised astrophysical bodies.

5.2 Mathematical formulation

We begin by considering a cylinder of radius, R, infinite length and uniform mass per unit length, M which rotates rigidly about its axis of symmetry with an angular velocity, Ω. In a co-rotating cylindrical coordinate system (ϖ, ϕ, z) where the z-axis is aligned with the rotation axis, the gravitational potential of this cylinder will be given by

$$\Psi = 2GM \ln(\varpi/R) \tag{5.1}$$

where the potential is normalised to 0 at $\varpi = R$. In a co-rotating frame of reference, we will need to solve the MHS equations as given in chapter 1 (equations (1.33), (1.33) and (1.34)) but where we now denote the combined centrifugal and gravitational potential ψ of equation (1.33) with V for which

$$V = -1/2\Omega^2\varpi^2 + 2\mathrm{G}M \ln(\varpi/R) \tag{5.2}$$

Following the method of the general theory outlined in Low (1991), we will seek solutions for which the current density takes the form

$$\mu_0 \mathbf{J} = \nabla F \times \nabla V \tag{5.3}$$

where the current density, $\mathbf{J}$ is perpendicular to the centrifugal and gravitational force and where the function F is a free function which we will need to specify later. Substituting the above equation into the force balance equation (equation (1.33)), we find

$$\begin{aligned} &\frac{1}{\mu_0}(\nabla F \times \nabla V) \times \mathbf{B} - \nabla p - \rho \nabla V = \\ &\qquad \frac{1}{\mu_0}(\mathbf{B} \cdot \nabla F)\nabla V - \frac{1}{\mu_0}(\mathbf{B} \cdot \nabla V)\nabla F - \nabla p - \rho \nabla V = 0. \end{aligned} \tag{5.4}$$

This implies the following pressure-density relation

$$p(\varpi, \phi, z) = p(F, V) \tag{5.5}$$

and thus

$$\left(\frac{\partial p}{\partial F}\right)_V = -\frac{1}{\mu_0}(\mathbf{B} \cdot \nabla V) \tag{5.6}$$

$$\rho = -\left(\frac{\partial p}{\partial V}\right)_F + \frac{1}{\mu_0}(\mathbf{B} \cdot \nabla F) \tag{5.7}$$

so that the pressure is now dependent upon our choice for the function F. Our choice is informed by Low (1991) as

$$F(\varpi, \phi, z) = \kappa(V)\mathbf{B} \cdot \nabla V \tag{5.8}$$

where $\kappa(V)$ is a free function of the theory. Because the gradient of $\kappa(V)$ is parallel to ∇V the current density becomes

$$\mu_0 \mathbf{j} = \kappa(V)\nabla(\mathbf{B} \cdot \nabla V) \times \nabla V \tag{5.9}$$

which depends linearly on the magnetic field so that Ampére's equation (1.33) will also be linear. Substituting our form of F (5.8) into equation (5.6) allows it to be rewritten in the following form

$$\left(\frac{\partial p}{\partial F}\right)_V = -\frac{1}{\mu_0 \kappa(V)} F \tag{5.10}$$

which we may integrate directly to yield the pressure

$$p = p_0(V) - \frac{1}{2\mu_0 \kappa(V)} F^2. \tag{5.11}$$

Upon substitution of equation (5.8) for F we then obtain the final form of the pressure

$$p = p_0(V) - \frac{1}{2\mu_0} \kappa(V) (\mathbf{B} \cdot \nabla V)^2 \tag{5.12}$$

where $p_0(V)$ is an arbitrary function which represents a hydrostatic background atmosphere. Turning our attention to evaluating the density from equation (5.7) we find that the first term may be calculated by making use of equation (5.11), to give

$$\left(\frac{\partial p}{\partial V}\right)_F = \frac{dp_0}{dV} + \frac{1}{2\mu_0 \kappa^2(V)} \frac{d\kappa}{dV} F^2. \tag{5.13}$$

which may then be substituted into the full form of the density together with the F-expression (equation (5.8)) to give the final expression for the density as

$$\begin{aligned}
\rho &= -\frac{dp_0}{dV} - \frac{1}{2\mu_0} \frac{d\kappa}{dV} (\mathbf{B} \cdot \nabla V)^2 + \frac{1}{\mu_0} \mathbf{B} \cdot \nabla (\kappa(V) \mathbf{B} \cdot \nabla V) \\
&= -\frac{dp_0}{dV} - \frac{1}{2\mu_0} \frac{d\kappa}{dV} (\mathbf{B} \cdot \nabla V)^2 + \frac{1}{\mu_0} \frac{d\kappa}{dV} (\mathbf{B} \cdot \nabla V)^2 + \frac{1}{\mu_0} \kappa(V) \mathbf{B} \cdot \nabla (\mathbf{B} \cdot \nabla V) \\
&= -\frac{dp_0}{dV} + \frac{1}{2\mu_0} \frac{d\kappa}{dV} (\mathbf{B} \cdot \nabla V)^2 + + \frac{1}{\mu_0} \kappa(V) \mathbf{B} \cdot \nabla (\mathbf{B} \cdot \nabla V)
\end{aligned} \tag{5.14}$$

Substitution of the total potential V (as given by equation (5.2)) would then give us the fully explicit forms for the pressure and density which we will omit for the sake of generality and brevity. In order to find the plasma temperature, we may once again make

the assumption that the plasma satisfies the equation of state of an ideal gas, as given by equation (1.63).

The magnetic field can be calculated using Ampére's law (equation (1.33)) to write the current density as

$$\mu_0 \mathbf{j} = \nabla \times (F \nabla V) \tag{5.15}$$

so that

$$\nabla \times \mathbf{B} = \nabla \times (F \nabla V). \tag{5.16}$$

which may be integrated once, with the result

$$\mathbf{B} = \nabla U + F \nabla V \tag{5.17}$$

and where U is a function which appears upon integration of equation (5.16). Substitution for F gives the full form of this equation as

$$\mathbf{B} = \nabla U + \kappa(V)(\mathbf{B} \cdot \nabla V)\nabla V. \tag{5.18}$$

However, it should be noted that this is not the final and full expression for $\mathbf{B}$ because we still have a right hand side which is dependent upon $\mathbf{B}$. The full form of this equation can be found, if we multiply equation (5.18) by ∇V

$$\mathbf{B} \cdot \nabla V = \nabla U \cdot \nabla V + \kappa(V)(\mathbf{B} \cdot \nabla V)(\nabla V)^2, \tag{5.19}$$

Solving this equation for $\mathbf{B} \cdot \nabla V$ gives us

$$\mathbf{B} \cdot \nabla V = \frac{\nabla U \cdot \nabla V}{1 - \kappa(V)(\nabla V)^2}. \tag{5.20}$$

which then allows us to write the final form of the magnetic field as

$$\mathbf{B} = \nabla U + \frac{\kappa(V)}{1 - \kappa(V)(\nabla V)^2}(\nabla U \cdot \nabla V)\nabla V. \tag{5.21}$$

The components of the **B** field are

$$B_\varpi = \frac{1}{1 - \kappa(V)(V')^2}\frac{\partial U}{\partial \varpi}, \tag{5.22}$$

$$B_\phi = \frac{1}{\varpi}\frac{\partial U}{\partial \phi}, \tag{5.23}$$

$$B_z = \frac{\partial U}{\partial z}. \tag{5.24}$$

where

$$V' = \frac{dV}{d\varpi}. \tag{5.25}$$

From the expression for B_ϖ above, we can see that the radial component of the field is modified relative to the corresponding radial component of a potential field which would only include the gradient of U (we therefore think of U as a pseudo-potential which determines **B** because ∇U is not a potential field, in general). The modification to equation (5.22) appears because of the presence of currents in the system, given by the factor $1/(1 - \kappa V'^2)$ which causes an increase of the radial magnetic field component compared to the field derived from the gradient of U (in general, this field will not be solenoidal) if the denominator of the factor is greater than one, i.e., $\kappa > 0$. This leads to the stretching of the field lines which one expect from a rotating plasma system. For cases where $\kappa < 0$ then there is a contraction of field lines which one would not expect in rotating plasma

systems.

To determine the pseudo-potential U, we substitute the full form of the magnetic field (5.21) into the divergence-free condition $\nabla \cdot \mathbf{B} = 0$ to give

$$\nabla \cdot \left(\nabla U + \frac{\kappa(V)}{1 - \kappa(V)(\nabla V)^2} (\nabla U \cdot \nabla V) \nabla V \right) = 0. \tag{5.26}$$

This may be rewritten if we define the following quantity

$$\xi(\varpi) = \kappa(V)(V')^2, \tag{5.27}$$

so that the equation for U takes the form of a single partial differential equation

$$\frac{1}{\varpi} \frac{\partial}{\partial \varpi} \left(\frac{\varpi}{1 - \xi(\varpi)} \frac{\partial U}{\partial \varpi} \right) + \frac{1}{\varpi^2} \frac{\partial^2 U}{\partial \phi^2} + \frac{\partial^2 U}{\partial z^2} = 0. \tag{5.28}$$

Equation (5.28) and its more general form, equation (5.26) will be of elliptic form if

$$1 - \kappa(V) V'^2 = 1 - \xi(\varpi) > 0 \tag{5.29}$$

and so we would be able to formulate the normal boundary conditions for U. However, in the case where

$$1 - \kappa(V) V'^2 = 1 - \xi(\varpi) < 0 \tag{5.30}$$

the equations will be hyperbolic and the establishment of the well-posed problem is less obvious. When $1 - \xi(\varpi) = 0$, (the transition point between the two classes of equations) there will be a singularity. In the interests of simplicity and of formulating a mathematically tractable model, we will confine our attention to the elliptic cases.

The functions $\kappa(V)$ (or $\xi(\varpi)$) are free functions of this formulation and may be chosen for mathematical convenience. Considering equation (5.28), we note that it is necessary

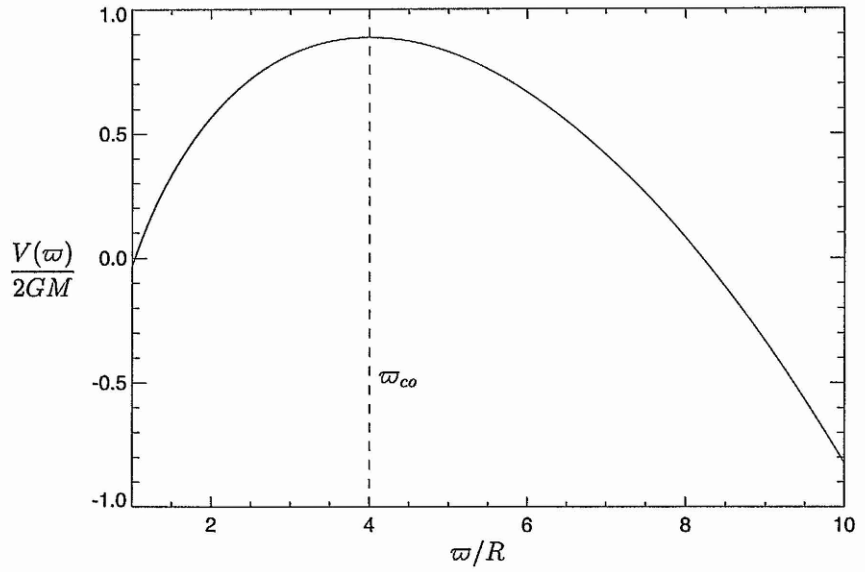

Figure 5.3: The combined potential $V(\varpi)$ for a corotation radius $\varpi_{co} = 4.0$.

to exercise caution when making a choice for $\xi(\varpi)$ directly instead of making a choice for $\kappa(V)$ and calculating $\xi(\varpi)$ from $\xi(\varpi) = \kappa(V(\varpi))V'^2(\varpi)$. This is because the function $V(\varpi)$ has a maximum at a finite radius and as such, is not a monotonic function of ϖ. To calculate this radius, it is necessary to solve the simple relation

$$V'(\varpi) = -\Omega^2\varpi + \frac{2GM}{\varpi} = 0. \tag{5.31}$$

which gives us a solution of the form

$$\varpi_{co} = \frac{\sqrt{2GM}}{|\Omega|}. \tag{5.32}$$

This has the same form as the corotation radius (equation (1.1)) and is the radius which a test particle in a circular and planar orbit would have if its orbital angular velocity would be equal to Ω so that it would co-rotate with the cylinder. When the radius of a rigidly rotating plasma on a cylindrical surface is equal to this corotation radius then the outward

centrifugal force is in exact balance with the inward gravitational force as shown by the expression

$$-\rho\nabla V = -\rho V' \mathbf{e}_{\varpi}$$

for the combination of the two forces. At $\varpi = \varpi_{co}$, V' vanishes and so the combined force is zero. For distances from the cylinder beyond the corotation radius, the centrifugal force will exceed the gravitational force ($V' < 0$) so that the combined forces must be directed outwards from the cylinder. The corotation radius has an additional role where it acts to separate the two ranges of $\varpi-$values for which a one-to-one mapping between $V(\varpi)$ and ϖ exists, i.e., $R < \varpi < \varpi_{co}$ and $\varpi_{co} < \varpi < \infty$. As choosing $\xi(\varpi)$ directly (instead of $\kappa(V)$) is equivalent to making a coordinate transformation from V to ϖ, such a choice is only mathematically well-defined in one of the two ranges of ϖ, but not in both of them together. This is corroborated by the fact that neglecting this condition generally leads to functions $\kappa(V)$ which are singular at the corotation radius, because

$$\kappa(V(\varpi)) = \frac{\xi(\varpi)}{V'^2(\varpi)}, \tag{5.33}$$

and clearly the denominator vanishes at $\varpi = \varpi_{co}$. Such a case will give rise to singularities in the density and the temperature but not in the pressure because

$$p = p_0(V) - \frac{1}{2\mu_0}\kappa(V)V'^2 B_{\varpi}^2 = p_0(V) - \frac{1}{2\mu_0}\xi(\varpi)B_{\varpi}^2. \tag{5.34}$$

However, if we express the density in terms of $\xi(\varpi)$ instead of $\kappa(V)$ then we would obtain

$$\rho = -\frac{dp_0}{dV} + \frac{1}{2\mu_0}\frac{d\kappa}{dV}V'^2 B_{\varpi}^2 + \frac{1}{\mu_0}\kappa(V)\ V'' B_{\varpi}^2 + \frac{1}{\mu_0}\kappa(V)\ V'\ \mathbf{B}\cdot\nabla B_{\varpi}. \tag{5.35}$$

This can be rewritten if we use the relation

$$\begin{aligned}\frac{d\xi}{d\varpi} &= \frac{d}{d\varpi}\left(\kappa(V)V'^2\right) \\ &= \frac{d\kappa}{dV}V'^3 + 2\kappa(V)V'\,V'' \end{aligned} \tag{5.36}$$

which allows us to rewrite Equation (5.35) in the form

$$\rho = -\frac{dp_0}{dV} + \frac{1}{V'}\frac{1}{2\mu_0}\frac{d\xi}{d\varpi}B_\varpi^2 + \frac{1}{V'}\frac{1}{\mu_0}\xi(\varpi)(\mathbf{B}\cdot\nabla B_\varpi), \tag{5.37}$$

with a clear singularity at the corotation radius ($V' = 0$). But even if a singularity of $\kappa(V)$ and ρ could be avoided for a suitable choice of $\xi(\varpi)$ (going through 0 quadratically at ϖ_{co}), the inverse mapping from ϖ to V would not be well-defined across ϖ_{co}, and therefore a given function $\xi(\varpi)/V'^2(\varpi)$ cannot generally be expressed as a function of V. This has to borne in mind when we discuss the analytical example solutions presented below.

The form of equation (5.28) is rather similar to that of Laplace's equation which suggests to us that we should seek separable solutions of the form

$$U(\varpi,\phi,z) = F_{mk}(\varpi)\exp(im\phi)\exp(ikz). \tag{5.38}$$

which may readily be seen to satisfy equation (5.28) upon substitution. In particular, the radial function $F_{mk}(\varpi)$ will satisfy the equation

$$\frac{1}{\varpi}\frac{d}{d\varpi}\left(\frac{\varpi}{1-\xi(\varpi)}\frac{dF_{mk}}{d\varpi}\right) - \left(\frac{m^2}{\varpi^2} + k^2\right)F_{mk} = 0 \tag{5.39}$$

The above equation is a second order ordinary differential equation for which we may find two linearly independent solutions, $F_{mk}^{(1)}(\varpi)$ and $F_{mk}^{(2)}(\varpi)$. Since the partial differential equation for U is linear, we can generate a superposition of solutions for different m

and k in order to generate other solutions. The two linearly independent radial functions $F^{(1)}_{mk}(\varpi)$ and $F^{(2)}_{mk}(\varpi)$ are required to allow us to match the boundary conditions imposed on the surface of the cylinder ($\varpi = R$) and on the outer boundary ($\varpi = \varpi_{out}$). It should be noted that whilst the outer boundary may be at infinity (in general), the problem should only be regarded on a finite domain since, for example, the rotational velocity of a rigidly rotating plasma will at some radius be equal to the velocity of light. However, the assumptions made for deriving our theory will usually break down well before that point. The most general form of a solution of (5.28) is

$$U(\varpi, \phi, z) = \sum_{m=-\infty}^{\infty} \exp(\mathrm{i}m\phi) \int_{-\infty}^{\infty} dk [A_m(k) F^{(1)}_{mk}(\varpi) + B_m(k) F^{(2)}_{mk}(\varpi)] \exp(\mathrm{i}kz). \tag{5.40}$$

Here the $A_m(k)$ and $B_m(k)$ are complex coefficients, which are determined by the boundary conditions. Thus, by superposition of separable solutions, general Dirichlet or von Neumann boundary conditions may be admissible (in the elliptic case).

5.3 Examples of analytic solutions

Whilst we have freedom in our choices for $\kappa(V)$ (or equivalently $\xi(\varpi)$), we are usually subject to the constraint that equation (5.28) or the corresponding radial equation (5.39) have to be solved using numerical methods. However, it is possible to recover some cases of exact solutions, which we will discuss below. It should be noted that an investigation of the full range of solutions to these equations using numerical methods is not impossible

but must be postponed for future study. In all our example solutions we will choose the form of $\xi(\varpi)$ in the context of the above discussion on the range of validity of the solutions and regarding any possible singularities at the corotation radius of the density. We will assume that the ϖ and z have been normalised to the cylindrical radius R, such that the radius of the cylinder is equal to one in these normalised coordinates.

Case 1: constant $\xi(\varpi)$

The simplest possible choice for $\xi(\varpi)$ is where

$$\xi(\varpi) = \xi_0 = \text{constant.} \tag{5.41}$$

Equation (5.39) will now take the form

$$\frac{1}{\varpi}\frac{d}{d\varpi}\left(\frac{\varpi}{1-\xi_0}\frac{dF_{mk}}{d\varpi}\right) - \left(\frac{m^2}{\varpi^2} + k^2\right)F_{mk} = 0 \tag{5.42}$$

with the general solutions

$$F_{mk}(\varpi) = a_{mk}\, I_\nu(k\sqrt{1-\xi_0}\,\varpi) + b_{mk}\, K_\nu(k\sqrt{1-\xi_0}\,\varpi) \tag{5.43}$$

for the radial function $F_{mk}(\varpi)$, where $I_\nu(x)$ and $K_\nu(x)$ are modified Bessel functions (see Abramowitz and Stegun , 1965, chap. 9), $\nu = m\sqrt{1-\xi_0}$ and a and b are constants which will be determined by the boundary conditions. Figure (5.4) shows a solution from this solution class for the parameter values

$$\xi_0 = \frac{3}{4}, \tag{5.44}$$

$$m = 2, \tag{5.45}$$

$$k = \frac{\pi}{5}, \tag{5.46}$$

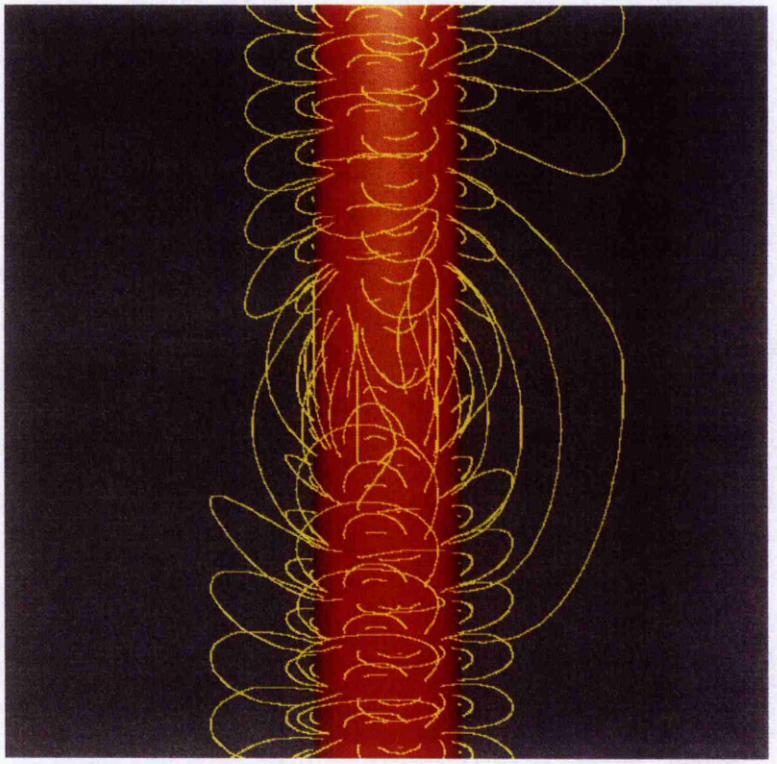

Figure 5.4: A 3D plot of selected field lines of the example solution for $\xi(\varpi) = \xi_0 = 3/4$. The other parameters used to calculate this plot are given in the main text. The plot extends from -2.0 to 2.0 in the z-direction so that the periodicity of this example in that direction is not really obvious.

$$a_{mk} = 0, \tag{5.47}$$

$$b_{mk} = B_0. \tag{5.48}$$

This choice of parameters leads to

$$\sqrt{1-\xi_0} = \frac{1}{2} \tag{5.49}$$

$$\nu \;=\; m\sqrt{1-\xi_0} = 1. \tag{5.50}$$

The coefficients a_{mk} and b_{mk} are chosen such that $F_{mk}(\varpi) \rightarrow 0$ for $\varpi \rightarrow \infty$. The magnetic field components are now given by

$$B_r \;=\; \frac{2\pi}{5} B_0 [\mathrm{K}_0(\pi\ \varpi/10) - \frac{10}{\pi\ \varpi}\mathrm{K}_1(\pi\ \varpi/10)] \sin(2\phi) \sin(\pi\ z/5) \tag{5.51}$$

$$B_\phi \;=\; \frac{2\ B_0}{\varpi}\mathrm{K}_1(\pi\ \varpi/10) \cos(2\phi) \sin(\pi\ z/5) \tag{5.52}$$

$$B_z \;=\; \frac{\pi\ B_0}{5}\mathrm{K}_1(\pi\ \varpi/10) \sin(2\phi) \cos(\pi\ z/5) \tag{5.53}$$

The pressure is given by

$$p = p_0(V) - \frac{\xi_0}{2\mu_0} B_\varpi^2, \tag{5.54}$$

which is non-singular at the corotation radius. The density, however, is given by

$$\rho = -\frac{dp_0}{dV} + \frac{\xi_0}{\mu_0\ V'}\mathbf{B} \cdot \nabla B_\varpi, \tag{5.55}$$

with a singularity at $V' = 0$ which forces us to confine our solutions to the range $\varpi < \varpi_{co}$. It should be noted that when we choose $\xi(\varpi)$ directly, the value of the corotation radius will affect the solution only through the presence of V' in the density. In the previous two chapters we considered the effect of increasing Ω on the emission from our model magnetospheres. However, were we to be interested in the effects of increasing Ω on the solutions then we would be frustrated by the fact that the rotation rate has been effectively eliminated from the solutions. This is because the corotation radius is the only parameter in which Ω appears, so that choosing $\xi(\varpi)$ instead of $\kappa(V)$ will eliminate Ω.

Case2: $\xi(\varpi) = 1 - q\varpi^2$

Solutions to equation (5.39) are also possible for a choice of $\xi(\varpi)$ of the following form

$$\xi(\varpi) = 1 - q\varpi^2 \tag{5.56}$$

for a constant, q. Equation (5.39) now becomes

$$\frac{1}{\varpi}\frac{d}{d\varpi}\left(\frac{1}{q\varpi}\frac{dF_{mk}}{d\varpi}\right) - \left(\frac{m^2}{\varpi^2} + k^2\right) F_{mk} = 0. \tag{5.57}$$

Under the coordinate transformation

$$w = \frac{1}{2}\varpi^2, \tag{5.58}$$

equation (5.39) will now be transformed to

$$\frac{d^2F_{mk}}{dw^2} - q\left(\frac{m^2}{2w} + k^2\right) F_{mk} = 0. \tag{5.59}$$

The solutions of equation (5.59) may be expressed in terms of confluent hypergeometric functions $M(a, b, x)$ and $U(a, b, x)$ as Abramowitz and Stegun (1965, chap. 13)

$$F_{mk} = 2\sqrt{qk^2}\,\varpi \quad \exp(-\sqrt{qk^2}\,\varpi)[\quad a_{mk} \quad M(1 + m^2/(8k^2), 1, 2\sqrt{qk^2}\,\varpi) + \\ b_{mk} \quad U(1 + m^2/(8k^2), 1, 2\sqrt{qk^2}\,\varpi)]. \tag{5.60}$$

The pressure and the density may be calculated using equations (5.34) and (5.37) in a similar manner as with case one, discussed previously. Solutions for different m and different k must be superposed if we wish to generate solutions for more realistic boundary conditions. However, the calculation of the expansion coefficients will (in most cases) have to be made numerically. Instead, it may be more preferable to solve equation (5.26)

directly for a more realistic $\kappa(V)$ using numerical methods in order to avoid singularities at the corotation radius. With this particular case, it might be better (and more realistic) to solve the appropriate equation for a spherical body rather a cylindrical one.

In the above formulation and analysis we have shown a relatively simple semi-analytical approach to the modelling of three-dimensional rigidly rotating magnetospheres for which we have to make a suitable choice for the free function $\kappa(V)$ (or $\xi(\varpi)$) that will allow us to make analytical progress with the problems associated with modelling planetary magnetospheres (given the cautionary remarks made above). However, a similar method may be developed for rotating spherical systems. In such systems, the combined gravitational and centrifugal potential of a body of mass M_0 with its rotation axis aligned with the $z-$axis has the following form (in spherical coordinates r, θ and ϕ)

$$V(r,\theta) = -\frac{1}{2}\Omega^2 r^2 \sin^2\theta - \frac{GM_0}{r}. \tag{5.61}$$

The dependence of V on two of the coordinates will lead to a more complicated form of equation (5.26) because B_r and B_θ depend on both $\frac{\partial U}{\partial r}$ and on $\frac{\partial U}{\partial \theta}$ which leads to mixed second derivative terms in the equation. Such an equation will probably not be of a form which would readily yield analytic solutions and it is doubtful that it would yield any such solutions at all. We would therefore have recourse to employing similar types of numerical methods that would be used to solve equation (5.26) in the cylindrical formulation. It is clear that there is much scope for further development of this approach, particularly from a numerical perspective. Developing a theory for rotating spherical massive bodies (along the lines outlined above) would be useful to extend our studies of the saturation of X-ray emission with increasing rotation rates (see previous chapters

and also Ryan et al. (2001)) from that of symmetric models to those of non-symmetric models. However, before developing such models it would be prudent to complete our analysis of the formulation and properties of cylindrical systems before we undertake the study of the more complex spherical systems.

Chapter 6

Concluding remarks

In the first part of this thesis (up to and including chapter four) we have used numerical methods to solve the magnetohydrostatic equations and to generate sequences of equilibria in order to model the changing behaviour of the X-ray emission from rigidly rotating stellar magnetospheres with increasing angular velocity. Whilst it has been necessary to make a number of strong assumptions, we have formulated our models to be simple but still physically plausible so that we may recover mathematically and computationally tractable equations to solve. In chapter 2 we discussed the numerical continuation method (due to Keller and Zwingmann), a more convenient formulation of this method and we discussed the finite element domain discretisation methods that form the basis of our numerical calculations. The third chapter then described the MHD formulation of our scaling models and in which we presented our results that showed a good agreement with the observed saturation (and supersaturation) seen in G-K dwarfs (and M-dwarfs)

of X-ray emission with increasing angular velocity. Chapter 4 discussed the extension of these models to include a toroidal component in the magnetic field and the presentation of results for that model. Both chapters 3 and 4 demonstrate the robustness and flexibility of our models that is independent of our major model assumptions. In addition, the inclusion of a toroidal magnetic field component is not seen to change our results greatly. Despite the success of these models there is clearly much room for further refinement and extension of these models. One such avenue is explored in chapter 5 where we present a simple semi-analytic method that should allow us to extend our models to fully three-dimensional, non-symmetric, rigidly rotating stellar and planetary magnetospheres. In the case of the work presented in chapter 5, we have only presented the analytic basis of this method in a cylindrical geometry and it is clearly desirable to extend this work to a spherical geometry. Furthermore, whilst we have made analytic progress with these models, it is still necessary for us to undertake extensive numerical calculations in order to complete this study.

Returning to the models of chapters 3 and 4 we find that there are other aspects of these models which need to be developed. For example, we must consider the full exploration of the parameter space. In particular, the nature of the parameters ξ_3 and λ_ϕ in our models, presents us with numerical difficulties that restrict our freedom of choice in the values of these parameters that we may take. Therefore, we need to consider different numerical approaches (such as discussed at the end of chapter 4) in order to progress. For the purposes of completion, it might also be worthwhile to repeat our M-dwarf calculations for models with toroidal magnetic field components included. Further information

can, however, be extracted from the models in their present form such as calculating helicity and considering stability criteria for our equilibria.

There is considerable potential for our models to incorporate other aspects of rotating magnetospheres. One such example is a model which departs from the ideal gas law which might allow us to consider filamentary structures. Another example is to extend our models to those of fully three-dimensional magnetospheres using the methods of chapter 5 and the numerical work of Romeou (2002). Other considerations such as mixed outer boundary conditions (that would allow us to include a proxy for a stellar wind into our models) are possible but would require considerable further development of our numerical codes. It is clear that both in terms of modelling and numerics we have considerable flexibility and scope to address questions concerning the modelling of rotating magnetospheres.

Appendix A

Derivation of pressure function by Vlasov approach

In the work of Neukirch (1993a), the author investigated the equilibrium and stability of rigidly rotating quasi-neutral axisymmetric magnetospheres that possess an aligned magnetic dipole moment. Using collisionless theory, this allowed a self-consistent description of trapped particle populations by making a choice of a mathematically simple (but still physically relevant) class of distribution functions. Calculation of solution branches was then found to be possible by varying the plasma density and then considering the bifurcation properties in typical cases. Following the method used in Neukirch (1993a) we wish to obtain some intuition as to the form of the free function $p_0(A)$ to apply to our coronal surface pressure distributions. Recalling our introductory discussion of kinetic theory we demonstrated how the theory gives the description of bulk plasma properties (such as

particle density and pressure) in terms of a distribution function, f_s where s labels the different particle species present in the plasma. We make the choice

$$f_s = f_{0s} \exp\left[-\beta_s \left(H - \Omega_s p_\phi\right)\right] \tag{A.1}$$

where f_{0s} is a normalisation constant and where Ω_s is the average angular velocity for a particle species s and $\beta_s = \frac{1}{k_B T_s}$. The energy (Hamiltonian) where $H := \frac{1}{2} m_s v^2 + q_s \Phi + m_s \psi$ and the canonical momentum $P_\phi := m_s r \sin\theta v_\phi + q_s A$ are both constants of the motion whose values determine the regions accessible to the particle in the magnetic dipole field. The variable q_s is the particle charge, v_ϕ is the component of the particle velocity in the azimuthal direction , Φ is the electric field potential and $\psi = -\frac{GM_*}{r}$ is the gravitational potential. (A more detailed exposition of these methods is available in Störmer (1955) and Rossi & Olbert (1970).) We begin by writing the quantity $\tilde{H} = H - \Omega_s p_\phi$ in a more convenient fashion

$$\begin{aligned} & H - \Omega_s p_\phi \\ & \qquad = \tfrac{1}{2} m_s \left(v_r^2 + v_\theta^2\right) + \tfrac{1}{2} m_s \left(\tilde{v_\phi}\right)^2 - \tfrac{1}{2} m_s \left(\Omega_s r \sin\theta\right)^2 + q_s \left(\Phi - \Omega_s A\right) + m_s \psi \end{aligned}$$

where $\tilde{v_\phi} = v_\phi - \Omega_s r \sin\theta$. The particle density may now be found by integrating the distribution function over the velocity space

$$n_s = \int_{-\infty}^{\infty} d^3 v f_s \left(H, p_\phi\right)$$

so that if we use $\tilde{H}$ as an integration variable, the particle density will take the following form

$$n_s = \frac{\sqrt{2} 4\pi}{\sqrt[3]{m_s}} \int_{\tilde{H}_{min}}^{\infty} d\tilde{H} \sqrt{\tilde{H} - q_s \left(\Phi - \Omega_s A\right) + \frac{1}{2} m_s \left(\Omega^2 r^2 \sin^2\theta\right) - m_s \psi} F\left(\tilde{H}\right)$$

$$= \frac{\sqrt{2}4\pi}{\sqrt[3]{m_s}} \int_{\tilde{H}_{min}}^{\infty} \sqrt{\tilde{H} - \tilde{H}_{min}} F\left(\tilde{H}\right) \tag{A.3}$$

where $\tilde{H}_{min}$ denotes the minimum energy available to the trapped particle population. Substitution of the distribution function (equation A.1) for $F(\tilde{H})$ into the integrand then yields

$$n_s = \frac{\sqrt{2}4\pi}{\sqrt[3]{m_s}} f_{0s} \int_{\tilde{H_{min}}}^{\infty} d\tilde{H} \sqrt{\tilde{H} - \tilde{H_{min}}} \exp\left[-\beta_s \tilde{H}\right] \tag{A.4}$$

which upon introduction of the new variable $z = \beta_s \left(\tilde{H} - \tilde{H}_{\min}\right)$ reduces to the a more simplified form

$$\begin{aligned} n_s &= \frac{\sqrt{2}4\pi}{\sqrt[3]{m_s}} f_{0s} \exp\left(-\beta_s \tilde{H}_{min}\right) \int_0^{\infty} dz z^{\frac{1}{2}} \exp\left(-z\right) \\ &= n_{0s} \exp\left[-\beta_s \{q_s \left(\Phi - \Omega_s A\right) - \frac{1}{2} m_s \Omega_s^2 r^2 \sin^2\theta + m_s \psi\}\right] \end{aligned} \tag{A.5}$$

where $n_{0s} = 4\sqrt{2} f_{0s} \left(\sqrt[3]{\frac{\pi}{\beta_s m_s}}\right)$ which incorporates the evaluation of the integral as a gamma function of the form $\Gamma\left(\frac{3}{2}\right) = \frac{\sqrt{\pi}}{2}$ (see Abramowitz and Stegun , 1965, chap. 6). Under the assumption that the principle particle species are those of electrons and ions (with particle densities n_e and n_i respectively) whose particle densities roughly equate and which will constitute a quasi-neutral plasma, the substitution of our expression for n_s (equation (A.5)) into the condition $n_e = n_i$ yields an equivalent expression of the form

$$n_{0e} \exp\left[-\beta_e \{-e\left(\Phi - \Omega_e A\right) - m_e \eta_e\}\right] = n_{0i} \exp\left[-\beta_i \{-e\left(\Phi - \Omega_i A\right) - m_i \eta_i\}\right] \tag{A.6}$$

where the subscripts e and i refer to the electronic or ionic populations respectively and where for convenience we denote η_i and η_e

$$\eta_i = \frac{1}{2}\Omega_i^2 r^2 \sin^2\theta - \psi \tag{A.7}$$

$$\eta_e = \frac{1}{2}\Omega_e^2 r^2 \sin^2\theta - \psi \tag{A.8}$$

The condition of quasi-neutrality allows us to neglect Poisson's equation and to solve the above expression for the electric field potential Φ as a function of the flux function, A, to give

$$\Phi = \frac{\beta_e\Omega_e + \beta_i\Omega_i}{\beta_e + \beta_i}A + \frac{\beta_i m_i\Omega_i^2 - \beta_e m_e\Omega_e^2}{e\left(\beta_e + \beta_i\right)}\frac{1}{2}r^2\sin^2\theta - \frac{\beta_i m_i - \beta_e m_e}{e\left(\beta_e + \beta_i\right)}\psi + \frac{1}{e\left(\beta_e + \beta_i\right)}\log\frac{n_{0i}}{n_{0e}} \tag{A.9}$$

which we may then substitute back into the argument of the exponential function of the particle density as given by equation (A.6). Together with the full expression for η_e given by equation (A.8) we may now recover the particle density in terms of the particles temperature (via β), angular velocity and mass

$$n_s = n_{0e}\exp\left[e\frac{\beta_e\beta_i}{\beta_e + \beta_i}\left(\Omega_i - \Omega_e\right)A + \frac{1}{2}\frac{\beta_e\beta_i\left(m_e\Omega_e^2 + m_i\Omega_i^2\right)}{\beta_e + \beta_i}r^2\sin^2\theta - \frac{\beta_e\beta_i}{\beta_e + \beta_i}\left(m_e + m_i\right)\psi + \frac{\beta_e}{\beta_i + \beta_e}\log\frac{n_{0i}}{n_{0e}}\right] \tag{A.10}$$

The last term of the argument can now be collected into a new constant, n_0, because the electron form of the term may be interchanged with the ion form but this will still result in the same factor

$$n = n_0\exp\left[\xi_3\tilde{A} + \frac{1}{2}\xi_2\tilde{r}^2\sin^2\theta + \xi_1\frac{1}{\tilde{r}}\right] \tag{A.11}$$

where

$$\xi_1 = \frac{\beta_e\beta_i}{\beta_e+\beta_i}\left(m_e+m_i\right)\frac{GM_\star}{R} \tag{A.12}$$

$$\xi_2 = \frac{\beta_e\beta_i}{\beta_e+\beta_i}\left(m_e\Omega^2+m_i\Omega_i^2\right)R^2 \tag{A.13}$$

$$\xi_3 = \frac{\beta_e\beta_i}{\beta_e+\beta_i}e\left(\Omega_i-\Omega_e\right)A_0 \tag{A.14}$$

Before we proceed any further, it is necessary to define a reference point for n_0 and for other model constants, on the stellar surface. At the pole of the stellar surface, $A=0, \theta=1$ and $r=1$ so that $n=n_0\exp(\xi_1)$. Defining $\bar{n_0}=n_0\exp\xi_1$ and inverting for n_0 we now obtain a modified form of equation (A.11) where n_0 is substituted for $\bar{n_0}$. This form of the particle density will now enable us to describe more useful and measurable physical quantities of the system and thence to determine and inform us with a good choice for the stellar coronal surface pressure function term, $p_0(A)$. The currents in the system result from the different toroidal drifts of the electron and ion particle populations with respect to any other velocities which will have already been averaged so that we now have a current density of the form

$$j_\phi = e\left(\Omega_i-\Omega_e\right)\bar{n}_0 r\sin\theta \tag{A.15}$$

Substitution of the current density together with that of the derived particle density, n (equation(A.11)) into a normalised form of the Grad-Shafranov equation (equation (3.9)

$$-\frac{\partial^2\tilde{A}}{\partial\tilde{r}^2}-\frac{\sin\theta}{\tilde{r}^2}\frac{\partial}{\partial\theta}\exp\left(\frac{1}{\sin\theta}\frac{\partial\tilde{A}}{\partial\theta}\right) = \lambda r^2\sin\theta\left[\xi_3\tilde{A}+\frac{1}{2}\xi_2\tilde{r}^2\sin^2\theta+\xi_1\frac{1}{\tilde{r}}\right] \tag{A.16}$$

where λ takes on the new form

$$\lambda = \frac{\mu_0 R^4\left(\Omega_i-\Omega_e\right)\bar{n_0}}{A_0} \tag{A.17}$$

and with $\bar{n}_0 = n_0 \exp(\xi_1)$.

In order to express the magnetic flux coefficient, ξ_3 (equation (A.14)), in terms of known quantities, we can combine ξ_3 with λ (equation(A.17)) together with the expression for stellar equatorial surface flux, $A_0 = B_0 R^2$ resulting in the following form of ξ_3

$$\xi_3 = \frac{\beta_e \beta_i}{\beta_e + \beta_i \bar{n}_0} \frac{B_0^2}{\mu_0} \lambda \tag{A.18}$$

Finally we may assume that the temperatures of both the ion and the electron populations are the same so that if $T_e = T_i = T$ then clearly $\beta_e = \beta_i = \beta = \frac{1}{k_B T}$ and we have

$$\xi_3 = \frac{\lambda}{\beta_p} \tag{A.19}$$

where

$$\beta_p = \frac{2\mu_0 k_B T \bar{n}_0}{B_0^2} \tag{A.20}$$

which is the plasma beta at the reference point of the surface of the stellar coronal pole and where the exponential terms are normalised in a similar manner to the normalisation of the Grad-Shafranov equation in the MHD formulation (as discussed earlier in chapter 3). In a stellar corona the plasma beta can be much smaller than unity resulting in a possible situation where $\xi_3 \gg 1$. The final form of the Grad-Shafranov equation would then be given by

$$-\frac{\partial^2 \tilde{A}}{\partial \tilde{r}^2} - \frac{\sin\theta}{\tilde{r}^2} \frac{\partial}{\partial \theta} \left(\frac{1}{\sin\theta} \frac{\partial \tilde{A}}{\partial \theta} \right) = \lambda r^2 \sin\theta \exp\left[\frac{1}{\beta_p} \lambda A + \frac{\xi_2}{2} \left(r^2 \sin^2\theta - 1 \right) + \xi_1 \left(\frac{1}{r} - 1 \right) \right]. \tag{A.21}$$

It follows from the form of the normalised Grad-Shafranov equation discussed earlier (3.9) that the pressure gradient which contributes to the current density will be

$$\frac{\partial p}{\partial A} \propto \lambda \exp\left[\frac{1}{\beta_p}\lambda A\right] \tag{A.22}$$

so that a simple first integration then gives us the final form of the pressure dependence

$$p \propto \beta_p \exp\left[\frac{1}{\beta_p}\lambda A\right] \tag{A.23}$$

In this appendix we have derived the form of pressure distribution appropriate to a collisionless, axisymmetric, quasi-neutral and rigidly rotating magnetosphere in the context of a Vlasov theory formulation. The MHD formulation of the scaling model (outlined in chapter 3) does not include a theoretical basis or any indication which might allow us to make our choice for the form of the free function, $p_0(A)$, of the coronal surface pressure distribution. Given the similarities between the plasma systems that we have considered within the Vlasov and MHD formalism, we feel confident in using a pressure function similar to that derived above in (A.23), as the basis for our choice of $p_0(A)$.

Bibliography

Abramowitz, M. & Stegun, I.A. 1965, *Handbook of Mathematical Functions*, Dover, New York

Alfvén, H. 1950, *Cosmical Electrodynamics*, Clarendon Press, Oxford

Allgower, E. L. & Georg, L. 1990, *Numerical Continuation Methods*, Springer-Verlag, Berlin-New York

Bagenal, F., 1992, Annu. Rev. Earth Planet Sci., 20, 289

Bogdan, T. J. and Low, B. C., 1986, ApJ, 306, 271

Becker, U. H., 1999, P.hD. thesis, Ruhr-Universität Bochum

Braess, D., 1997, *Finite Elements*, Cambridge University Press, England

Braginskii, S.I., 1965, Rev. Plasma. Phys., 1, 205

Browning, P.K. and Priest, E.R., 1984, Geophys. Astrophys. Fluid Dynamics, 28, 141

Campbell, C. G., 1997, *Magnetohydrodynamics in Binary Stars*, Kluwer Academic

Chandrasekhar,S., 1961, *Hydrodynamic and Hydromagnetic Stability*, Oxford University Press, England

Charbonneau, P., & MacGregor, K. B., 1992, ApJ, 387, 639

Collier Cameron, A. and Robinson R. D., 1989, MNRAS, 236, 57

Collier Cameron, A., L. Jianke and Mestel, L., 1991 in NATO ASI Series Angular Momentum Evolution of Young Stars, eds. Catano, S. and Stauffer, J. R., 297

Collier Cameron, A., Jardine, M. M. and Donati, J.-F., 2001 in Stellar Coronae in the Chandra and XMM-Newton Era, eds. Favata, F. and Drake, J., ASP Conf. Series, in press

Donati, J.-F. and Collier Cameron, A., 1997, MNRAS, 291, 1

Doyle, J., 1996, A. & A., 162, 307

Durney, B. R., 1972 in Asilomar Conference on the Solar Wind, eds. Sonnett, C. P., Coleman Jr., P. J. and Wilcox, J. M., p282, NASA, Washington

Favata, F., Reale, F., Micela, G., Sciortino, S., Maggio, A. and Schmidt, J. H. M. M., 2001 in ASP Conf. Ser. Vol.223, 11th Cambridge Workshop on Cool Stars, Stellar Systems and the Sun, eds. Lopez, R. J. G., Rebolo, R. and Osorio, M., San Franscisco (CD-ROM directory:contribs/favata)

Ferreira, J. M., 1998, A. & A., 335, 248

Ferreira, J. M., 2000, MNRAS, 316, 647

Fleck, B., 1997, Rev. Mod. Astron., 10, 273

Grad, H., 1960, Rev. Mod. Phys., 32, 830

Heinemann, M. and Olbert, D., 1978, J. Geophys. Res., 82, 2457

Hempelmann, A., Schmidt, J. H. M. M., Schultz, M., Rüdiger, G. and Stępień, K., 1995, A & A, 294, 515

Houdebine, E. R., Foing, B.H., Doyle, J. G. and Rodono, M., 1993, A & A, 278, 109

Hundhausen, J. R., Hundhausen, A. R. and Zweibel, E. G., 1981, J. Geophys. Res., 86,

11117

Hundhausen, A. J., *Coronal Diagnostics and Some Dynamics*, unpublished report

James, D., Jardine, M. M., Jeffries, R. D., Randich, S., Collier Cameron, A. and Ferreira, J. M., 2000, MNRAS, 318, 1217

Jardine, M. M. and Collier Cameron, A., 1991, Sol. Phys., 131, 269

Jardine, M. M. and Unruh, Y. C., 1999, A. & A., 346, 883

Keller, H. B., 1977, Numerical Solution of Bifurcation and nonlinear Eigenvalue Problems, in Applications of Bifurcation Theory, Academic, San Diego, Calif, 395

Kopp, A., Space Physics Page, http://www.linmpi.mpg.de/~kopp/index_p.html

Kennel, C. F. and Coronti, F. V., 1977, Ann. Rev. Astron. Astrophys., 15, 389

Kitchatinov, L. L., Jardine, M. M. and Donati, J.-F., 2000a, MNRAS, 318, 1171

Kitchatinov, L. L., Mazur, M. V. and Jardine, M. M., 2000b, A. & A., 359, 531

Kraft, R. P., 1967, Astrophys. J., 150, 551

Krall, N. A and Trivelpiece, A. W., 1973, *Principles of Plasma Physics*, McGraw-Hill

Krishnamurthi, A., Pinsonneault, M. H., Barnes, S. and Sofia, S., 1997, ApJ, 480, 303

Low, B. C., 1985, ApJ, 293, 31

Low, B. C., 1991, ApJ, 370, 427

Low, B. C., 1992, ApJ, 399, 300

Low, B. C., 1993a, ApJ, 408, 689

Low, B. C., 1993b, ApJ, 408, 693

Mathioudakis, M., Fruscione, A., Drake, J., McDonald, K., Bowyer, S. and Malina, R. F., 1985, A. & A., 300, 773

Mestel, L. and Spruit, H. C., 1987, MNRAS, 226, 57

Mestel, L., *Stellar Magnetism*, Oxford University Press, England

Moss, D. and Smith, R. C., 1981, Rep. Prog. Phys., 44, 831

Neukirch, T., 1993a, J. Geophys. Res., 98, 3753

Neukirch, T., 1993b, A. & A., 274, 319

Neukirch, T., 1995, A. & A., 301, 628

Neukirch, T., 1997, A. & A., 325, 847

Neukirch, T., 1998, *Introduction to the theory of MHD equilibria*, lecture notes, http://www-solar.mcs.st-andrews.ac.uk/thomas/teaching/mhdlect.ps.gz, University of St. Andrews

Noyes, R. W., Hartmann, L. W., Baliumas, S. L., Duncan, D. K. and Vaughan, A. H., 1984, ApJ, 279, 763

O'Dell, M. A., Panagi, P. M., Hendry, M. A. and Collier Cameron, A., 1995, A. & A., 294, 715

Osherovich, V. A., 1985a, Aust. J. Phys., 38, 975

Osherovich, V. A., 1985b, ApJ, 298, 235

Pallavicini, R., Golub, L., Rosner, R., Vaiana, G. S., Ayres, T. R. and Linsky,J., 1981, ApJ, 248, 279

Parker, E. N., 1955, ApJ, 122, 293

Parker, E. N., 1979, *Cosmical Electric Fields*, Oxford University Press, England

Petrie, G. J. D. and Neukirch, N., 2000, A. & A., 356, 735

Prosser, C. F., Randich, S., Stauffer, J. R. and Schmidt, J. H. M. M., 1996, Astron. J., 112,

1570

Randich, S., 1998 in ASP Conf. Ser. Vol. 154, 10th Cambridge Workshop on Cool Stars, Stellar Systems and the Sun, eds. Donahue, D. and Bookbinder, J., 501

Rastätter, L. and Neukirch, T., 1999, A. & A., 348, 1000

Reale, F., 2001 in Stellar Coronae in the Chandra and XMM-Newton Era, eds. Favata, F. and Drake, J., ASP Conf. Series, in press

Ritz, W., 1908, J. Reine angew. Math, 135, 1-61

Roberts, P. H., 1967, *An Introduction to Magnetohydrodynamics*, Longmans, London

Robinson, R. D., Worden, P. W. and Harvey, J. W., 1980, ApJ, 236, L155

Romeou, Z., 2002, P.hD. thesis, University of St. Andrews

Rosner, R., Golub, L. and Vaiana, G. S., 1985, Ann. Rev. Astron, Astrophys., 23, 413

Rosner, R., 2000, Phil. Trans. R. Soc. Lond, 358, 689

Rossi, B. and Olbert, S., 1970, *Introduction to the Physics of Space*, McGraw-Hill, New York

Ryan, R. D., Neukirch, T. and M. M. Jardine, 2001 in ASP Conf. Ser. Vol. 248, Magnetic Fields Across the Hertzsprung-Russell Diagram, eds. G. Mathys, S. K. Solanki and D. T. Wickramasinghe, 251

Saar, S. and Linsky, J., 1985, ApJ, 299, L47

Saar, S., 2001 in Stellar Coronae in the Chandra and XMM-Newton Era, eds. Favata, F. and Drake, J., ASP Conf. Series, in press

Schrijver, C. J. and Zwaan, C., *Solar and Stellar Magnetic Activity*, Cambridge University Press, England

Solanki, S. K., S. Motamen and R. Keppens, 1997, A. & A., 325, 1039

Spitzer, L., 1962, *Physics of Fully Ionized Gases*, Interscience, New York

Stauffer, J. R., Hartmann, L. W., Prosser, C. F., Randich, S., Balachandran, S., Patten, B. M. Simon, T. and Giampapa, M., 1997, ApJ, 479, 776

Störmer, C., 1955, *The Polar Aurora*, Oxford University Press, England

Strassmeier, K .G. and Rice, J. B., 1998, A. & A, 330, 685

Stern, D. P. and Ness, N. F., 1982, A. Rev. Astron. Astrophys., 20, 139

Sturrock, P. A., 1994, *Plasma Physics*, Cambridge University Press, England

Vaiana, G. S. and Rosner, R., 1978, Annu. Rev. Astron. Astrophys., 16, 393

Ventura, P., Zeppieri, A., Mazzitelli, I. and D'Antona, F., 1998, A. & A., 334, 953

Vilhu, O. and Walter, F. M., 1987, ApJ, 321, 958

Wait, R. and Mitchell, A. R., 1985, *Finite Element Analysis and Applications*, John Wiley, New York

Wilson, O. C., 1966, ApJ, 144, 695

Wolfson, R. and Dlamini, B., 1999, ApJ, 526, 1046

Zombeck, M. V., 1990, *Handbook of Space Astronomy and Astrophysics*, Cambridge University Press, England

Zwingmann, W., 1987, Sol. Phys., 111, 309